Harpur Hill, Buxton
Derbyshire, SK17 9JN
T: +44 (0)1298 218000
F: +44 (0)1298 218590
W: www.hsl.gov.uk

HEALTH & SAFETY LABORATORY

Flammability of Hydrocarbon and Carbon Dioxide Gas Mixtures: Measurements and Modelling

MSU/2010/21

Project Leader: **Richard Bettis**

Author(s): **S. E. Gant**
C. J. Lea
M. Pursell
J. Fletcher
W. Rattigan
A. Thyer

DISTRIBUTION

S. Connolly	HSE OSD3.2, Customer Authorising Officer
A. M. Grey	HSE Customer Project Officer
M. J. Ivings	Fluid Dynamics Team Leader, Mathematical Sciences Unit, HSL
L. Cusco	Fire and Process Safety Unit Head, HSL
D. Morgan	Mathematical Sciences Unit Head, HSL
A. D. Curran	Science Director, HSL

PRIVACY MARKING:

Available to the public (and will not be published by HSE)
SCS Clearance given by Professor Andrew Curran, Science and Resources Director

HSL report approval:	**A. D. Curran**
Date of issue:	**1 March 2011**
Job number:	**PH03009**
Registry file:	**029674**
Electronic file name:	**MSU201021.doc**

ACKNOWLEDGEMENTS

The authors would like to thank Professor Mike Fairweather and Dr. Reza Alvani (University of Leeds), Andrew Wells (ANSYS) and Dr. Adrian Kelsey (Health & Safety Laboratory) for their help and assistance in preparing this report.

CONTENTS

EXECUTIVE SUMMARY

The next decade is likely to see a rapid increase in the transport offshore of carbon dioxide (CO_2) for enhanced oil recovery and sequestration into depleted oil and gas fields. As a result, hydrocarbon gas streams may become increasingly contaminated by CO_2, and indeed it may sometimes be advantageous to mix the two streams to reduce the hazard posed by fires and explosions from unintended releases.

In addition to these considerations, ageing offshore installations are also now being decommissioned or dismantled at an increasing rate. Dismantling of poorly-inerted former hydrocarbon processing plant has been known to cause fires and explosions resulting in fatalities.

In developing a safety case for Major Accident Hazard (MAH) plant where CO_2 is used, risk assessments may therefore need to incorporate consequence modelling that takes into account the presence of CO_2 and the new or modified hazards, including changes in fire and explosion properties. This includes consideration of:

- Premixed and non-premixed gas streams
- Ignition sources
- Gas dispersion and flammability

In particular, it is important to appreciate that gas mixtures may be flammable even when the local mean concentration is below the Lower Flammability Limit (LFL) or above the Upper Flammability Limit (UFL), due to turbulent fluctuations in concentration above and below the mean level.

To help provide information to both HSE and industry on the characteristics of mixtures of hydrocarbon and inert gases, the present work examines the flammability of premixed and non-premixed hydrocarbon and CO_2 gas mixtures.

Measurements from explosion tests are presented using a 20 litre explosion sphere and an 8 m long section of 1.04 m diameter pipeline with premixed CO_2 and propane or methane mixtures in air. These show that the explosion overpressure decreases as the CO_2 concentration is increased, as anticipated. For the 20 litre sphere, it is found that CO_2 concentrations greater than 15% vol/vol in the CO_2-methane-air mixture are needed in order to suppress completely the explosion. These results agree well with the previous flammability measurements of Kondo *et al*. (2006). In the larger-scale pipe tests, no ignition of the gas mixture is found to occur for a CO_2 concentration of 12% vol/vol, although the mixture should be within the flammable range for this case. This result is attributed to incomplete mixing of the gases and highlights the fact that poor mixing of the inerting gas needs to be considered when analysing certain fire and explosion events.

The flammability of non-premixed jets is then examined. A brief introduction to various analytical techniques is first provided. Using a combination of empirical relations taken from the literature, a simple predictive model is presented for the flammability factor in free, unobstructed, gas jets. The predicted flammability factor provides an indication of the ignition probability, i.e. the likelihood of the gas mixture being ignitable at a given location and time. The model is validated against the previously published works of Birch *et al*. (1981) and Smith *et al*. (1986), and then used to model the ignition of free-jets of methane and CO_2, for which new experimental data is also presented.

The measurements and model predictions show that the ignitable region in a jet of methane containing 20% CO_2 is smaller than that of the equivalent pure methane release, as expected. It is demonstrated that it is possible to ignite the gas jets at points in the flow where the mean concentration is either below LFL or above the UFL. The agreement between the flammability factor predicted by the empirical model and the measured ignition probability is reasonably good in the near-field of the jet but it deteriorates further downstream in the far-field. The model predictions here are significantly higher than those measured, with the measured ignition probabilities remaining below 60% even where it is predicted for gas concentrations to be within the flammable range for the vast majority of the time. These differences are attributed mainly to the effect of the wind in the experiments, which were conducted in a walled courtyard that was open to the atmosphere, whereas the model assumed that the ambient environment was quiescent.

The results from bulk ignition experiments are also reported, from tests in which jets of methane, mixed with varying quantities of CO_2, were released in air and ignited using a propane blow torch. Three different release velocities are examined and the resulting ignition behaviour is classified according to a set of five criteria. The results show that in some situations where a stable flame cannot be sustained, the fuel present in the CO_2-methane jet still promotes combustion. If, in a MAH event, a partially inerted mixture is released onto a continuous ignition source, such as an on-going hydrocarbon fire, these results show that it could potentially add to the severity of the fire.

A final section of this report examines the feasibility of using Computational Fluid Dynamics (CFD) to extend predictions of the flammability factor beyond simple jet flows. Previous work in this field is examined in detail, and a simplified methodology is proposed which retains many of the benefits of more sophisticated approaches.

Models for the flammability of hydrocarbon and CO_2 gas clouds presented in this report can easily be extended to consider other gas mixtures. Applications include discharges from storage tanks with nitrogen-inerting or flue gas systems, and hydrogen and inert gas mixtures used in pre-combustion CO_2-capture power stations. The same fundamental principles of the flammability factor can also be used to analyse the toxic load a person may receive from atmospheric exposure to fluctuating concentrations of a toxic gas, aerosol or dust.

1 INTRODUCTION

The next decade is likely to see a rapid increase in the transport offshore of carbon dioxide (CO_2) for enhanced oil recovery and sequestration into depleted oil and gas fields. As a result, hydrocarbon gas streams may become increasingly contaminated by CO_2, and indeed it may sometimes be advantageous to mix the two streams to reduce the hazard posed by fires and explosions from unintended releases. Risk assessments may therefore need to incorporate consequence modelling that takes into account the presence of CO_2 and the new or modified hazards, including changes in fire and explosion properties.

In addition to these considerations, ageing offshore installations are also now being decommissioned or dismantled at an increasing rate. Dismantling of poorly-inerted former hydrocarbon processing plant has been known to cause fires and explosions resulting in fatalities.

To help provide information to both HSE and industry on the characteristics of mixtures of hydrocarbon and inert gases, the present work examines the flammability of premixed and non-premixed hydrocarbon and CO_2 gas mixtures. The study takes forward knowledge gained during the earlier work of Thyer *et al.* (2009).

Explosion measurements undertaken with premixed CO_2 and propane or methane mixtures are first presented for two different scale tests: a 20 litre sphere and a 1.04 m diameter pipe.

The flammability of non-premixed jets is then examined. A brief introduction to various analytical techniques is provided and a new empirically-based model is applied to study jets of methane and CO_2, for which experimental data is also presented. Rather than focus on mean gas concentrations, which provides only an indirect indictor of flammability, the present work examines the flammability of gas jets using the concept of the "flammability factor". This provides a prediction of the ignition probability, i.e. the likelihood of the gas mixture being ignitable at any particular location and time.

Bulk ignition experiments are also reported, in which jets of methane mixed with varying quantities of CO_2 are released in air and ignited using a propane blow torch. Three different release velocities are examined and the resulting ignition behaviour is classified according to a set of five criteria.

Section 5 of this report examines the feasibility of using Computational Fluid Dynamics (CFD) to extend predictions of the flammability factor beyond simple jet flows. Previous work in this field is examined, and a simplified methodology is proposed which retains many of the benefits of more sophisticated approaches.

Conclusions and recommendations for further work are then provided. Details of the experimental measurements and the flammability factor model, together with further analysis of the CFD models, are given in Appendices.

2 IGNITION OF PREMIXED HYDROCARBON-CO_2 GAS CLOUDS

2.1 INTRODUCTION

This section describes a set of experiments that have been performed to measure the over-pressure generated by igniting mixtures of methane or propane with CO_2. The gases tested were "premixed" with air, i.e. the gas composition was approximately homogeneous, or constant through space. This is in contrast to the work described later, in Sections 3 and 4, where non-premixed gas jets are considered.

The premixed explosion tests were performed on two scales: the first being a standard 20 litre explosion sphere; the second being a larger 8 m long section of 1.04 m diameter pipe, which had a total volume of 6.8 m^3.

In the following description of the tests, the quoted experimental gas concentrations are, unless otherwise stated, in terms of a volume percentage (% vol/vol) 'feed' concentration of either the fuel (methane or propane) or CO_2 in the absence of air, as defined by Equations (2.1) and (2.2). This allows comparison between the premixed explosion tests and the source conditions in the non-premixed jet release experiments, described later.

$$C_{Fuel,Feed} = \frac{V_{Fuel}}{V_{Fuel} + V_{CO_2}} \tag{2.1}$$

$$C_{CO_2,Feed} = \frac{V_{CO_2}}{V_{Fuel} + V_{CO_2}} \tag{2.2}$$

When air has been added to the system prior to ignition, the concentrations of fuel, CO_2 or air in the combined fuel-CO_2-air system are expressed as 'final' concentrations, by volume, according to Equations (2.3) to (2.5).

$$C_{Fuel,Final} = \frac{V_{Fuel}}{V_{Fuel} + V_{CO_2} + V_{Air}} \tag{2.3}$$

$$C_{CO_2,Final} = \frac{V_{CO_2}}{V_{Fuel} + V_{CO_2} + V_{Air}} \tag{2.4}$$

$$C_{Air,Final} = \frac{V_{Air}}{V_{Fuel} + V_{CO_2} + V_{Air}} \tag{2.4}$$

2.2 PREVIOUS STUDIES

It is well known that the experimental mode of investigation can have a significant bearing on the observed flammability behaviour of hydrocarbon mixtures (De Smedt *et al.*, 1999, Beyler, 2002). Different flammability limits are observed when experiments are conducted with a spark ignition or pilot flame. Most studies reported in the literature use one of the standard test procedures (ASTM, 2005, 2009, BSI, 2004, ISO, 2010) and the prescribed apparatus to determine the upper and lower concentrations where the flame will propagate.

The effect of inert gases on the flammability limits of hydrocarbon gases in air has been examined previously by, amongst others, Coward and Jones (1952), Zabetakis (1965) and Molnarne *et al.* (2005). The study by Kondo *et al.* (2006) examined a number of hydrocarbons (methane, propane, ethylene, propylene, methyl ether, methyl formate, 1,1-difluoroethane, and ammonia) with different quantities of CO_2, and determined the flammability limits using an explosion bomb similar to that described by ASTM (2009). The change in their measured flammability limits for methane is shown in Figure 1. Increasing the CO_2 concentration decreased the extent of the flammability window and it was determined that ignition of the mixture would not be possible for CO_2 feed concentrations above 80% vol/vol in the source gas stream.

Unlike chorine and bromine containing compounds that chemically react with radicals to inhibit the combustion process, CO_2 acts as an effective inerting compound due to its high specific heat capacity. Essentially, as the CO_2 concentration is increased, more thermal energy is required to raise the temperature of the combusting mixture, and the reaction rate is therefore reduced (Drysdale, 1999).

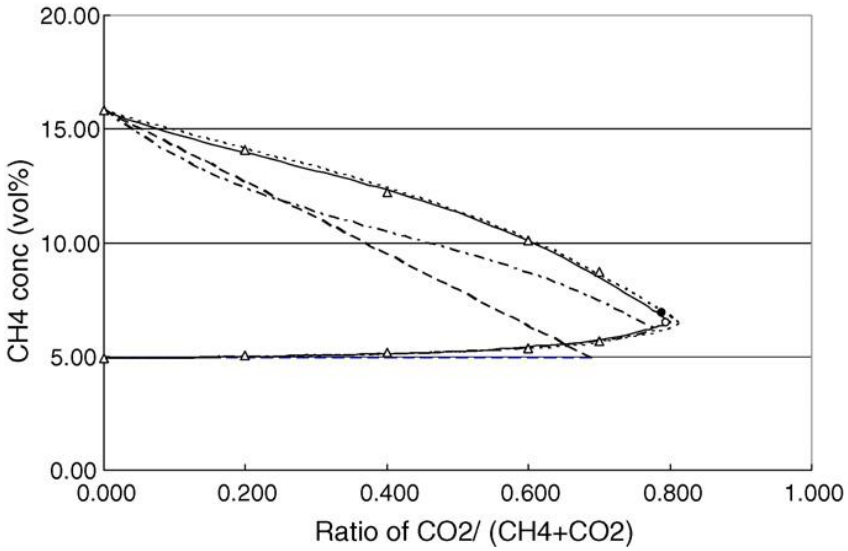

Figure 1 Flammability limits of methane and CO_2 mixtures, from Kondo *et al.* (2006). Symbols show measurements and lines indicate different model predictions. Reprinted with permission from Elsevier.

2.3 SMALL-SCALE EXPLOSION TESTS

2.3.1 Measurement Technique

The tests reported here were carried out in accordance with the principles of British Standard, BS EN 1839:2003 "Determination of explosion limits of gases and vapours" (BSI, 2004), using a 20 litre stainless steel sphere fitted with a manifold for the introduction of gas mixtures.

The vessel was first evacuated to an absolute pressure of approximately 100 mbar before the hydrocarbon, CO_2 and air gases were introduced to the vessel via the manifold. The quantities of each substance were measured by partial pressure readings using a high precision digital pressure gauge. For all of the tests, the fuel concentration was chosen to be close to the stoichiometric concentration. The final methane concentration in the vessel was 10% vol/vol, and the final propane concentration was 5% vol/vol. Five tests were performed for each gas

with final CO_2 concentrations varying from 0% to 20% vol/vol. This corresponds to CO_2 feed concentrations of 0% to 80% vol/vol. Individual component concentrations are given in Appendix A. The vessel temperature was maintained at 25ºC using heating fluid in the vessel jacket.

The gas mixture was ignited using a 10 kV spark generated across two stainless steel electrode tips. Control of the ignition system was via a computer linked to the spark generator unit, with an interlock on the fume cupboard sash to prevent accidental activation.

Explosion overpressures were monitored using two calibrated Kistler (type 701A) pressure transducers. The data was logged at 50,000 readings per second and saved to a computer hard drive automatically.

2.3.2 Results

Figures 2 and 3 present the results of the explosions tests performed in the 20 litre explosion sphere, for methane and propane respectively. For both gases it was found that increasing the CO_2 concentration caused a decrease in both the maximum overpressure (P_{max}), and the rate of change of pressure (dP/dt). For both gases, the rate of change of pressure was greatly reduced in all tests where CO_2 was present. The maximum ignitable CO_2 feed concentration was 60% vol/vol for methane, and 78% vol/vol for propane, although in the latter case a slight overpressure was still recorded for this condition. In terms of final concentrations of CO_2, these values are 15% vol/vol and 17.5% vol/vol, for the methane and propane tests, respectively. For the same conditions, Kondo *et al*. (2006) obtained maximum ignitable feed concentrations of 60.7% vol/vol and 81.6% vol/vol for methane and propane. The slightly higher values recorded by Kondo *et al*. (2006) may be due to their use of a smaller reaction vessel and a higher spark energy. Flammability measurements are known to be sensitive to both these parameters. Overall, the agreement with the current test results and those of Kondo et al. (2006) is considered to be good, and the results show that under well-defined controllable conditions, similar flammability ranges can be obtained.

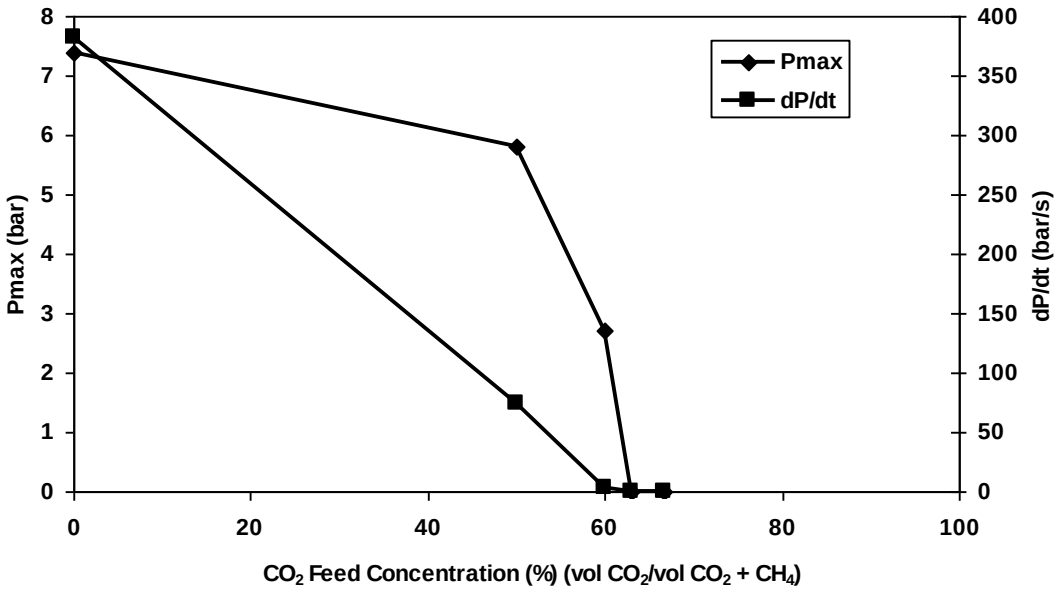

Figure 2 Measured maximum overpressure (P_{max}) and maximum rate of change of pressure (dP/dt) for methane and CO_2 mixtures in the 20 litre explosion sphere.

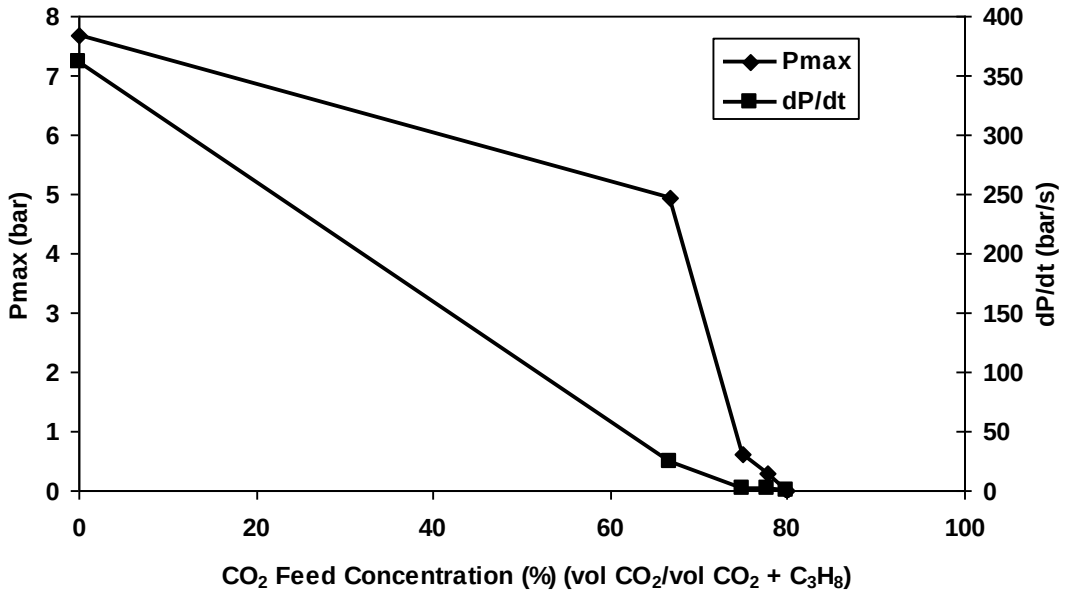

Figure 3 Measured maximum overpressure (P_{max}) and maximum rate of change of pressure (dP/dt) for propane and CO_2 mixtures in the 20 litre explosion sphere.

2.4 LARGE-SCALE EXPLOSION TESTS

2.4.1 Measurement Technique

The large-scale explosion facility was constructed from a number of 1.04 m internal diameter steel pipe sections. Methane and CO_2 was introduced into the vessel, mixed using an electrically driven fan, and ignited using a 5 grain blackpowder fuse. The general appearance of the pipes and target support frame is shown in Figures 4 to 6.

The three-quarters open area vent arrangement that can be used to tune to explosion pressure to the desired range is shown in Figure 6. As well as being able to alter the explosion pressure in the pipeline, the pressure received by the target can be tuned by moving the frame closer to, or further away from, the open mouth of the pipe (see Figure 5). For the tests described in this report, the gap between the open end of the pipe and the test sample was set to 74 cm.

Figure 4 General view of 1.04 m diameter explosion vessel

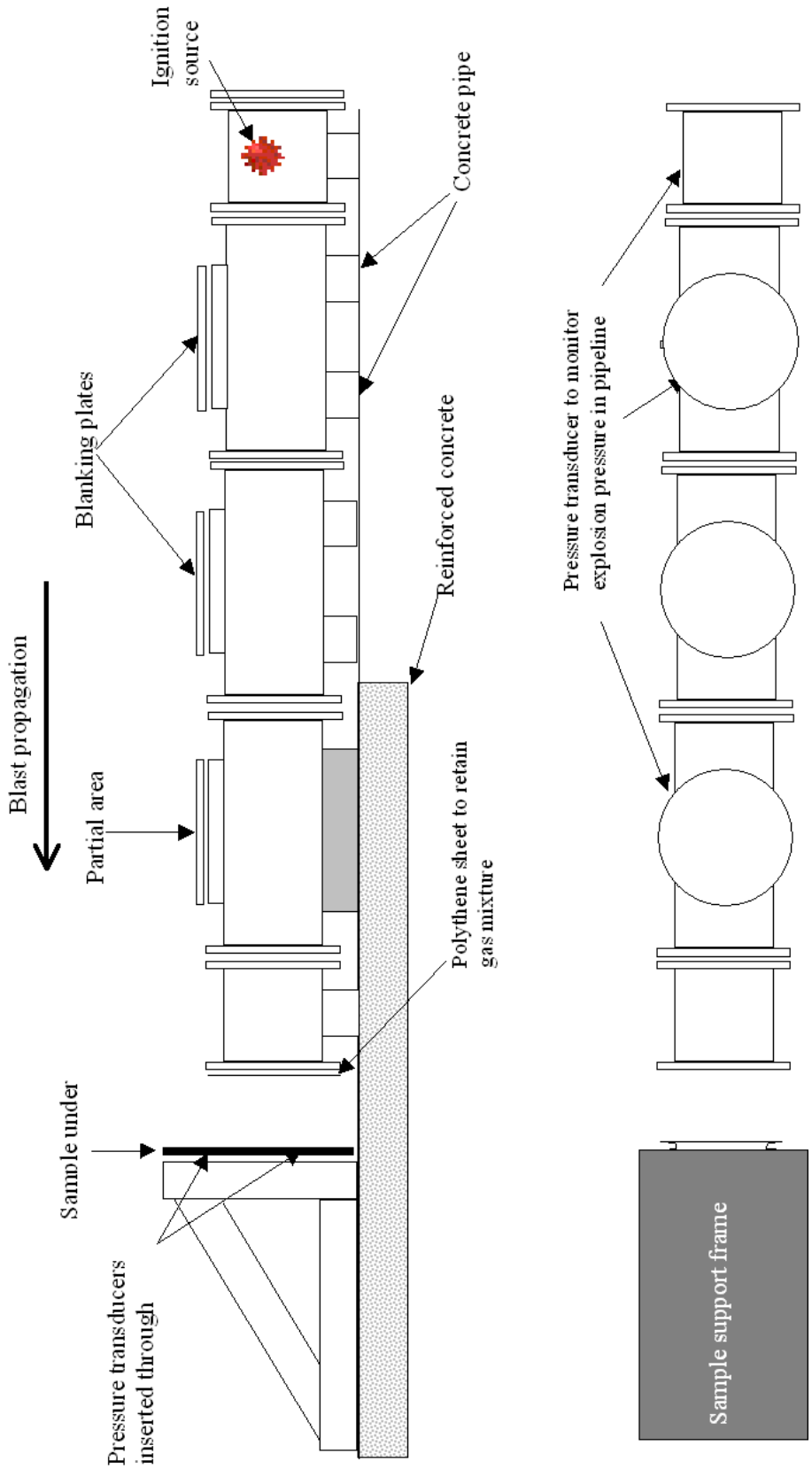

Figure 5 Schematic of large-scale explosion test rig

Figure 6 View of the ¾ open area top vent

2.4.2 Results

The effect of the CO_2 concentration on the overpressure in the large-scale gas explosion tests is presented in Figure 7. The results show similar trends to those observed in the 20 litre explosion sphere. Increasing the CO_2 concentration caused a decrease in the maximum overpressure. Ignition occurred for a feed concentration of 40% vol/vol CO_2, but no ignition was detected with a feed concentration of 59.4% vol/vol CO_2 (equivalent to a final CO_2 concentration in the CO_2-methane-air mixture of 12% vol/vol). In the latter case, the gas concentrations should have been within the flammable range.

These results are compared to those obtained in the 20 litre sphere in Figure 8, where the overpressures are normalised using the maximum pressures obtained from the experiments with pure methane, which were 7.40 bar and 0.72 bar in the in the 20 litre sphere and pipeline tests, respectively. Higher pressures were obtained in the explosion sphere as it was fully enclosed, whereas the pipeline was open at one end and had additional vents. In addition, the shape of geometry in the 20 litre sphere tests will have contributed to a pressure piling effect due to reflection of the pressure waves, giving rise to higher overpressures. Figure 8 shows that the effect of the CO_2 concentration on the maximum overpressure was more pronounced in the 1.04 m diameter pipe. Again, this may be due to the tubular geometry and the venting of the pipeline dissipating the pressure wave

The results from the 20 litre sphere and 1.04 m diameter pipe are compared to the flammability measurements obtained previously by Kondo *et al*. (2006) in Figure 9. All but one of the measurements agree with the findings of Kondo *et al*. (2006). The only exception is the 1.04 m diameter pipe test with CO_2 feed concentration of 59.4%, where no ignition was recorded, although the measurements of Kondo *et al*. (2006) suggest that the mixture should have been flammable. It is possible that for this test, there was incomplete mixing of the gases in the pipe. Whilst conditions could be controlled accurately in the 20 litre explosion sphere, in the larger pipe, mixing was induced by a fan positioned at one end of the pipe. It was therefore possible that an ignition failed even when the mean concentration in the pipe was within the flammable range. This behaviour is equally possible in practical applications, such as hydrocarbon storage vessels. Incomplete mixing should be considered in analysis of fire and explosion events involving inerted gas mixtures.

During one of the tests (Test 4) the gas mixture did not ignite when the first blackpowder fuse was fired. At this point in the test, the final gas concentrations were 7.7% vol/vol CO_2 and 10.4% vol/vol methane (with the remainder being air). Once the second fuse had been wired to the igniter the final gas concentrations had reduced slightly to 7.0% vol/vol CO_2 and 10.0% vol/vol methane and explosive ignition was achieved. It is unlikely that this small reduction in CO_2 concentration had a bearing on the ignition potential of the gas mixture and the initial ignition was most likely to have failed due to a faulty fuse.

The variation between the present results obtained from two quite different experimental setups highlights the potential uncertainty that can exist when identifying the correct inertization concentration for different geometries and scenarios where uncertain degrees of mixing and turbulence may be present. Incomplete mixing should be considered in the analysis of fire and explosion events involving inerted gas mixtures.

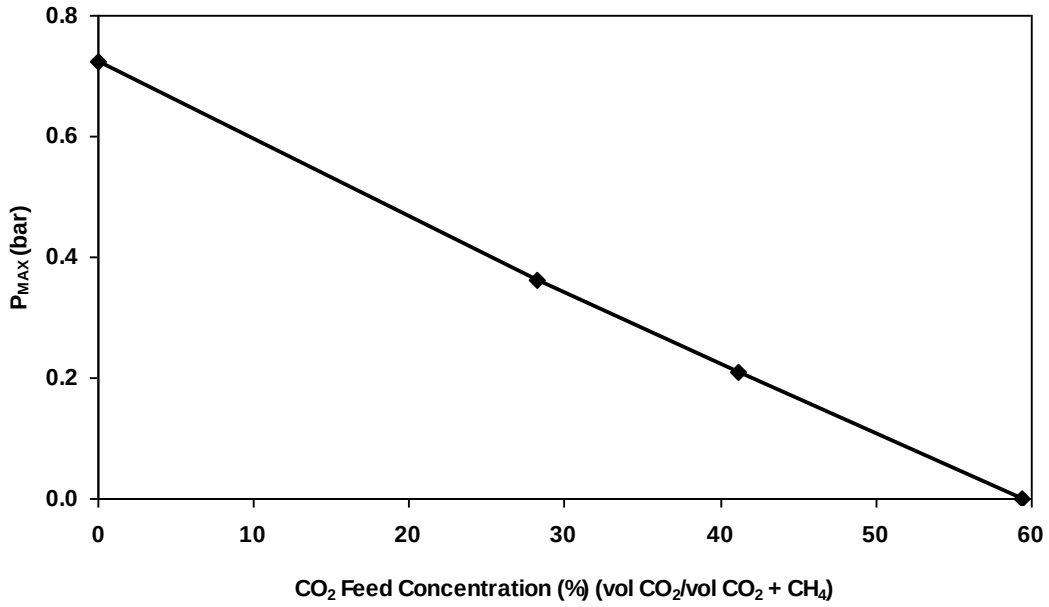

Figure 7 Measured maximum overpressures for methane and CO_2 mixtures in the 1.04 m diameter pipeline. Symbols indicate measurement points.

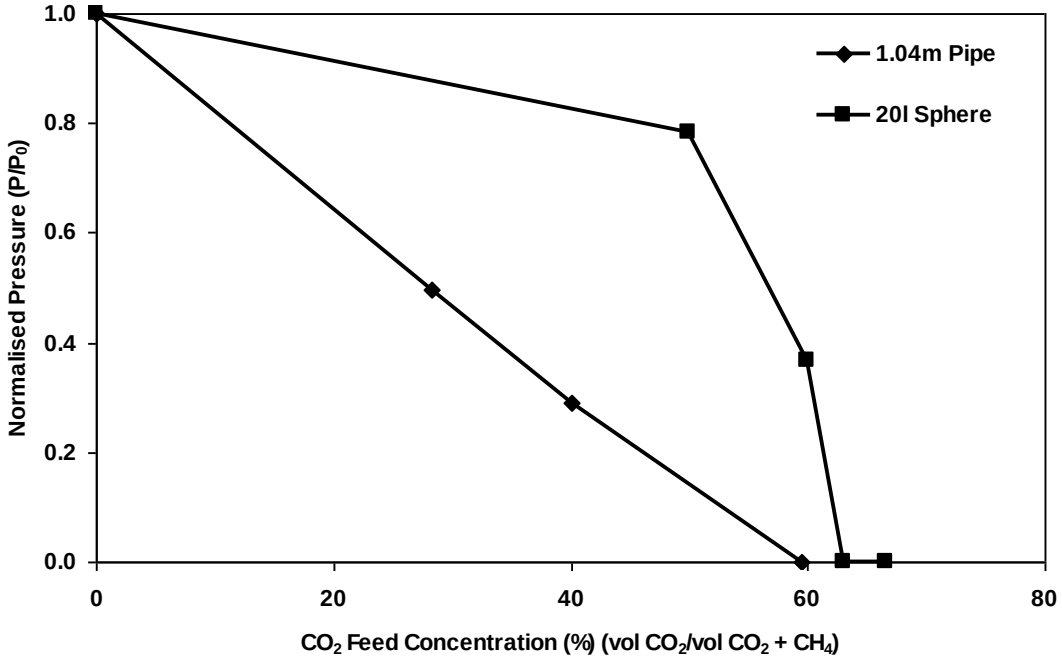

Figure 8 Maximum normalised overpressure for explosion tests conducted in the 20 litre explosion sphere and the 1.04 m diameter pipeline.

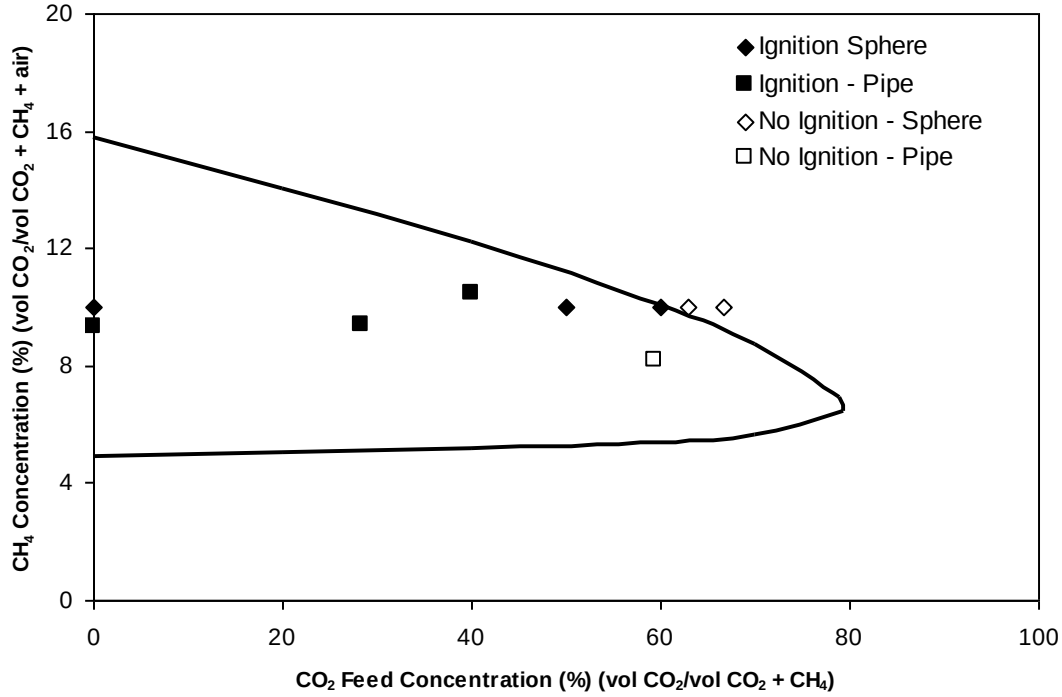

Figure 9 Flammability limits resulting from explosion tests (symbols) compared to the measurements of Kondo et al. (2006) (solid line); ♦ : 20 litre sphere tests; ■ : 1.04 m diameter pipeline; filled symbols indicate where ignition occurred..

3 IGNITION OF NON-PREMIXED FLOWS

3.1 INTRODUCTION

In non-premixed flows, the concentration of gases changes in space and, in most cases, over time. For example, an un-ignited Bunsen burner will have high concentrations of gas near the jet orifice and pure air in the far-field. The nature of the mixing processes in the jet will determine when and where in the flow the fuel and air will be in the correct proportions for the mixture to be flammable.

In the majority of applications of engineering interest, the fuel gas is stored or transported at pressure and therefore releases will tend to involve relatively high-speed gas jets. Due to the shear between the fast-moving gas and the slower background air flow, the jet will be turbulent. An understanding of turbulent mixing processes is therefore key to understanding the flammability of these flows.

The following sections examine the physics of turbulent jets and provide an introduction to the analytical techniques that can be used to quantify turbulent mixing processes. The concepts also apply to a wider range of turbulent flows than just jets. Any flow in which there is shear between the fuel and air streams would, in principle, be amenable to this analysis. This includes releases that impinge on surfaces or are affected by crosswinds, or releases in which buoyancy-effects become appreciable.

3.2 STRUCTURE OF TURBULENT JETS

A classical representation of a turbulent gas jet is shown in Figure 10. A virtual point origin for the jet is located a distance x_o upstream of the orifice, where the spreading jet converges to a point. As the jet evolves with distance downstream, the velocity on the centreline of the jet gradually decays and the jet continually increases in width. This increase in the width of the jet is caused by the entrainment of ambient air as a result of shear-generated turbulence.

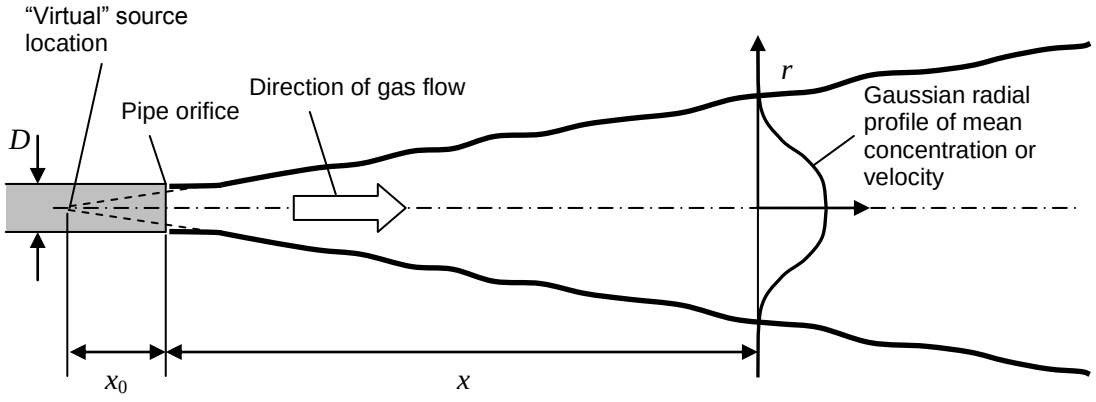

Figure 10 Schematic of a gas jet

Sufficiently far downstream from the point of release, the cross-stream profiles of mean velocity and mean concentration adopt a similar form, which is approximately Gaussian, i.e. the familiar bell-shaped curve shown in Figure 10. The profiles here are termed "self-similar"

in that the shape of the distributions remains the same at different axial positions, and by applying appropriate scaling factors the curves at these axial positions are coincident when plotted on the same graph axes (see Figure 11).

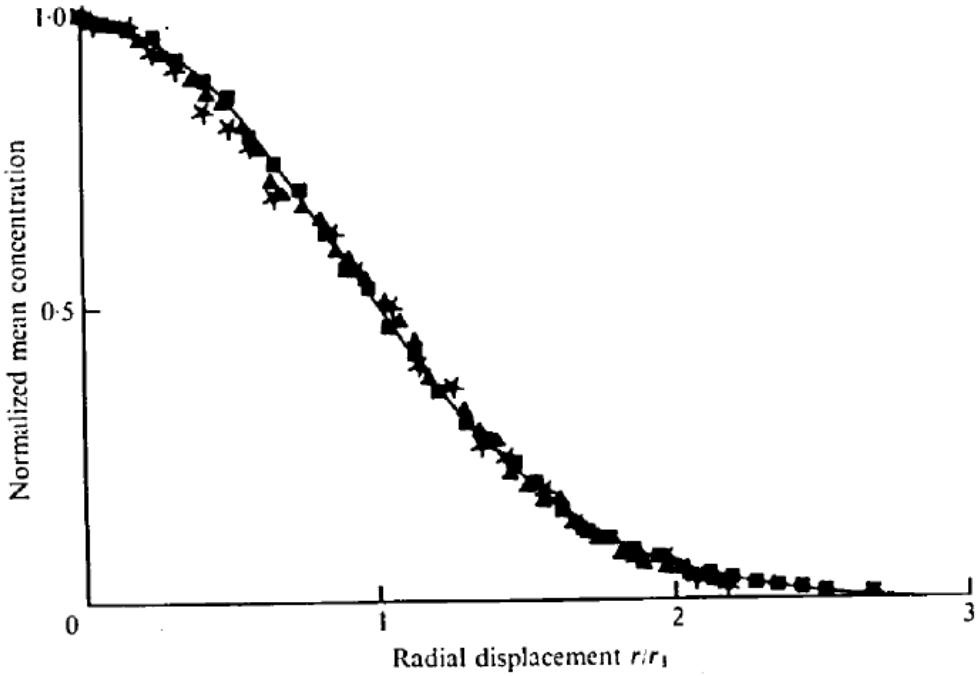

Figure 11 Radial profiles of normalised mean concentration at three axial positions in a turbulent gas jet: ■ x/D = 20; ▲ x/D = 30; ★ x/D = 40, where D is the orifice diameter. Reproduced with the permission of Cambridge University Press from Birch *et al.* (1978).

Empirical correlations describing how mean velocity and concentration vary in a turbulent jets are well-established. For the momentum-dominated region, both the mean centreline velocity and concentration decay with the inverse of axial distance from the source:

$$U_{cl} \propto \frac{1}{x'} \quad ; \quad C_{cl} \propto \frac{1}{x'} \tag{3.1}$$

where x' is the distance from the virtual origin:

$$x' = x + x_0 \tag{3.2}$$

In the radial direction, the empirical Gaussian mean velocity and mean concentration profiles are expressed as follows:

$$\frac{U}{U_{cl}} = \exp\left[-K_U\left(\frac{r}{x'}\right)^2\right] \tag{3.3}$$

$$\frac{C}{C_{cl}} = \exp\left[-K_C\left(\frac{r}{x'}\right)^2\right] \tag{3.4}$$

where K_U and K_C are empirically-derived constants.

This classical description of a turbulent jet gives the impression that velocity and concentration vary smoothly in gas jets, decaying gradually from maximum values on the jet

centreline to zero in the far field. Whilst this is true if one examines the *average* behaviour over a long period of time, the instantaneous structure of a turbulent jet exhibits large temporal and spatial variations, as shown in Figure 12. These fluctuations are of crucial significance when analysing the likelihood of the gas being within its flammable range.

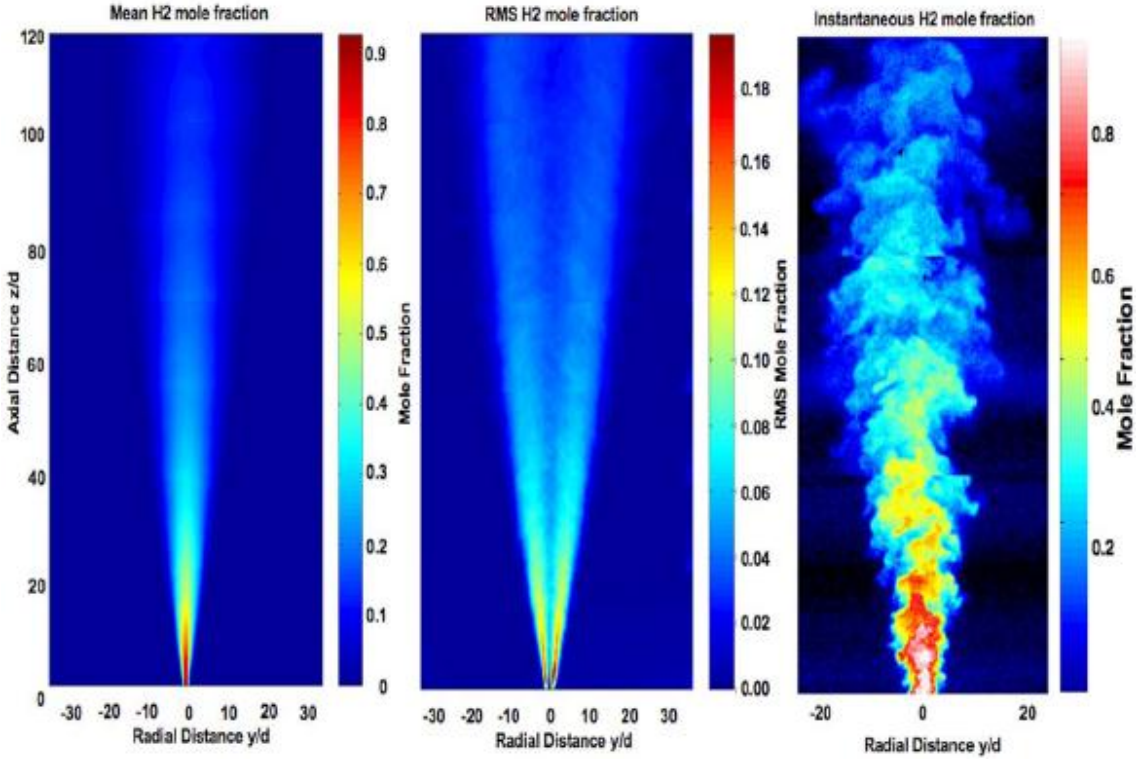

Figure 12 Measured mean concentration, RMS concentration and instantaneous concentration for a hydrogen jet in air. Reproduced with the permission of Dr. Jay Keller, Sandia National Laboratories.

The central image in Figure 12 shows Root Mean Square values (RMS) concentrations, which are obtained by taking a long time-average of fluctuations in concentration about the mean value. The highest RMS values do not occur on the axis of the jet, but in the regions of highest mean shear on the jet periphery. The image on the right in Figure 12 shows clearly that the instantaneous concentration in a turbulent jet is highly complex and that turbulent eddies have a wide variation of length-scales. The largest eddies have dimensions of the same order of magnitude as the width of the jet, whilst the smallest eddies are probably too small to be visible. This large range of eddy length-scales is typical of turbulent flow at high Reynolds number.

Many hydrocarbon fuel gases of interest in engineering applications have a density different to that of air. For example, natural gas (mainly methane) is around 40% less dense and hydrogen is 14 times less dense than air at the same temperature and pressure. Far downstream from the point of release, the buoyancy of the gas will eventually become more influential in driving the flow than its momentum. A jet in which the density of the material released is different to the ambient evolves through several stages as its initial momentum diminishes: from momentum-dominated to a forced plume, and then to a buoyant plume. In each of these stages, the rate at which the velocity and concentration decays with distance from the source is different.

The key parameter which governs the transition from momentum-dominated to buoyancy-dominated flow is the Froude number, *Fr*. Following the convention adopted by Chen &

Rodi, (1980), the densimetric Froude number, which expresses the ratio of inertial to buoyancy forces, is given by:

$$Fr = \frac{U_0^2}{gD(\rho_a - \rho_0)/\rho_0} \qquad (3.5)$$

where U_0 is the velocity at the jet orifice, g is the acceleration due to gravity, D is the orifice diameter, ρ the density and subscripts "a" and "0" refer to ambient and jet orifice values respectively. In the empirical relations used later in this report, the absolute value of the Froude number is used.

3.3 FLUCTUATIONS

The velocity and concentration field in a turbulent jet is in a constant state of change. Large fluctuations occur both in time and space. This behaviour is illustrated well in Figure 13, which shows a snapshot of the concentration field in the far-field of a turbulent jet. Ambient fluid is entrained from the surroundings by turbulent eddies and almost penetrates to the jet axis. Also, pockets of relatively high concentration can be seen far-removed from the centreline of the jet.

A sensor (or point source of ignition) located close to the boundary of the jet is exposed to large variations in concentration over time, including periods when the concentration is zero. This is illustrated in Figure 14, which shows velocity, rather than concentration, although the concepts are essentially the same. The uppermost diagram in Figure 14 is a simple illustration of the irregular boundary of a jet and the middle diagram shows the instantaneous value of axial velocity at a point close to this boundary. For much of the time, the velocity is fluctuating wildly as turbulent eddies pass over the sensor. However, for a period of time the fluctuations cease, when the sensor is outside the jet in the ambient non-turbulent fluid. Formally, it can be said that the sensor is located in an intermittent region of turbulent flow. If periods in which the sensor is fully located in the turbulent fluid are denoted as having a value of one, and periods in which it is located in the non-turbulent fluid as having a value of zero, then the lowermost graph in Figure 14 is constructed. Averaged over time, this measure represents the fraction of time that the sensor is in the turbulent flow, and this is defined as the turbulence intermittency, I. In practice, turbulence intermittency is measured by setting a very small threshold for concentration. Any concentration measurements larger than the threshold are given an intermittency indicator value of one, whilst those below are given a value of zero.

Intermittency is an important phenomenon in non-premixed combustion. For further details, see Bilger (1980) or Cant and Mastorakos (2008).

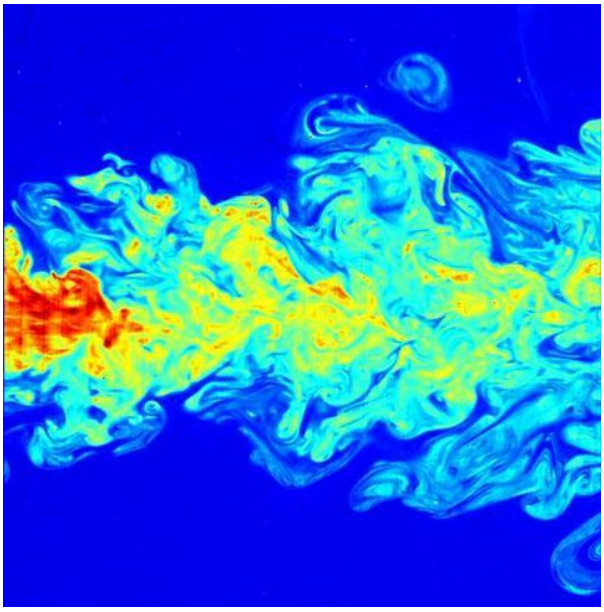

Figure 13 Instantaenous concentration in the far-field of a submerged jet, made visible by means of laser induced fluoresence. Image courtesy of C. Fukushima and J. Westerweel, Delft University of Technology (the Netherlands).

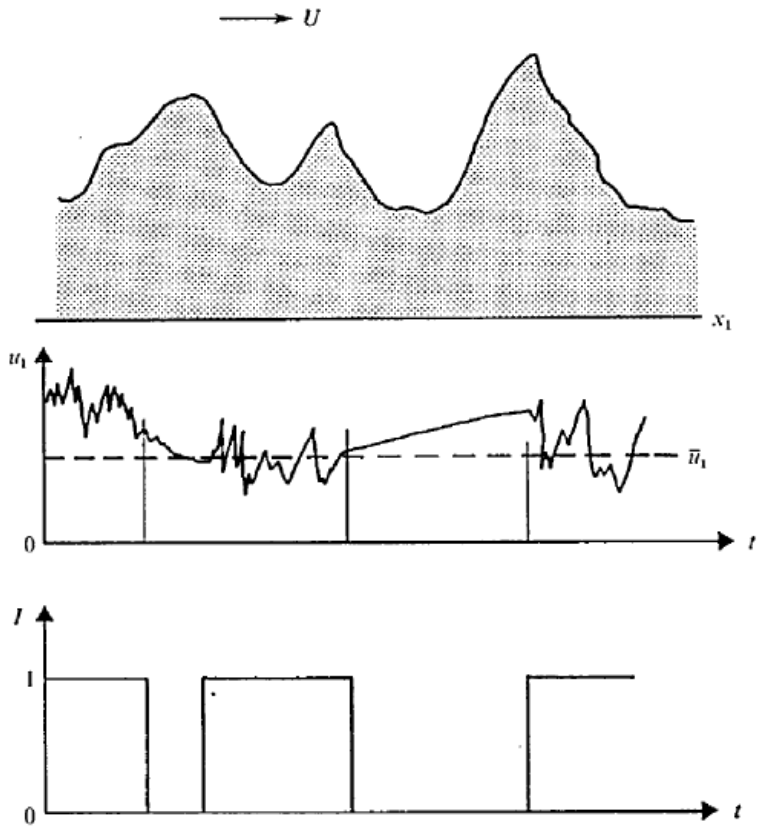

Figure 14 Intermittency at the boundary of a turbulent flow. Reproduced with the permission of Cambridge University Press from Libby (1975).

3.4 TIME AVERAGING

We now introduce formal definitions and time-averaging procedures for dealing with fluctuating turbulent fields. Throughout this analysis, mean values refer to time-averages where the averaging period is long in relation to the time-scales of the turbulent fluctuations.

The time-varying instantaneous concentration at any point in space, $\tilde{c}$, is decomposed into two parts: a mean concentration, *C*, and a time-varying fluctuation, *c*, where:

$$\tilde{c} = C + c \qquad (3.6)$$

The mean concentration remains constant over time, although clearly it varies through space. In the turbulent region of the flow, the time-average of the concentration fluctuation is zero $\left(\overline{c} = 0\right)$, but the time-average of the square of the fluctuation is non-zero $\left(\overline{c^2} \neq 0\right)$. The quantity, $\overline{c^2}$, is referred to as the "variance" of the concentration.

The RMS of the concentration fluctuation is denoted as follows:

$$c' = \sqrt{\overline{c^2}} \qquad (3.7)$$

Similarly, the mean, fluctuating and RMS values of velocity are denoted as *U*, *u* and *u*', respectively.

3.5 PROBABILITY DENSITY FUNCTIONS

The fraction of time any particular fuel-air concentration exists at a point in a flow is expressed by a Probability Density Function (PDF). This function, *P*(*f*) describes the likelihood of the concentration taking a particular value. PDFs for a turbulent natural gas jet measured by Birch *et al.* (1978) are shown in Figure 15. Near the centreline, the shape of the PDF is nearly Gaussian, whilst on the periphery of the jet the PDF develops into a delta function, as more of the time is spent with a concentration close to zero.

If the concentration is measured in terms of mass or molar fractions, the maximum possible value is one and the minimum value is zero, anywhere in the flow. These values are the upper and lower bounds of the sample space. If the PDF is then integrated between these bounds, it must sum to unity, since there is 100% probability that the concentration will lie between zero and one. This is expressed as follows:

$$\int_0^1 P(\tilde{c})\,d\tilde{c} = 1 \qquad (3.8)$$

The probability that the concentration lies between the upper and lower flammability limits of c_U and c_L is given by:

$$\int_{c_L}^{c_U} P(\tilde{c})\,d\tilde{c} \qquad (3.9)$$

This expression will be used later to help define the proportion of time that the gas is flammable.

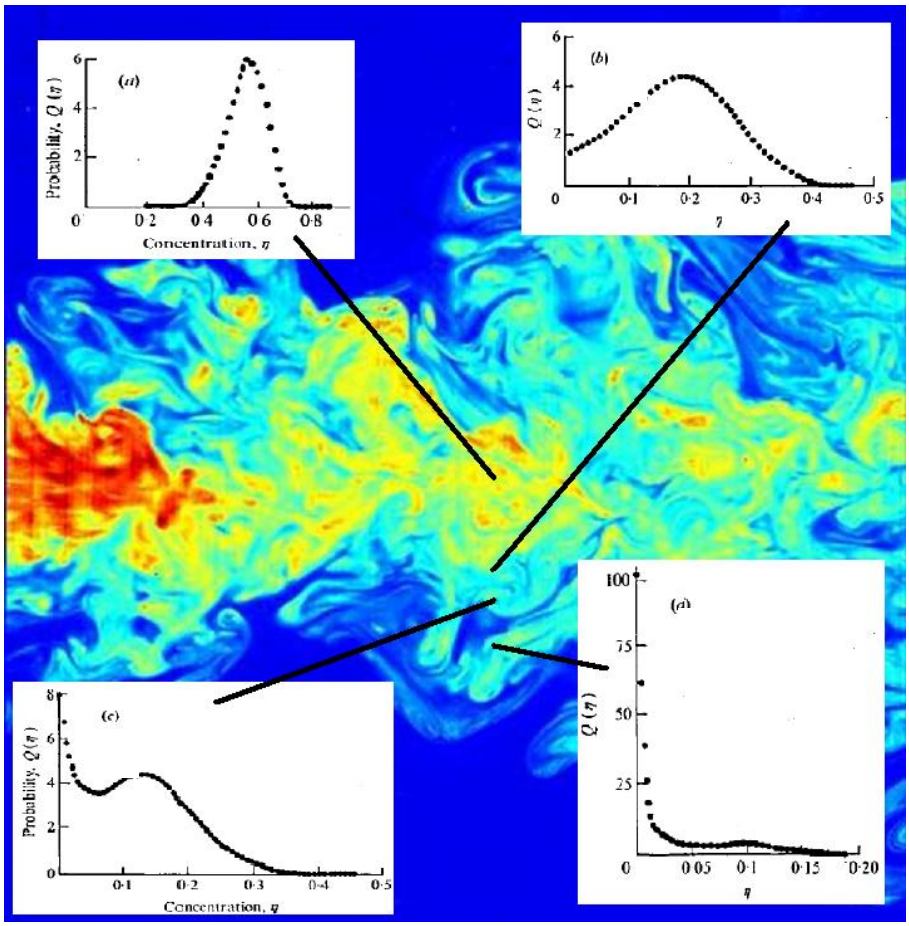

Figure 15 PDFs of concentration measured by Birch *et al*. (1978), superimposed on an image of the instantaneous concentration field in a turbulent jet. Reproduced with the permission of C. Fukushima and J. Westerweel, Delft University of Technology (the Netherlands) and Cambridge University Press.

The mean concentration at a particular point in the flow is obtained by integrating the product of the PDF and the concentration over the sample space, as follows:

$$C = \int_0^1 \tilde{c} P(\tilde{c}) d\tilde{c} \qquad (3.10)$$

The most commonly-encountered PDF is the Gaussian distribution. Often, the 'tails' of a Gaussian PDF may be unnecessary in representing a turbulent flow, in which case a 'clipped', or truncated, Gaussian may be used.

The delta PDF, $\delta(f)$, is a useful function, as this is zero everywhere except at the boundary of the sample space, where it has an infinitely sharp peak. Outside of a gas jet the concentration is usually zero, so the delta function provides a way of expressing this probability as being 100%. Often a delta function will be used in combination with another PDF to model such a sharp spike.

A particularly useful PDF in the context of turbulent flows and the modelling of ignition and combustion is the beta function, $P_\beta(f)$. The shape of this PDF can be altered, with the exact shape being governed by the value of two parameters – which themselves depend only on the

mean and the variance of a scalar. If the mean and variance of a relevant scalar can be computed, then the beta function is fully defined. Details of the beta function are given in mathematical texts and CFD modelling literature, such as Versteeg & Malalasekera (2007).

Usually, the best and most flexible representations of measured PDFs in turbulent flow are found by combining several PDFs. For example, the empirical model described later in Section 4.2 combines Gaussian and delta functions. One means of blending the two PDFs is by weighting the functions by the intermittency. For instance, in the following function the PDF blends from a delta function when the intermittency is zero to the beta-PDF when the intermittency has a value of one:

$$P(f) = (1-I)\delta(f) + IP_{\beta}(f) \qquad (3.11)$$

3.6 IGNITION PROBABILITY AND FLAMMABILITY FACTOR

Although the time-averaged mean concentration at a particular point in a turbulent flow may be below the LFL, the presence of turbulent fluctuations can lead at times to the instantaneous concentration rising above the LFL. If there is a point source of ignition present at this location then the gas mixture may ignite – even though the mean concentration would suggest that this is not possible.

At the boundary of a turbulent jet it is possible for ignition to be possible even where the mean concentration is as low as 10% of the LFL.

In summary, mean concentrations are a poor predictor of ignitability in turbulent flows.

To be able to predict the probability of ignition it is necessary to know the fraction of time that a source of ignition may encounter gas concentrations that are between the LFL and UFL. This fraction of time that gas mixture is flammable is very closely related to the PDF of concentration at the ignition location.

We now introduce the concept of flammability factor, *F*. Formally, *F* is the cumulative probability of a potentially flammable mixture occurring at a given point (Birch *et al.*, 1981):

$$F = \int_{c_L}^{c_U} P(\tilde{c})d\tilde{c} \qquad (3.12)$$

This is equivalent to the area under the curve of the PDF for concentration, between the upper and lower flammability limits, as shown in Figure 16. The PDFs are shown at four different radial positions (marked A to D) for a natural gas jet at a position 10 orifice diameters downstream from the jet orifice. The LFL and UFL in this case are 0.05 vol/vol and 0.15 vol/vol, respectively.

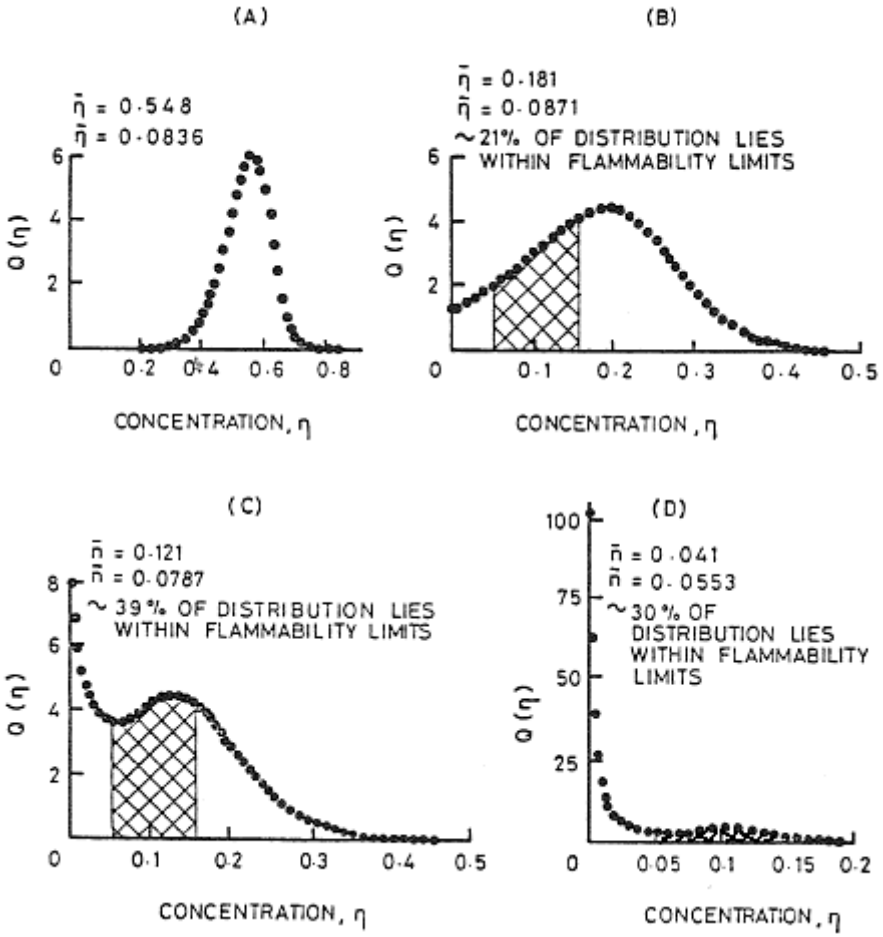

Figure 16 PDFs of concentration measured at four radial locations in a natural gas jet. Shaded areas indicate those parts of the distribution within flammability limits Reproduced with the permission of The Combustion Institute from Birch *et al*. (1981).

The validity of the flammability factor concept is demonstrated by Figure 17, which compares measurements of ignition probability against the calculated flammability factor on the axis of the gas jet examined by Birch *et al.* (1981). In the experiments, the ignition probability was found by recording the proportion of successful attempts to obtain ignition. A spark igniter was used with a spark gap of 3 mm, i.e. approximating a point source of ignition. To ensure that statistical errors were small, 400 ignition attempts were made at each measurement location. To calculate the flammability factor, the PDF of concentration was assumed to be Gaussian on the axis of the jet. There is clearly excellent agreement between the measured ignition probability and the calculated flammability factor.

Flammability factors have also been computed and compared to measurements of ignition probability for propane jets by Smith *et al.* (1986) and recently for hydrogen jets by Schefer *et al.* (2010). In both cases there was good agreement between the predicted flammability factor and the measured ignition probability. Saima and Higaki (1988) also measured ignition probabilities for propane and carbon dioxide gas mixtures, although there are concerns that insufficient ignition attempts were used to generate reliable statistics (Alvani, 2004).

In the propane jet measurements made by Smith *et al*. (1986), shown in Figure 18, it is particularly interesting to note that where the mean gas concentration is equal to the lower flammability limit (indicated by η_L) there is still a 50% probability of ignition.

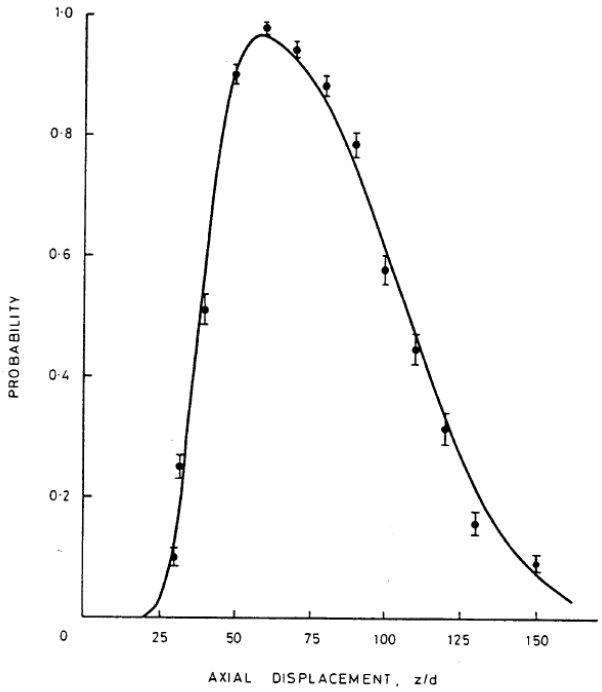

Figure 17 Measured ignition probability (point data) and calculated flammability factor (line) on the centreline of a turbulent natural gas jet. Reproduced with the permission of The Combustion Institute from Birch *et al.* (1981).

The ignition probability can depend on factors other than the instantaneous concentration. The temperature of the ignition source is one such factor, with ignition probability decreasing as the temperature of the ignition source decreases. However, the ignition probability becomes independent of source temperature if the ignition source is above 1400 K, and this condition will apply for electrical sparks of sufficient energy (Birch *et al.*, 1979).

When measuring ignition probability, the duration of an ignition source such as a spark, should not be longer than a turbulent eddy time-scale, as otherwise a point source of ignition will be 'sampling' from a wide range of concentrations. In the work of Birch *et al.* (1981), a spark duration of approximately 20 ms was used. There is evidence from Birch *et al.* (1978) that this somewhat exceeded the measured eddy time-scales for locations on the axis of a jet close to the source of release. However, further downstream, at a distance of more than 50 orifice diameters, this 20 ms spark duration should have been sufficiently short. Nevertheless, the flammability factor concept is largely validated by measurements of ignition probability. Methods for computing the eddy time-scales in CFD simulations are presented by, for example, Gant (2009).

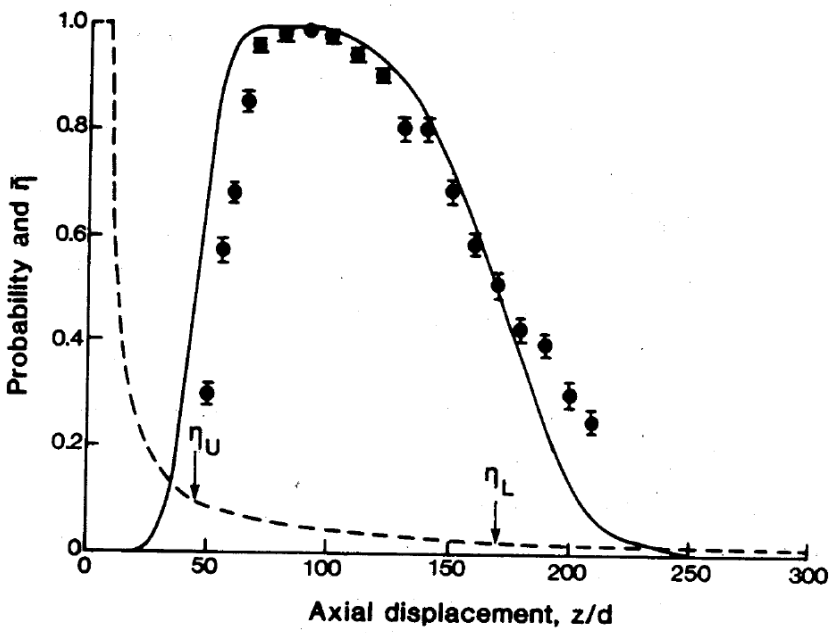

Figure 18 Measured ignition probability (point data) and computed flammability factor (solid line) on the axis of a turbulent propane gas jet. The dashed line is time-averaged mean concentration. Reproduced with the permission of The Combustion Institute from Smith *et al*. (1986).

3.7 LOCALISED IGNITION AND FLAME LIGHT-UP

Following ignition, a flame kernel may be convected downstream in the jet and eventually be extinguished, or alternatively it may grow both downstream and upstream to light-up the whole jet. The extent of the region where light-up occurs is smaller than the region where a localised ignition is possible. Localised ignition only requires instantaneous gas concentrations to be within the flammability limits and for there to be present an ignition source of sufficient energy. However, light-up of the whole release depends on other factors, such as the existence of a pathway for the flame to propagate from one flammable region to another, and for the local flame speed to exceed the local flow speed.

Measurements of ignition and light-up probability are compared in Figures 19 and 20. On the axis of a turbulent jet, the probability of light-up decreases much more quickly than that of localised ignition. Figure 20 shows that for the natural gas jet of Birch *et al*. (1981) the maximum downstream location at which light-up was possible occurred before the LFL was reached. This was also found to be the case for the propane jets studied by Smith *et al*. (1986). These studies also showed that on the centreline of the jet beyond the point where the mean gas concentration fell below 50% of the LFL, the ignition probability dropped essentially to zero. However, as previously noted, the measurements also showed that ignition was possible away from the centreline of the jet at mean gas concentrations down to as low as 10% of the LFL.

The flammability factor predicts the probability of only a flame kernel being produced. Subsequently, this kernel may or may not lead to light-up of the jet. Model predictions of the flammability factor should be compared to measured probabilities of the production of a flame kernel, rather than jet light-up.

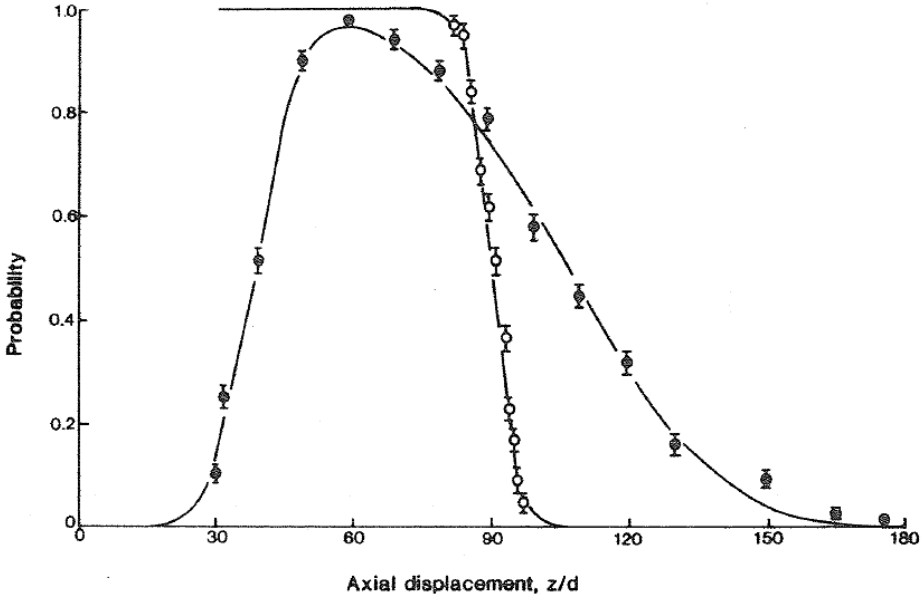

Figure 19 Measured ignition probability (closed point data) and light-up probability (open point data), on the axis of a natural gas jet. Reproduced with the permission of The Combustion Institute from Smith *et al*. (1986).

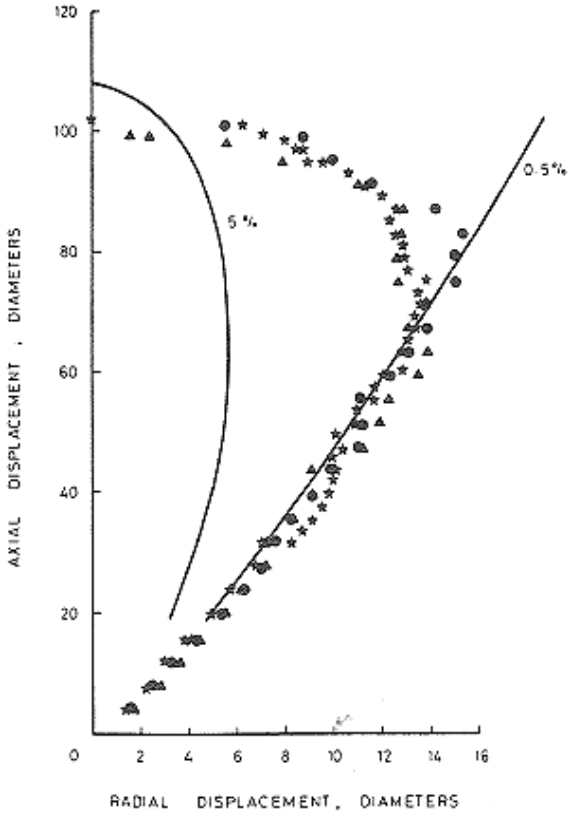

Figure 20 Measured boundary for complete light-up of the jet (point data), for natural gas jets with Reynolds numbers: ● *Re* = 20,900; ★ *Re* = 16,700; ▲ *Re* = 12,500. Solid lines are time-averaged mean concentrations at the LFL and 10% of the LFL. Reproduced with the permission of The Combustion Institute from Birch *et al*. (1981).

The concept of the flammability factor is therefore consistent with the philosophy used commonly in risk assessments, where a source of ignition in the presence of a flammable mixture is assumed to pose a hazard, and it is not required to demonstrate the presence of a flammable pathway back to the source.

It is very difficult to predict jet light-up, rather than localised ignition. To do so requires prediction of the time-varying 'connectedness' of flammable regions in a turbulent flow, such that flame propagation can occur. This is possible in principle, using CFD methods based on Large-Eddy Simulation (LES), as shown by Triantafyllidis *et al.* (2009), but it requires large computing resources.

The two major studies by Birch *et al.* (1981) and Smith *et al.* (1986) examined relatively low-speed turbulent jets, with release velocities typically between 20 m/s and 30 m/s, in quiescent air that was undisturbed by crosswinds. Subsequent experiments were performed by Birch *et al.* (1988) on high-pressure releases where the flow was sonic at the source. These indicated that the flammability factor should also be a valid indicator of ignition probability for high-speed releases once the jet has decelerated to sub-sonic flow. Birch *et al.* (1989) also later investigated the ignition behaviour of jets in a cross-flow.

The addition of CO_2, nitrogen or other inert gases to a fuel does not affect the validity of the flammability factor concept for predicting ignition probability. The same physics applies and all that is required is to modify the LFL and UFL for the particular gas mixture.

4 IGNITION PROBABILITY OF GAS JETS

4.1 INTRODUCTION

The analytical concepts introduced in Section 3 are applied here to study the flammability of gas jets comprising mixtures of hydrocarbon and CO_2 gases. An empirically-based model is first presented to calculate the flammability factor in a free jet. A series of experiments undertaken to assess the flammability of hydrocarbon and CO_2 jets are then described. Predictions made using the new flammability factor model are then compared to measurements of the ignition probability.

4.2 EMPIRICAL FLAMMABILITY FACTOR MODEL

To calculate the flammability factor it is necessary to determine the proportion of time that the gas concentration spends between the LFL and UFL. The present model determines this proportion of time using a PDF, the shape of which varies across the flow according to the mean and RMS gas concentration, and the intermittency. These parameters are all determined using empirical profiles obtained from experiments involving sub-sonic free-jets. The following list provides a summary of the sources of empirical data:

- The mean velocity and mean concentration along the centreline of the jet are determined from empirical profiles from Chen & Rodi (1980), with some minor changes (described below).
- In the radial direction, Gaussian profiles are assumed for the mean velocity and mean concentration, using spreading rates given by Chen & Rodi (1980) and Birch *et al*. (1978).
- The RMS concentration fluctuation is determined using the α-β model of Chatwin & Sullivan (1990).
- The turbulent intermittency in the jet is determined using the empirical model of Kent & Bilger (1976).
- A two-part PDF is used for the concentration fluctuations, comprising the sum of a delta function and a truncated Gaussian, using conditionally sampled mean and RMS values, based on the model of Birch *et al*. (1981).
- The two-part PDF is integrated using error functions between upper and lower flammability limits which are calculated for hydrocarbon-CO_2 mixtures using a modified Le Chatelier's law developed by Kondo *et al*. (2006).

The model based on these empirical correlations has many similarities to that presented by Birch *et al*. (1981), except that they did not describe the profiles used for intermittency and mean and RMS concentration[1]. The mathematical formulae and model constants are described briefly below. The model is relatively simple to implement in a programming language such as MatLab[2] or Octave[3]. A related model that is applicable only along the jet centreline can be coded in Microsoft Excel. Further details of these models, their implementation and their sensitivity to the choice of constants are provided in Appendix B.

The mean velocity and concentration profiles along the centreline of the jet, taken from Chen & Rodi (1980), consist of two equations which are valid in separate regions of the flow: the momentum-dominated region near the jet orifice and an intermediate region further

[1] *These were probably taken from unpublished experimental measurements (M. Fairweather, Private Communication, 2010)*
[2] *http://www.mathworks.com, accessed July 2010.*
[3] *http://www.gnu.org/software/octave/, accessed July 2010.*

downstream where inertial forces are weaker and buoyancy forces start to become important. The boundary between these two regions is defined using a dimensionless axial distance, x^*, given by:

$$x^* = Fr^{-1/2}\left(\frac{\rho_0}{\rho_a}\right)^{-1/4}\left(\frac{x'}{D}\right) \qquad (4.1)$$

where x' is the axial distance from the virtual origin of the jet (see Section 3)

In the momentum-dominated region near the jet, where $x^* < 0.5$, the mean centreline velocity, U_{cl}, and centreline concentration, C_{cl}, are given by:

$$U_{cl} = 6.2U_0\left(\frac{\rho_0}{\rho_a}\right)^{1/2}\left(\frac{x'}{D}\right)^{-1} \qquad (4.2)$$

$$C_{cl} = 5C_0\left(\frac{\rho_0}{\rho_a}\right)^{-1/2}\left(\frac{x'}{D}\right)^{-1} \qquad (4.3)$$

whilst in the intermediate region, where x^* is between 0.5 and 5.0, they are given by:

$$U_{cl} = a_U U_0 Fr^{-1/10}\left(\frac{\rho_0}{\rho_a}\right)^{9/20}\left(\frac{x'}{D}\right)^{-4/5} \qquad (4.4)$$

$$C_{cl} = a_C C_0 Fr^{1/8}\left(\frac{\rho_0}{\rho_a}\right)^{-7/16}\left(\frac{x'}{D}\right)^{-5/4} \qquad (4.5)$$

Beyond the intermediate region, where x^* is greater than 5.0, buoyancy forces become dominant and the flow exhibits plume-like behaviour. However, since the fluctuating gas concentrations in this region of the flow are below the LFL, it is only necessary here to consider the momentum-dominated and intermediate regions.

Values of 7.1 and 4.2 are taken for the constants a_U and a_C in Equations (4.4) and (4.5), respectively. These differ slightly from the values given by Chen & Rodi (1980) and Smith *et al*. (1986) who used, respectively, a_U = 7.26 and a_C = 0.44, and a_C = 4.4. The values have been chosen in the present study to produce smooth transitions in the velocity and concentration between the momentum-dominated and intermediate regions, see Appendix B for further details.

In the radial direction, the mean velocity and mean concentration are approximated using Gaussian profiles:

$$\frac{U}{U_{cl}} = \exp\left[-K_U\left(\frac{r}{x'}\right)^2\right] \qquad (4.6)$$

$$\frac{C}{C_{cl}} = \exp\left[-K_C\left(\frac{r}{x'}\right)^2\right] \qquad (4.7)$$

where constants K_U and K_C are given values 94 and 73.6, based on values given by Chen & Rodi (1980) and Birch *et al*. (1978), respectively.

The RMS concentration is determined using the α-β model of Chatwin & Sullivan (1990):

$$\overline{c^2} = \beta C\left(\alpha C_{cl} - C\right) \qquad (4.8)$$

where constants α and β are given values of 1.27 and 0.14, respectively, based on Chatwin & Sullivan's (1990) analysis of the methane jet experiments of Birch *et al*. (1978).

The turbulent intermittency, I, is calculated using the empirical formula of Kent & Bilger (1976):

$$I = \frac{K+1}{\left[\left(\frac{\overline{c^2}}{\overline{C^2}}\right)+1\right]} \qquad (4.9)$$

where K is a constant given a value of 0.25 by Kent & Bilger (1976).

On the axis of a free-jet, the concentration PDF is well approximated using a Gaussian distribution (Birch *et al.*, 1981). However, away from the jet axis, the PDF changes shape and in the far field, where the concentration is zero, the distribution tends to a delta-function. To account for the change in shape of the distribution with radius, the present model adopts the two-part PDF proposed by Birch *et al*. (1981) which smoothly varies between a truncated Gaussian distribution and a delta-function, based on the intermittency:

$$P\left(\tilde{c}\right) = \underbrace{\left(1-I\right)\delta\left(\tilde{c}\right)}_{} + \frac{IA}{\sqrt{2\pi\overline{c_c^2}}}\exp\left[-\frac{\left(\tilde{c}-C_c\right)^2}{2\overline{c_c^2}}\right] \qquad (4.10)$$

where the subscript "*c*" denotes conditionally sampled values, which are calculated as follows:

$$C_c = \frac{C}{I} \qquad (4.11)$$

$$\overline{c_c^2} = \frac{\overline{c^2}}{I} - \frac{C^2\left(1-I\right)}{I^2} \qquad (4.12)$$

and scaling factor, A, is given by:

$$A = \frac{2}{ERF\left(\frac{1-C_c}{\sqrt{2\overline{c_c^2}}}\right) - ERF\left(\frac{-C_c}{\sqrt{2\overline{c_c^2}}}\right)} \qquad (4.13)$$

where *ERF*() denotes the error function.

As noted in Section 3.3, due to the turbulent eddy motion in a free jet, at a given position towards the edge of the jet there will be times when the flow is turbulent and other times when it is quiescent. The 'conditional' values of concentration determined by Equations (4.11) and (4.12) relate to those concentrations within the fully turbulent jet, i.e. concentrations that exclude the influence of any intermittent intervals when the flow is quiescent or at the ambient condition (when the concentration is zero).

To calculate the flammability factor requires the integration of Equation (4.10) between the upper and lower flammability limits. Since the delta function only has finite amplitude at concentrations approaching zero (i.e. below the lower flammability limit of the gas) the underbraced part of Equation (4.10) can effectively be ignored. The remaining part is integrated using error functions as follows:

$$F = \frac{IA}{2}\left[ERF\left(\frac{c_U - C_c}{\sqrt{2\overline{c_c^2}}} \right) - ERF\left(\frac{c_L - C_c}{\sqrt{2\overline{c_c^2}}} \right) \right] \qquad (4.14)$$

To account for the presence of carbon dioxide in the gas mixtures, the upper and lower flammability limits (c_U and c_L) are determined here using a modified version of Le Chatelier's law developed by Kondo *et al*. (2006), given by:

$$c_L = \frac{\sum_i c_i}{\sum_i \frac{c_i}{L_i} - 0.01094 c_{co2}} \qquad (4.15)$$

$$c_U = \left(\sum_i c_i \right) \left[100 - \frac{\left(\sum_i c_i n_i \right)}{B} \right] \qquad (4.16)$$

where B is given by:

$$B = \sum_i \frac{c_i n_i}{100 - U_i} + 0.00105 c_{CO2} + 0.00106 c_{CO2}^2 - 0.00106 c_{CO2}^3 \qquad (4.17)$$

The concentrations of each of the flammable gases, c_i, have upper and lower flammable limits of U_i and L_i respectively, and c_{CO2} is the concentration of carbon dioxide. The parameters c_i, L_i, U_i and c_{CO2} are all expressed in terms of percentage by volume in Equations (4.15) to (4.17), i.e. the LFL of methane is included in the equations as L_i = 5.0, not 0.050. The parameter n_i is the number of moles of oxygen consumed by one mole of fuel when the mixture is at the upper flammability limit. Assuming the combustion takes place in air, this is given by:

$$n_i = \frac{(100/U_i) - 1}{1 + (79/21)} \qquad (4.18)$$

This model for c_L and c_U was shown to provide good agreement with flammability measurements undertaken by Kondo *et al*. (2006) using a 12 litre explosion sphere.

4.3 MODEL VALIDATION

To check that the choice of empirical profiles described in the previous section is appropriate for sub-sonic free jets, the model has been used to reproduce the work of Birch *et al*. (1981)

and Smith *et al*. (1986). The former study compared predictions of the flammability factor to measurements of ignition probability in natural gas jets. The gas was composed of 95% methane, 3% ethane and 2% higher hydrocarbons (assumed here to be propane), and the jet issued from an orifice with diameter of 12.65 mm. Three different release velocities were examined: 32.2 m/s, 25.7 m/s and 19.2 m/s. Unfortunately, Birch *et al*. (1981) did not clearly state which of these three velocities was used in their results comparisons. Predictions of the flammability factor for all three velocities are therefore shown in Figure 21. The measured ignition probabilities and the model results of Birch *et al*. (1981) shown in this figure have been digitally scanned in from their paper.

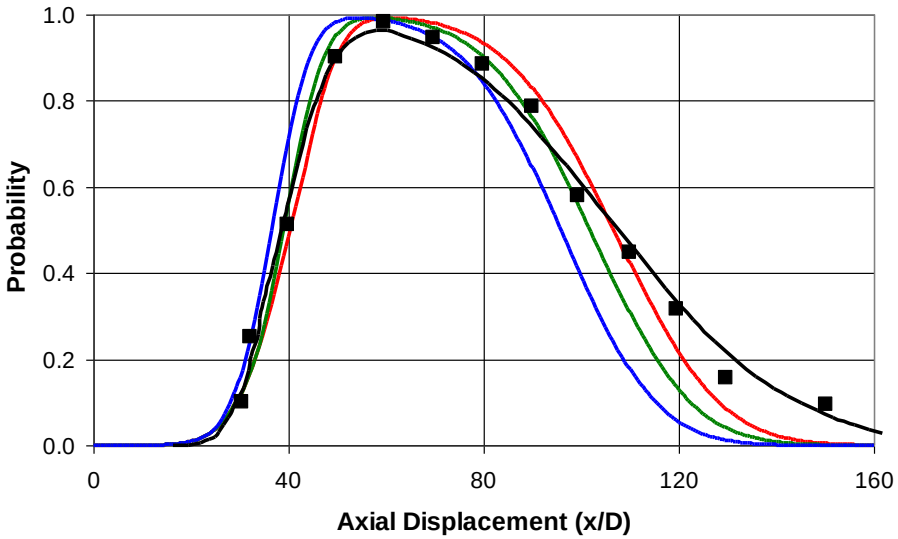

Figure 21 Comparison of flammability factor predictions (lines) to ignition probability measurements (symbols) for the natural gas jets studied by Birch *et al*. (1981). The black line is the previous prediction of Birch *et al*. (1981) and coloured lines are the present model predictions with exit velocities of: – 32.2 m/s; – 25.7 m/s; – 19.2 m/s.

Comparison of the present model predictions and those of Birch *et al*. (1981) along the centreline of the jet (Figure 19) suggests that their results were probably presented for the middle of the three velocities (25.7 m/s). There is reasonably good agreement between the predictions of the present model and the approach used by Birch *et al*. (1981). Both models show good agreement between the predicted flammability factor and measured ignition probability along the axis of the jet, with the previous model of Birch *et al*. (1981) producing a slightly higher flammability factor in the far field ($x/D > 100$), in better agreement with the measurements. The differences here are likely to have been due to slightly different profiles being adopted for the mean and fluctuating gas concentrations in the present model, compared to those used by Birch *et al*. (1981).

Radial profiles of concentration and flammability factor are compared to the previous predictions and experimental measurements from Birch *et al*. (1981) in Figure 22. Again, three profiles are shown for the different velocities. The predicted peak flammability factor using the new model is around 5% higher than their peak value, in better agreement with the experiments. This is likely to be a consequence of different fluctuating gas concentration profiles being used. Overall, the agreement between the predicted flammability factor and the measured ignition probabilities is very good.

Figures 23 and 24 compare the results of the new model to those presented by Smith *et al*. (1986) for jets of natural gas and propane, respectively. For the natural gas jet, the release velocity was 50 m/s whilst for the propane tests it was 20 m/s. In both cases, the orifice diameter was 6.35 mm. Smith *et al*. (1986) assumed that the virtual source of the gas jet was located four diameters upstream of the orifice. The same offset is used in the present model results, and the results are plotted in Figures 23 and 24 with the axial displacement measured from the virtual jet origin rather than the orifice. Despite this, the model of Smith *et al*. (1986) predicted the potential core of the jet, where the gas concentration has a volume fraction of one, to extend nearly twice as far in the axial direction as the present model predictions. The source of discrepancy between their predictions and those of the present model are unclear. However, these differences are limited to the region very close to the orifice ($x/D < 30$) where the gas concentrations are well above the UFL, and so they have little bearing on the flammability factor. Further downstream, the agreement between the model predictions of the mean gas concentration is good.

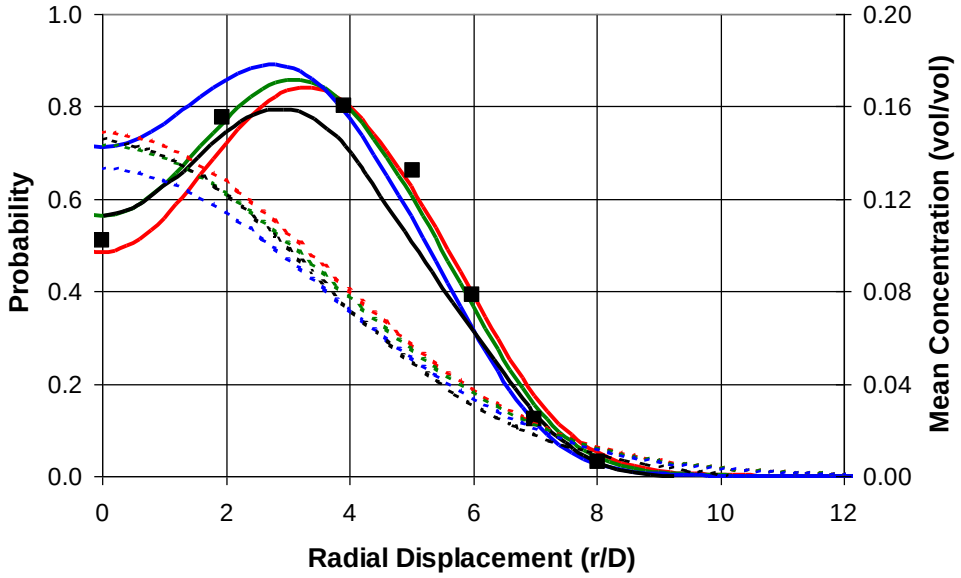

Figure 22 Comparison of flammability factor predictions (solid lines) and mean concentrations (dashed lines) to ignition probability measurements (symbols) for the natural gas jets studied by Birch *et al*. (1981). The black lines are the previous predictions of Birch *et al*. (1981) and coloured lines are the present model predictions with exit velocities of: – 32.2 m/s; – 25.7 m/s; – 19.2 m/s.

The flammability factor predicted by the present model shows some small differences compared to the previous results of Smith *et al*. (1986). For both the natural gas and propane jets it predicts the flammability factor to decay more rapidly to zero than the Smith *et al*. (1986) model in the far field, where the mean concentrations fall below the LFL. In the natural gas jet, the results are therefore in slightly better agreement with the experiments, whilst in the propane jet case they are slightly worse. These differences are fairly minor, however, and overall the predicted flammability factor is in good agreement with the measured ignition probabilities.

In summary, comparison of the present model predictions to the cases previously examined by Birch *et al*. (1981) and Smith *et al*. (1986) indicates that the model provides reliable predictions of the flammability factor for free jets in a quiescent environment.

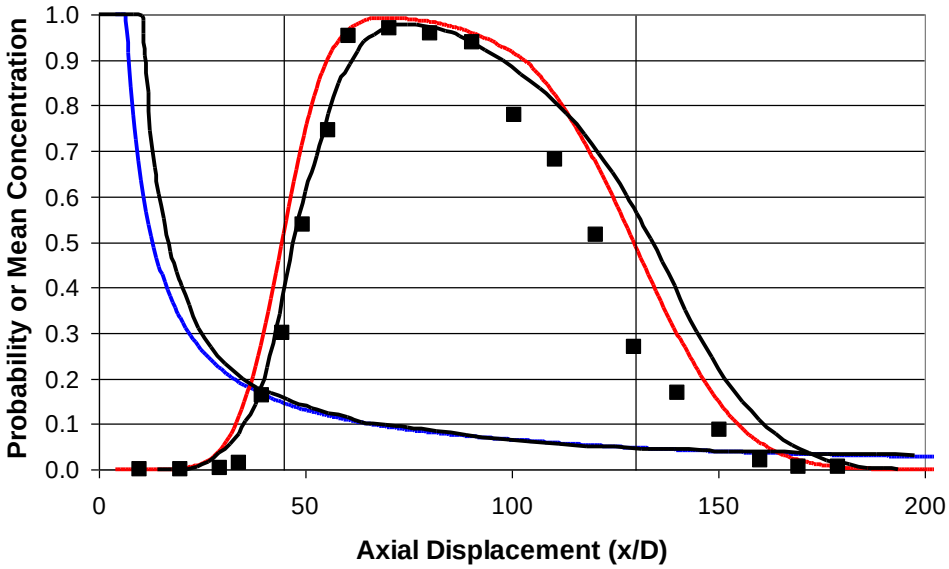

Figure 23 Comparison of flammability factor predictions and mean concentrations to ignition probability measurements for the natural gas jet studied by Smith *et al*. (1986). The black lines are the previous prediction of Smith *et al*. (1986) and coloured lines are the present model predictions. Vertical lines indicate the positions of the mean UFL and LFL.

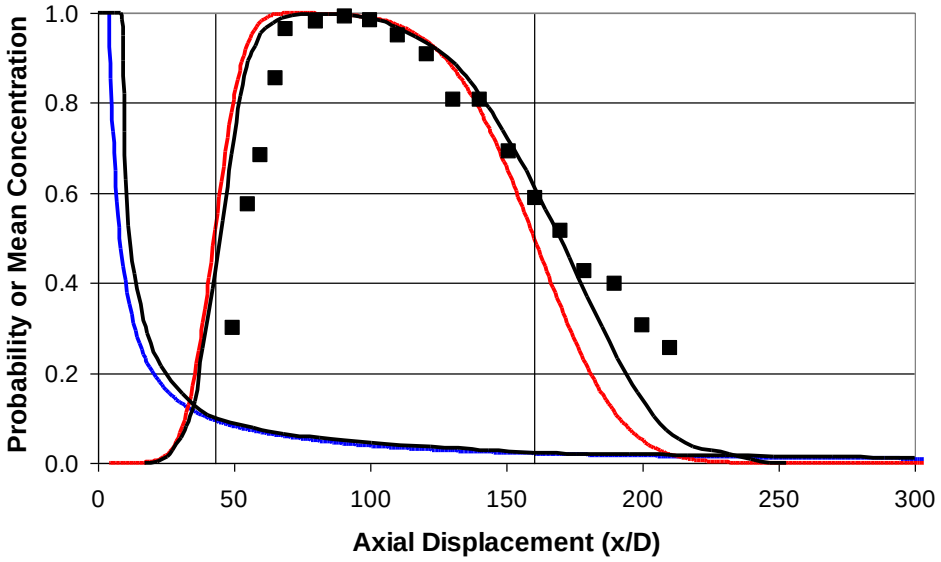

Figure 24 Comparison of flammability factor predictions and mean concentrations to ignition probability measurements for the propane gas jet studied by Smith *et al*. (1986). The black lines are the previous predictions of Smith *et al*. (1986) and coloured lines are the present model predictions. Vertical lines indicate the positions of the mean UFL and LFL.

4.4 JET IGNITION EXPERIMENTS

In the gas jet experiments performed at the Health & Safety Laboratory, two sets of ignition tests were performed. The first involved bulk ignition tests using a large ignition source (a propane blow torch), which were undertaken to assess the inerting effect of CO_2 on methane, and to give an indication of a suitable CO_2 to methane ratio for the subsequent ignition tests.

The second series of tests involved detailed ignition probability measurements using 100% methane and an 80:20 mixture of methane to CO_2 concentration, by volume. The ignition probability was determined in a number of axial and radial positions and measurements of the mean gas concentration in the unignited jet were also taken.

4.4.1 Gas Release System

The methane and CO_2 gases were supplied from pressurised gas cylinders that were pressure-regulated to 3 barg. Each cylinder was connected to a separate rotameter and manual flow controller that allowed the flow rate to be adjusted to between 10 litres/min and 90 litres/min. The flow of methane and CO_2 gas from the rotameters was combined at a T-junction, and further downstream in the supply line there was a shut-off valve. This valve allowed the total gas flow to be stopped immediately without adjusting the settings for each of the individual gases. The shut off valve was connected to the release pipe by a further five metres of fire resistant gas tubing.

The release pipe had an internal diameter of 6 mm and was 400 mm in length. It was oriented vertically such that the gas issued upwards and was attached to a metal frame that also secured the spark ignition system and the concentration analysis tubing (Figure 25). Ignition and concentration measurements were possible up to a distance of 1.20 m from the release point. The sampling tube used to measure the gas concentrations and the spark ignition electrodes are shown in Figures 26 and 27.

4.4.2 Bulk Ignition Tests

Bulk ignition tests were performed using a propane blowtorch to ignite the gas jet. The tests were categorised based on the observed response, as shown in Table 1. For Classes 1, 2, and 3 the lighted blowtorch remained in the gas jet during the test, whereas for Classes 4 and 5 the torch was removed as soon as ignition occurred.

Table 1 Ignition response classification

Class	*Ignition response*
1	No effect on pilot flame
2	Enhances combustion of pilot flame
3	Burns only in the presence of the pilot flame
4	Burns for a short period
5	Stable combustion, burns continuously

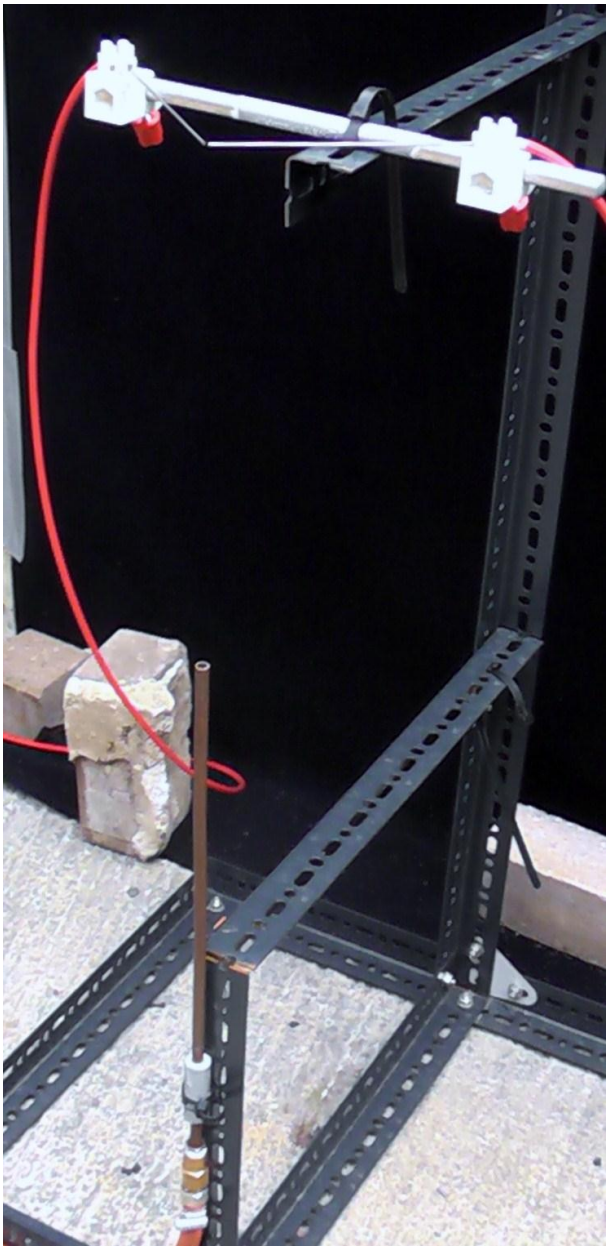

Figure 25 Experimental apparatus showing the release pipe and the spark electrodes attached to the supporting frame.

Figure 26 Gas sampling tube positioned above the gas release point.

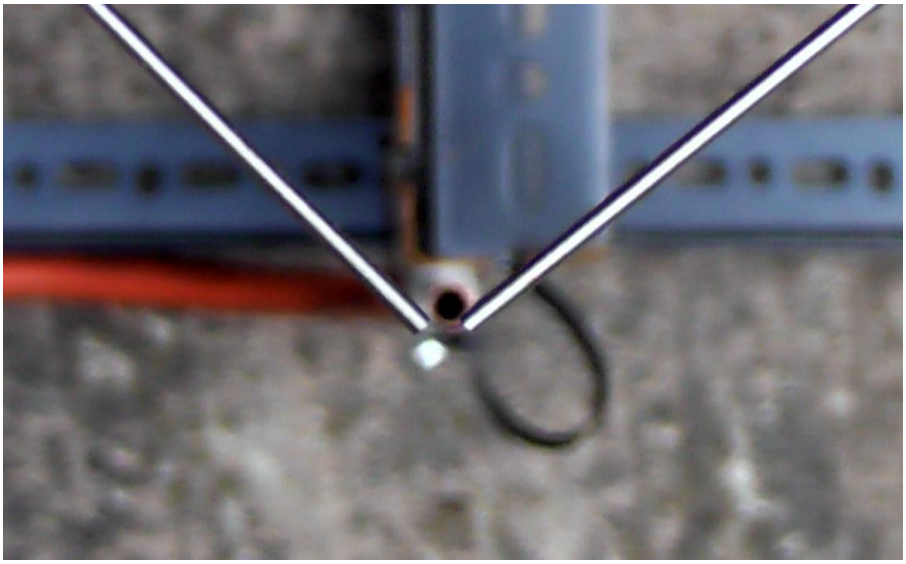

Figure 27 Seen from above, the spark electrodes positioned above the release point.

4.4.3 Ignition Probability Tests

The ignition probability was measured using a sparking system which comprised a variable voltage power source, two 1 GOhm resistors, a 2 nF capacitor, high tension wires and tungsten electrodes. The power source was set to 16 kV, allowing the capacitor to be charged to 15 kV. When sufficient energy was charged in the capacitor to break down across the gap between the electrodes, the capacitor would discharge and a spark would be produced. The combination of resistors and capacitor dictated the capacitor charge time, and this was chosen to produce a spark every four seconds. The tungsten electrodes of diameter 1.6 mm and length 150 mm were positioned in the jet with a separation distance of 2 mm.

Ignition tests were performed in batches, with the gas shut off for a period of 20 to 30 seconds between each batch to avoid build up of combustible gases, or to allow venting of combustion products when ignition had occurred. Each batch consisted of a maximum of ten sparks. However, when ignition occurred the batch was terminated. For each ignition location, a total of 100 batches were performed. In many cases, ignition occurred before the maximum of ten ignition attempts had been reached. On average 250 ignition attempts were performed at each location. Photos showing the ignition of a gas cloud are shown in Figure 28.

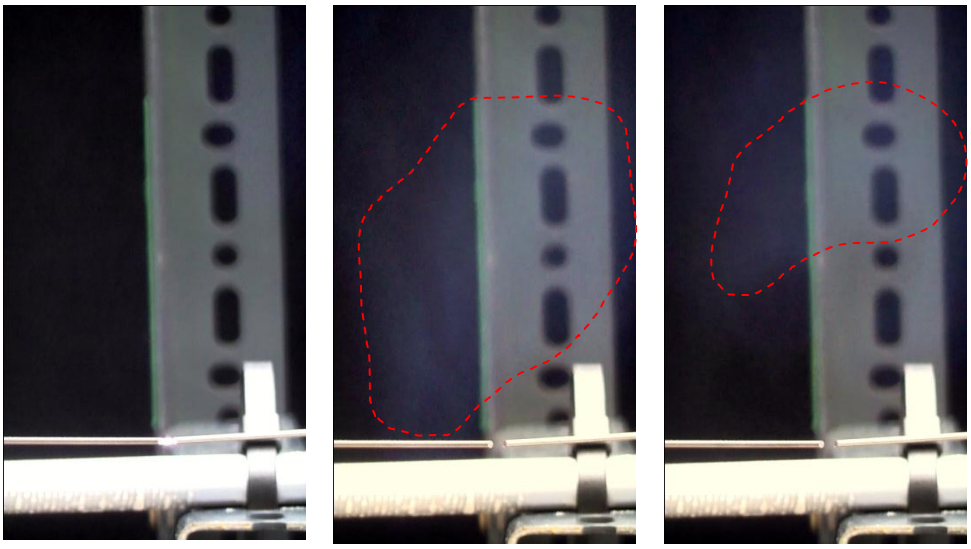

Figure 28 Photogrpahs showing the spark at the electrodes followed by the ignited gas moving downstream. Image time step = 1/25 second

4.4.4 Gas Analysis

The concentrations of methane and CO_2 in the unignited gas jet were determined prior to conducting any ignition tests using a GA 2000 Portable Gas Analyser (Geotechnical Instruments, UK). The accuracy of the analyser was ±0.5% vol/vol over the range 0% to 15% vol/vol, ±1.0% vol/vol over the range 15% vol/vol to 30% vol/vol, and ±3.0% vol/vol over the range 30% vol/vol to 100% vol/vol. Gases were sampled via a stainless steel tube of internal diameter 4 mm and length 300 mm that was positioned in the gas jet and connected to the analyser by 5 meters of flexible tubing. The internal pump of the gas analyser operated at a flow rate of 620 ml/min, giving a residence time in the sampling tube of roughly 16 s. The gas jet was therefore sampled for 60 s prior to readings being taken, and an average reading

was calculated over a further 60 seconds using values recorded at a rate of 1Hz. The standard deviation of the reported reading was ±0.8% vol/vol for methane and ±0.1% vol/vol for CO_2.

4.4.5 Rotameter calibration

Calibration of the rotameters was performed using a water displacement method. The time required to displace the contents of an 18 litre bottle was determined for each graduation mark on the rotameter scale. The method assumed that there was negligible solubility of the gas in the water. Calibrations were performed using the same fittings and length of tubing as used in the actual experiments so that pressure losses were accounted for in the measured flow rates at each calibration point.

4.4.6 Experimental conditions

All of the ignition experiments were performed in a sheltered courtyard that was walled on four sides and open to the atmosphere. Tests could only be performed in low to moderate wind speeds since higher wind speeds clearly affected the gas jet dispersion behaviour.

The bulk ignition tests examined three different flow rates (30 litres/min, 50 litres/min and 90 litres/min), whereas for the ignition probability tests only one flow rate was used (90 litres/min). This condition was chosen so as to be comparable with the previous work of Birch *et al.* (1981) and Smith *et al.* (1986) who used similar Reynolds Numbers of between 12,500 and 22,000. Details of the conditions tested are summarised in Table 2.

Table 2 Experimental release conditions

Volumetric Flow rate (l/min)	30	50	90
Exit velocity (m/s)	17.7	29.5	53.1
Reynolds number[4]	6,453	10,755	19,359

4.5 RESULTS

4.5.1 Gas Concentration

The concentrations of methane and CO_2 were measured in the unburnt gas jet at a number of axial and radial positions. For the tests conducted with a gas exit velocity of 53.1 m/s, the measured centreline concentrations are compared to those predicted by the empirical jet model (described in Section 4.2) in Figures 29 and 30 for the pure methane and the methane-CO_2 mixture (comprising 80% vol/vol methane and 20% vol/vol CO_2), respectively. The upper and lower flammability limits shown in these graphs are those given by Drysdale (1999) for methane (15% and 5%) and those determined from the model of Kondo *et al.* (2006) for the methane-CO_2 mixture (13.4% and 5.1%).

[4] *Reynolds numbers are for the pure methane releases, based on the release velocity and pipe diameter.*

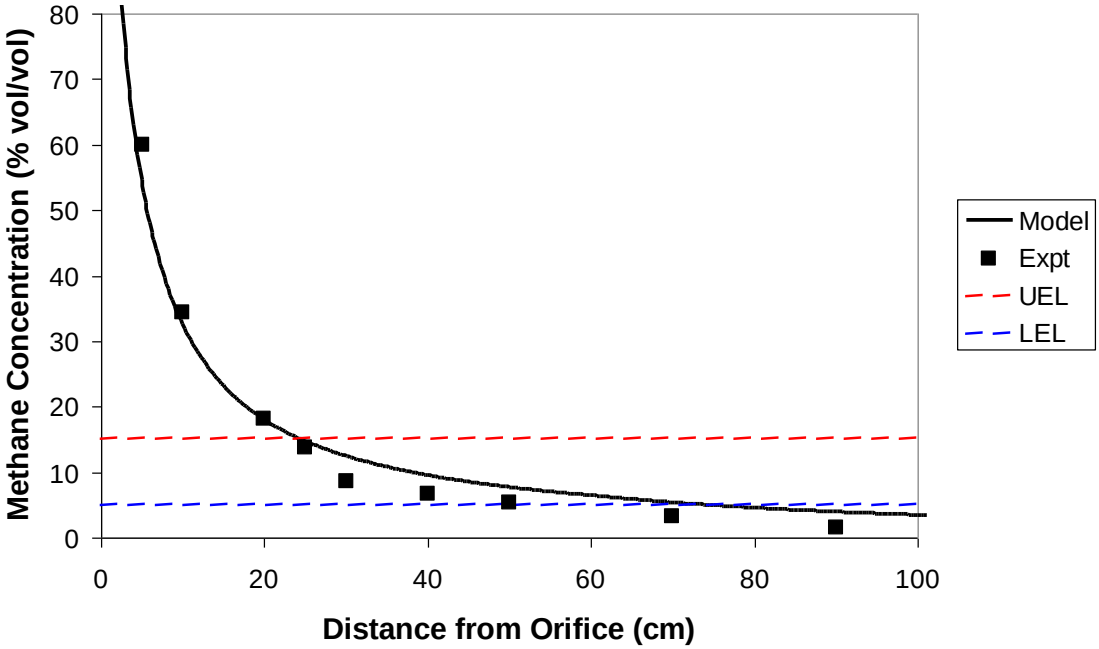

Figure 29 Methane concentrations along the jet axis for the 100% methane release with an exit velocity of 53.1 m/s.

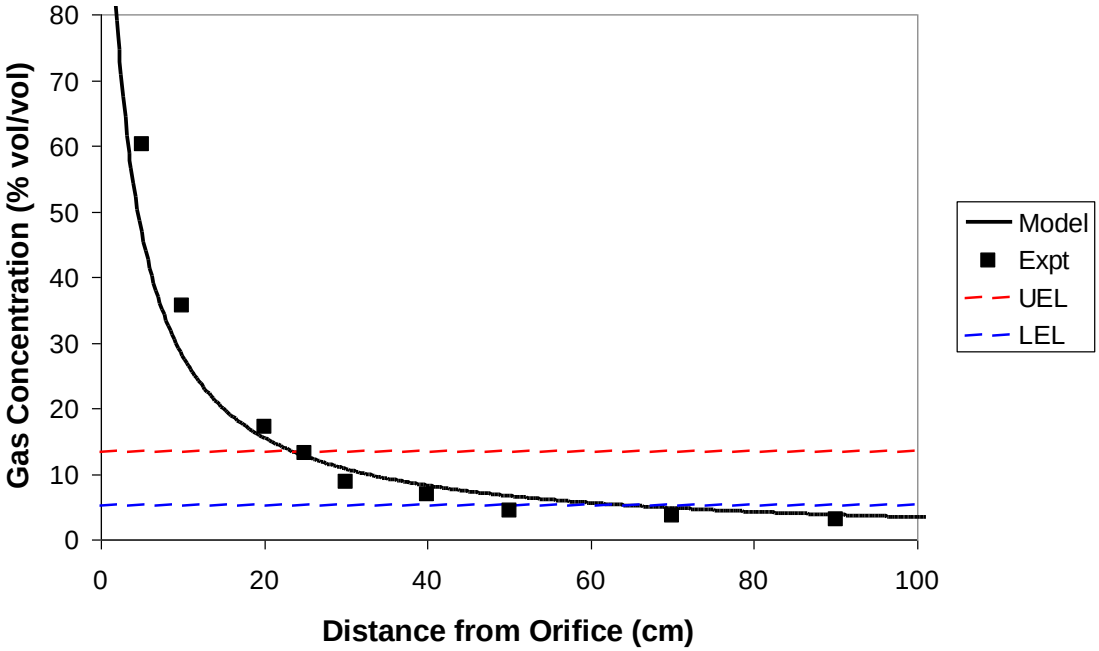

Figure 30 Combined methane plus CO_2 concentrations along the jet axis for the 80% methane, 20% CO_2 release with an exit velocity of 53.1 m/s.

Along the centreline of the jet, the mean gas concentrations were in the flammable range for an axial distance of between 25 cm and 74 cm for the pure methane jet, and between 24 cm and 66 cm for the methane-CO_2 jet.

The agreement between the measured and predicted mean gas concentrations was generally good. For the pure methane jet, all of the results were within 5% vol/vol, although at an axial distance greater than 25 cm the model was consistently higher than the measured concentrations. For the methane-CO_2 mixture, the model agreed with the measurements within 3% vol/vol for all but the first two measurement positions at 5 cm and 10 cm from the release point, where the gas concentrations were under-predicted by around 20% in relative terms.

Radial profiles of the gas concentration are also shown in Figures 31 and 32. The jet in the experiment spread at a faster rate than was predicted by the model. On the centreline of the jet, the model over-predicted the gas concentration at axial distances of 30 cm, 40 cm and 70 cm downstream from the jet source. However, at a radial offset of 4 cm from the centreline, the model under-predicted the measured gas concentrations at the 30 cm and 40 cm positions.

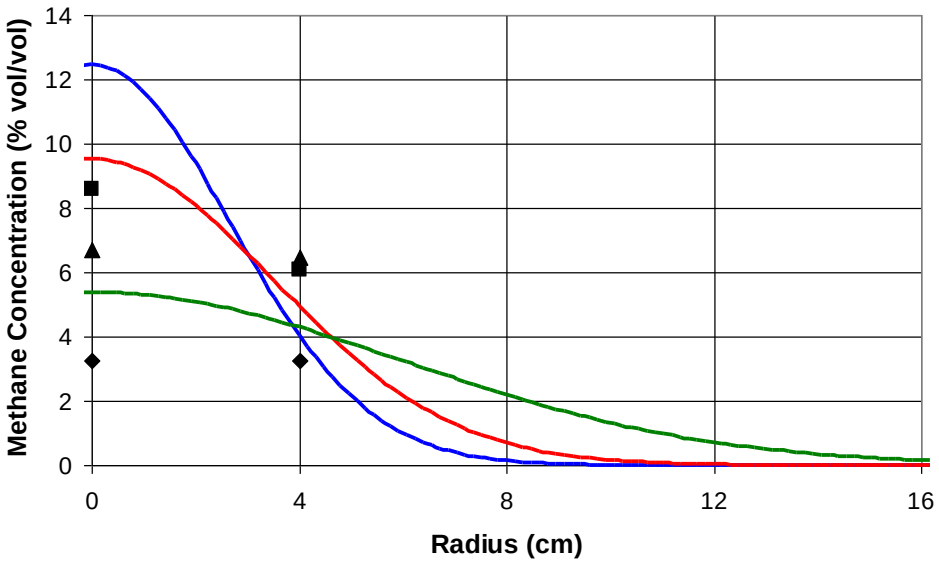

Figure 31 Radial profiles of measured and predicted gas concentration for the 100% methane release with an exit velocity of 53.1 m/s at three distances from the jet source. Model results: – 30 cm; – 40 cm; – 70 cm; measured values: ■ 30 cm, ▲ 40 cm, ◆ 70 cm.

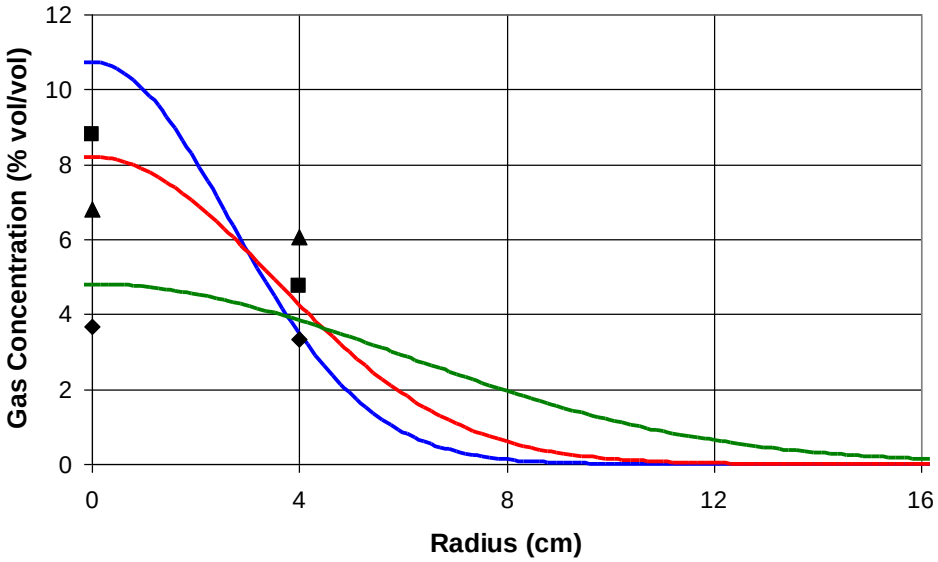

Figure 32 Radial profiles of combined methane plus CO_2 concentration for the 80% methane, 20% CO_2 with an exit velocity of 53.1 m/s at three distances from the jet source. Model results: – 30 cm; – 40 cm; – 70 cm; measured values: ■ 30 cm, ▲ 40 cm, ◆ 70 cm.

4.5.2 Bulk Ignition Characteristics

The bulk ignition behaviour of methane and CO_2 gas mixtures was examined at three different gas exit velocities with CO_2 feed concentrations up to 70% vol/vol. The response of the gas mixture to the ignition source was classified according to the criteria given in Table 1 and results are presented in Figure 33. For all three of the gas velocities that were examined, the severity of the ignition response decreased with increasing CO_2 concentration, as expected. For gas velocities of 29.5 m/s and 17.7 m/s the methane was completely inert with CO_2 concentrations in the region of 60% to 70% vol/vol in the feed gas, respectively. Due to the limited range of the available gas flow meters it was not possible to explore CO_2 mixture concentrations above 45% for the highest release rate (53.1 m/s). However, it is expected that the behaviour at this velocity would follow a similar trend to the other two conditions, and that the gas mixture would be completely inerted with CO_2 feed concentrations of around 60% vol/vol.

Figure 33 shows that the lower velocity gas jets maintained a higher ignition class over a wider range of CO_2 concentrations. In these circumstances, a lower flame front speed is require to maintain a stable flame and avoid flame blow out. The CO_2 feed concentrations that gave rise to complete inertisation in these tests (approx. 60% vol/vol and 70% vol/vol) are less than the concentrations reported by Coward and Jones (1952) and Kondo *et al*. (2006), who found that a feed concentration of 80% vol/vol CO_2 was necessary to render static mixtures of CO_2, methane and air completely inert. The trends identified in Figure 33 show that for free jets the release velocity provides an additional inhibiting factor in the ignition and formation of stable flames. Standard static tests of flammability may therefore be considered to provide conservative estimates of the CO_2 concentration necessary to inert releases from pressurized systems.

For the two higher gas velocities (29.5m/s and 53.1 m/s) the pure methane flame was not attached to the release pipe but adopted a stable location downstream from the release point.

The location of this lift off distance was determined using image analysis of the video footage, and the results are given in Table 3. The flame front location at the higher velocity of 53.1 m/s was roughly twice that of the lower gas release velocity of 29.5m/s (12.84 cm as compared to 6.91 cm). The local gas velocity at the lift off distance is also shown in Table 3 for the two tests, determined using the empirical jet model developed presented in Section 4.2. Although the distance from the flame front to the release point increased with release velocity, the local velocity at the flame front for each condition was independent of the release velocity, falling within the region of 9.20 ± 0.44 m/s. This demonstrated the competition between the advancing gas velocity and the flame front speed in determining the location of the stable flame.

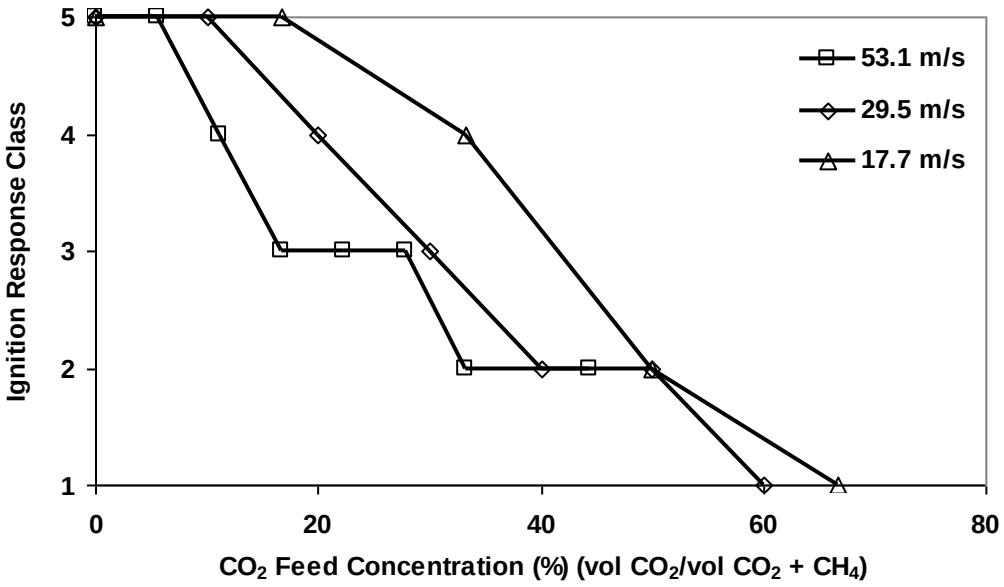

Figure 33 Ignition response of gas mixtures containing CO_2 concentrations up to 70% vol/vol with gas exit velocities of 17.7 m/s, 29.5 m/s and 53.1 m/s.

Table 3 Flame front lift off distance and local velocity for pure methane flames

Release Velocity (m/s)	*Lift Off Distance (cm)*	*Local Velocity (m/s)*
29.5	6.91	8.77
53.1	12.84	9.64

The analysis of the flame lift off position and velocity was also undertaken for the tests where the methane jet was diluted with CO_2 where a stable flame was observed (stability classes 4 and 5, in Table 1). Results are presented for the two highest gas flowrates (29.5 m/s and 51.1 m/s) in Figure 34. At the lower gas velocity of 17.7 m/s, the flame was not sufficiently stable to provide reliable measurements.

For release velocities of both 29.5 m/s and 51.1m/s, the flame front moved further downstream with increasing CO_2 concentration. This translates into a reduced flame front speed, as shown by Figure 34. Over the limited range considered, the relationship between the flame front speed and CO_2 concentration was linear, however a number of factors will dictate the location of the stable flame front, including the local gas velocity, the local gas

composition, the calorific value of the mixture, the chemistry of the combustion reaction and the effect of the inert gas on the reaction rate.

Ishizuka and Tsuji (1981) examined the effect of inert gases on flame stability in counter-current diffusion flames and found a limiting inert concentration beyond which a stable flame could not be maintained, which was attributed to chemical limitations on the combustion rate. They also observed that the flame temperature decreased as the inert concentration in the fuel mixture was increased.

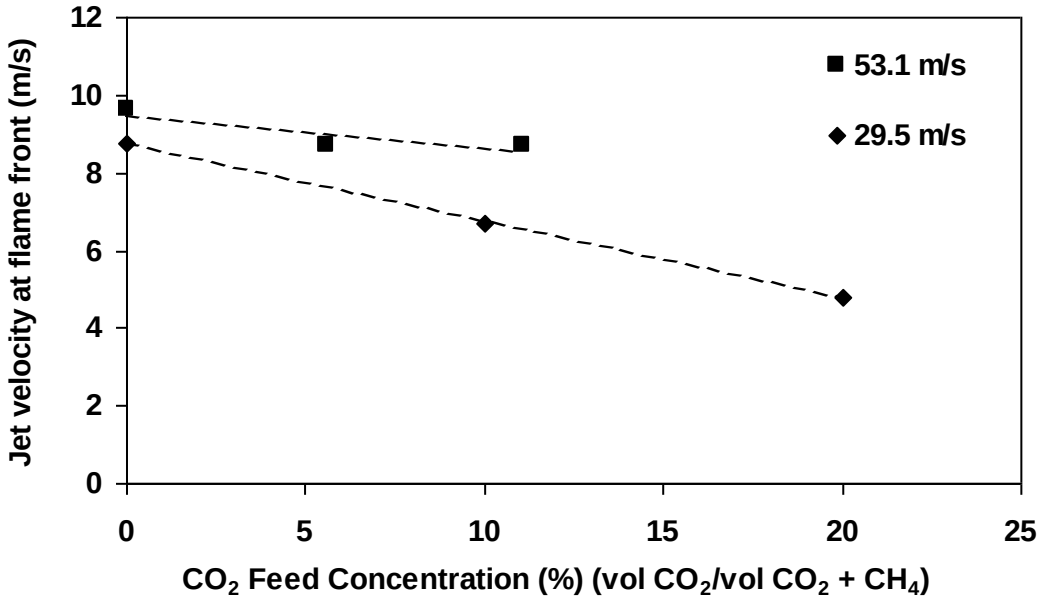

Figure 34 The effect of the CO_2 feed concentration on the local jet velocity at the flame lift off position for initial release velocities of 29.5 m/s (♦) and 53.1 m/s (■)

4.5.3 Ignition Probability

The measured probability of ignition at different axial and radial positions is presented in Figures 35 to 38, compared to predictions of flammability factor from the model presented in Section 4.2. Figures 35 examines the ignition behaviour along the jet centreline for the pure methane and methane-CO_2 releases. The measured ignition probabilities are shown with error bars representing the statistical uncertainty associated with one standard deviation, using the same approach taken by Birch *et al*. (1981). In the experiments, the addition of 20% vol/vol CO_2 to the gas mixture increased the likelihood of ignition slightly close to the orifice and decreased it markedly further downstream. At a distance of 20 cm, close to the orifice where the mean gas concentrations were above the UFL, the ignition probability was 13% and 32% for the pure methane and methane-CO_2 mixtures, respectively. Further downstream, at a distance of 50 cm, the pure methane jet was ignited in 33% of the ignition attempts, whereas for the methane-CO_2 mixture it was only ignited in 1% of the ignition attempts.

There is reasonable agreement between the measured and predicted ignition probabilities up to a distance of around 30 cm from the nozzle. Further downstream, the model produced significantly higher values than were measured experimentally, by a factor of two or more. The experiments measured a practically zero ignition probability at distances more than 70 cm and 50 cm for pure methane and methane-CO_2, respectively, whilst the model predicted the jet to be ignitable at distances up to 100 cm downstream from the source in both cases. At

the two off-axis positions 30 cm and 40 cm downstream from the jet source, the agreement between the experiments and the model predictions was significantly better than along the centreline (Figures 36 and 37).

It was shown earlier that the predicted concentration did not match exactly that measured in the experiments (Figures 29 and 30). To provide a more direct comparison of the model and measured ignition probabilities, the data along the centreline of the jet are plotted against the mean concentration, instead of the axial displacement, in Figure 38. When the data are plotted in this way, the measured ignition probabilities span a similar range of mean concentration to that predicted by the model. This highlights how even a relatively small change in mean concentration can have a significant affect on the ignition probability, particularly in regions where the gas concentration is close to the LFL. Despite these improvements in agreement between the measured and predicted values, the measured ignition probabilities are still significantly lower than those predicted by the empirical model. All of the measured ignition probabilities are less than 60% whereas they are predicted to reach nearly 100% in places.

One of the possible explanations for the low ignition probability measured in the experiments is that not all of the ignitions were detected. Very small pockets of gas could have been ignited that were too small to be visible. However, this is not considered to offer a plausible explanation for the discrepancy of 40% in the ignition probability. Ignitions were detected both audibly and visibly and there is confidence that the vast majority of ignitions were detected. In those cases where bright sunshine partially obscured the directly visible flame, its presence was detected by the shadow produced on an adjacent wall, from the Schlieren effect.

Another, more likely, explanation is that gusts of wind disturbed the jet and led to gas concentrations varying significantly over time. The test area used in the experiments was open to the atmosphere and although tests were conducted in low to moderate wind speeds to minimise its effect, some disturbances still occurred. These would have been more significant in the far-field of the jet, where its momentum diminished. Beyond a distance of 30 cm, the maximum velocity on the centreline of the jet was predicted to fall below 5 m/s (approximately 11 mph). Although Figure 38 accounts for the reduction in mean gas concentration due to these disturbances, the turbulent fluctuations in the jet will have been affected. The same mean gas concentration can be produced by varying the gas concentration between wider limits, which could reduce the proportion of time the mixture spends within the flammable range, and hence lower its likelihood of ignition.

In realistic release conditions, following a failure on an offshore platform for example, it is unlikely that the flow around the release point will be quiescent. The results presented here are useful in demonstrating that even relatively small gusts of wind may have a significant effect on the dispersion of the gas and its chances of igniting in such cases.

In the results presented here, the model predicted higher ignition probabilities along the axis of the jet than were measured, i.e. the model results were conservative in terms of the predicted hazard. However, without further analysis it is unclear whether the model will always return conservative values, or whether under certain conditions, such as a co-flowing wind, turbulent fluctuations could be suppressed, leading to higher ignition probabilities.

Contours of the predicted flammability factor for the free jet in quiescent air are presented in Figures 39 and 40 for the pure methane and methane-CO2 jets, respectively. These show that the addition of CO_2 decreases the area over which the gas mixture can be ignited. Where the mean gas concentration is at LFL or UFL, indicated by the red lines in the figures, the predicted flammability factor is around 50%, in agreement with the previous findings of Smith *et al*. (1986).

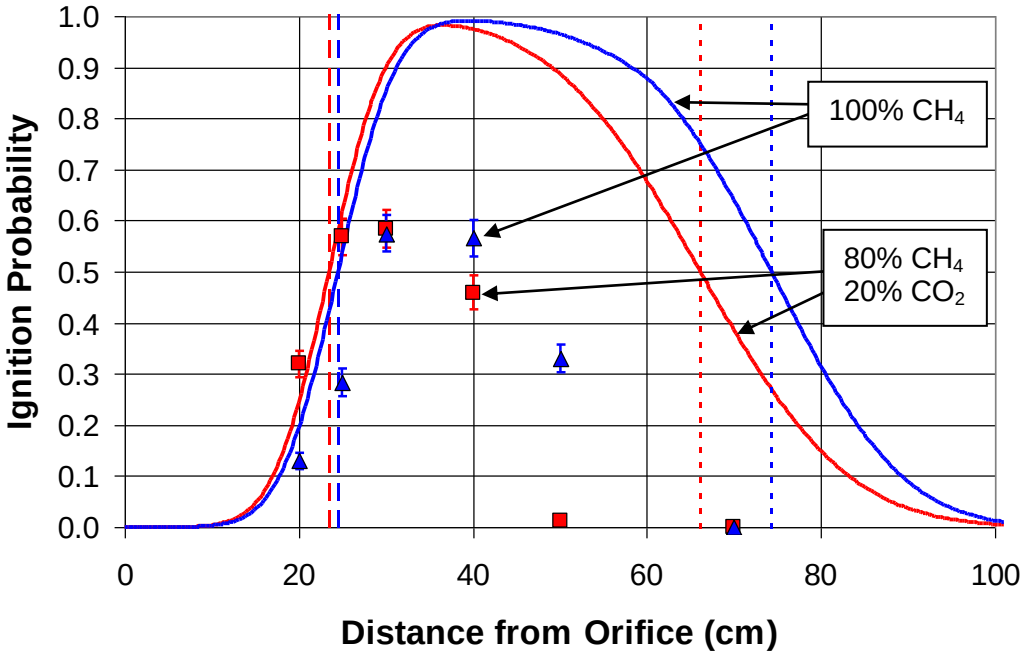

Figure 35 Measured ignition probability (symbols) and predicted flammability factor (solid line) along the centreline of the jet with an exit velocity of 53.1 m/s. Broken lines show the location of the LFL and UFL, based on the predicted mean concentrations.

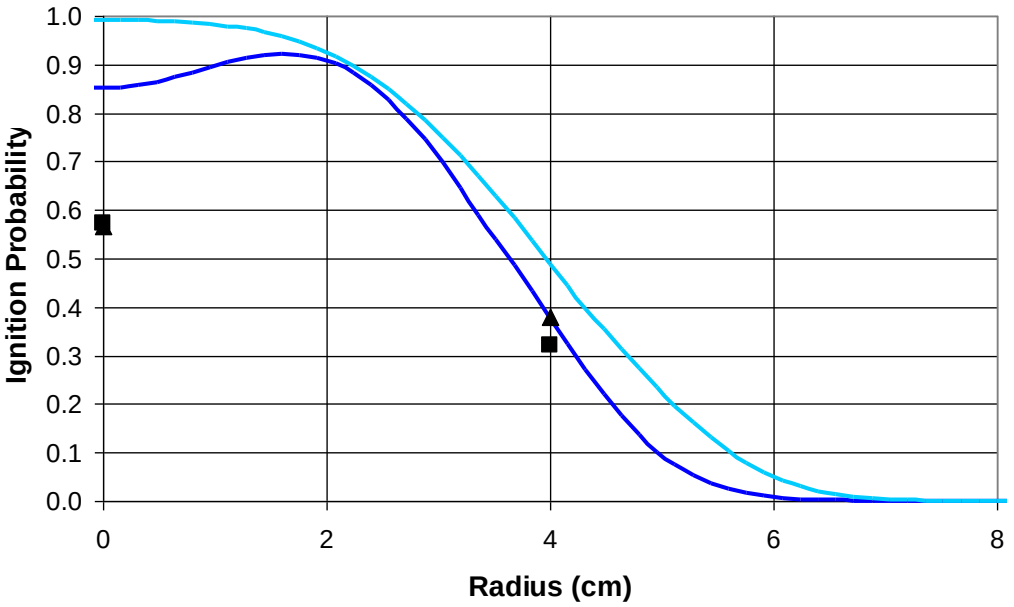

Figure 36 Measured ignition probability (symbols) and predicted flammability factor (solid lines) for the 100% methane release with an exit velocity of 53.1 m/s at two distances from the jet source. Model results: – 30 cm; – 40 cm; measured values: ■ 30 cm, ▲ 40 cm.

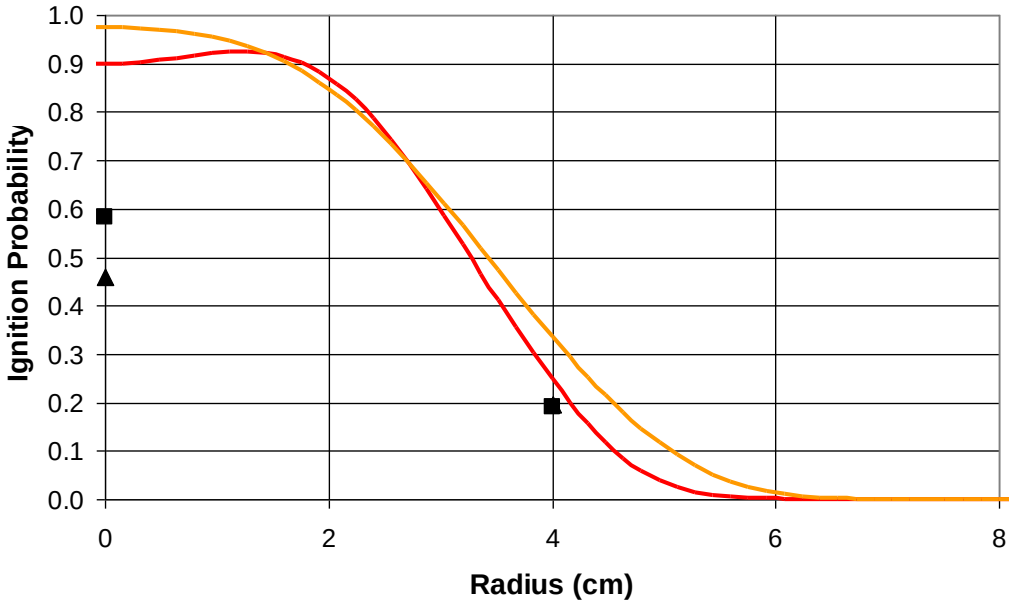

Figure 37 Measured ignition probability (symbols) and predicted flammability factor (solid lines) for the 80% methane 20% CO_2 mixture with an exit velocity of 53.1 m/s at two distances from the jet source. Model results: – 30 cm; – 40 cm; measured values: ■ 30 cm, ▲ 40 cm.

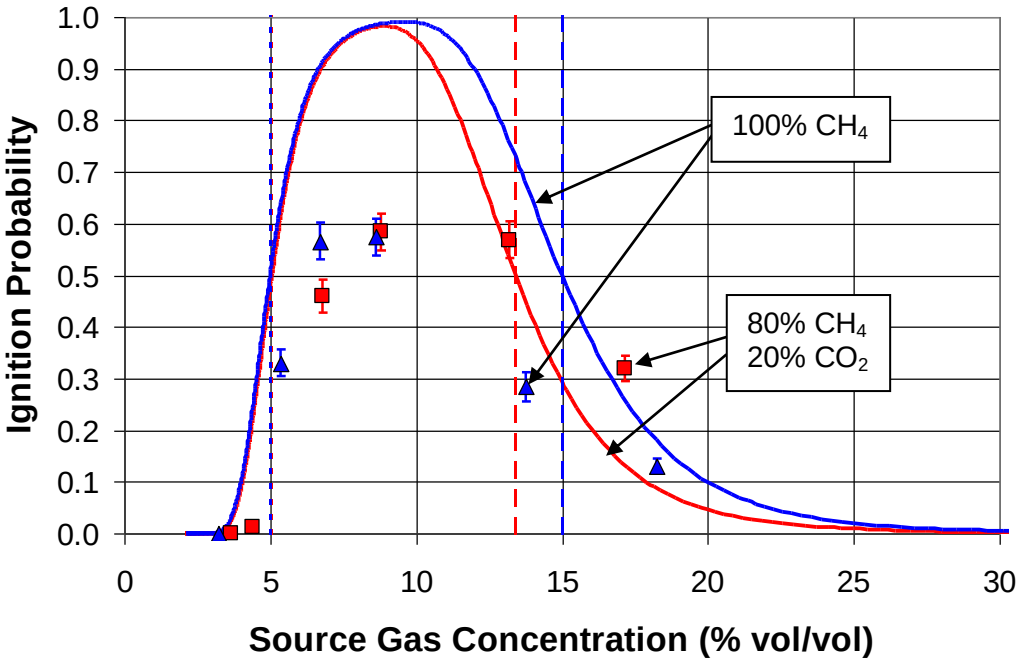

Figure 38 Measured ignition probability (symbols) and predicted flammability factor (solid line) along the centreline of the jet with an exit velocity of 53.1 m/s. Broken lines show the location of the LFL and UFL, based on the predicted mean concentrations.

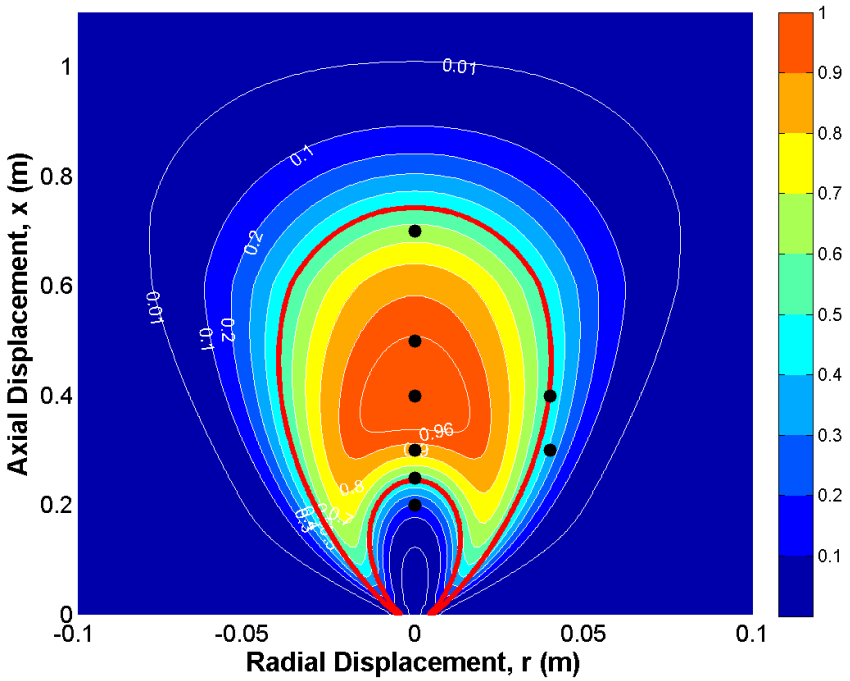

Figure 39 Predicted flammability factor for the 100% methane release with an exit velocity of 53.1 m/s. Red lines indicate the position of the LFL and UFL, based on the predicted mean gas concentration and symbols show the locations where the ignition probability was measured in the experiments.

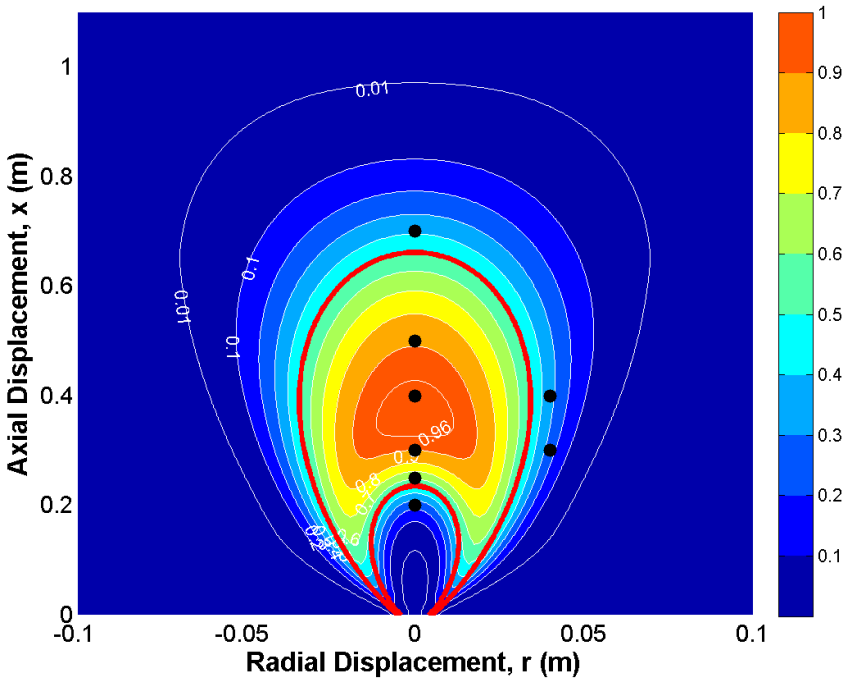

Figure 40 Predicted flammability factor for the methane-CO2 mixture with an exit velocity of 53.1 m/s. Red lines indicate the position of the LFL and UFL, based on the predicted mean gas concentration and symbols show the locations where the ignition probability was measured in the experiments.

5 CFD MODELS OF IGNITION PROBABILITY

5.1 INTRODUCTION

Sections 3 and 4 presented the fundamental physics of mixing processes and demonstrated a method for determining the ignition probability in jets of methane and CO_2. The empirically-based model presented in Section 4 is suitable for simulating free, unobstructed gas jets in quiescent environments only. For practical application to risk assessment and incident investigation, there is a need to model more complex scenarios which may involve cross-winds, flow impingement and interaction of the jet with shear layers. Such complicated flow behaviour is not amenable to simple empirically-based models. Instead, a more general-purpose approach such as CFD is required.

CFD models are capable of predicting the complex flow field around buildings, complicated structures and terrain, and can produce values of the mean and RMS concentration and intermittency that are needed in order to calculate the flammability factor. Recent research has demonstrated the feasibility of using CFD to predict the flammability factor in simple jet flows (Alvani & Fairweather, 2008, Schefer *et al.*, 2010). However, there are a number of practical issues that need to be addressed before this work can be extended to consider more realistic scenarios of interest.

A brief review of the previous work undertaken in this field is provided below and a relatively simple methodology is presented that is practicable to implement in commercial CFD codes. A plan for verification and validation of the model is described and potential applications are discussed. Further detailed analysis of the CFD modelling of flammability factor is provided in Appendix C.

5.2 PREVIOUS STUDIES

There have been very few works examining the use of CFD to model the ignition probability of non-premixed flows relevant to industrial hazards. The most in-depth study is that of Alvani & Fairweather (2008), who presented CFD simulations of the flammability factor for turbulent jets of natural gas, propane and town gas. This followed on from an earlier study by Alvani & Fairweather (2002) and work documented in Alvani's PhD thesis (Alvani, 2004). Very recently, Schefer *et al.*(2010) presented some simulations of hydrogen jets, although their work is less well-developed than that of Alvani and Fairweather. There may be related research in the internal combustion engine and gas turbine combustor fields, but these are outside the scope of the present study.

In the work of Alvani & Fairweather (2008), two different turbulence models were tested: the *k-ε-I* model of Cho & Chung (1992) and the Reynolds stress model of Jones & Musonge (1988). The former model involved the solution of transport equations for the turbulent kinetic energy, its dissipation rate and the intermittency, whilst the latter involved transport equations for each of the Reynolds stresses and the turbulent scalar fluxes, turbulence energy dissipation rate and the intermittency. In both cases, further transport equations were solved for momentum, mixture fraction and mixture fraction variance. A three-part PDF was used to determine the flammability factor which comprised a fully-turbulent part, modelled with a beta function, a super-layer part that was modelled using a approach derived from the work of Effelsberg & Peters (1983), and an outer layer part that was modelled using a delta function.

Alvani & Fairweather (2008) compared the computed flammability factor to measurements of the ignition probability from Birch *et al*. (1981) and Smith *et al*. (1986). Overall, there was good agreement between computations and measurements. They also evaluated the validity of

the underlying models used in their approach by comparing CFD predictions of mean and RMS concentration, turbulent intermittency and PDFs of concentration, against data obtained from measurements in air, propane and natural gas jets, again with good overall agreement. Their study clearly demonstrated that CFD can be used successfully to calculate the flammability factor in turbulent jets. Sample results from their work are shown in Figures 41 and 42. Further work on this topic is ongoing at the University of Leeds, led by Professor Fairweather.

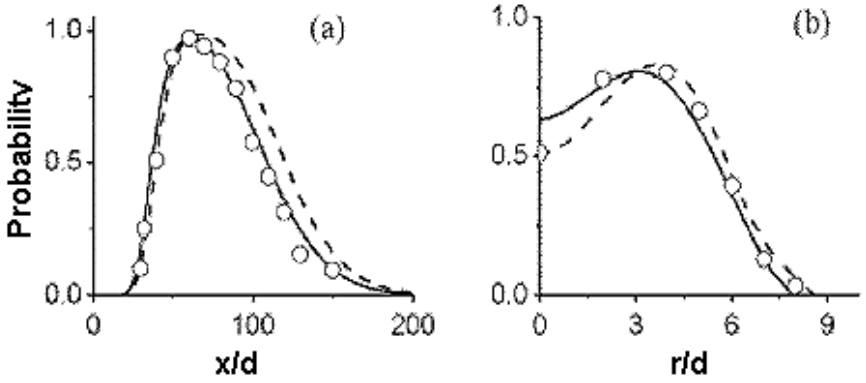

Figure 41 CFD simulations of computed flammability factor versus measured ignition probability (open circles) for the natural gas jet of Birch *et al*. (1981). Solid line: Reynolds stress model, dashed line: *k-ε-I* model. a.) axial profile along the jet centreline; b.) radial profile at an axial position of *x*/*D* = 40. Reproduced with the permission of Prof. Fairweather, University of Leeds.

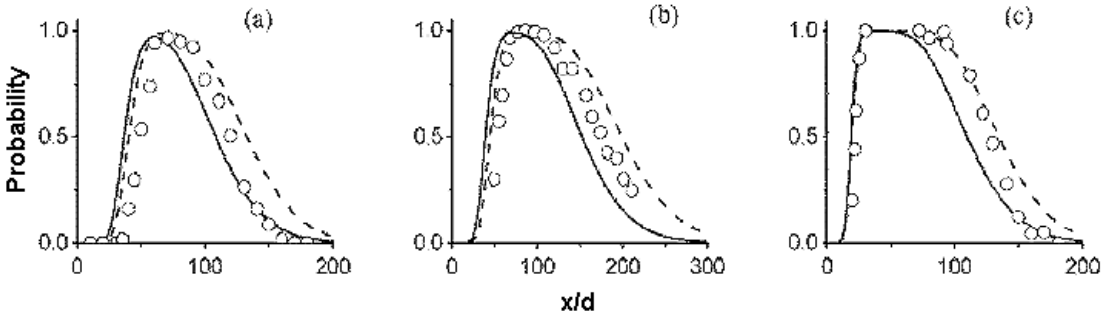

Figure 42 CFD simulations of computed flammability factor versus measured ignition probability (open circles) for the natural gas jet of Smith *et al*. (1986). Solid line: Reynolds stress model, dashed line: *k-ε-I* model. a.) natural gas; b.) propane; c.) simulated town gas. Reproduced with the permission of Prof. Fairweather, University of Leeds.

In the work of Schefer *et al*.(2010), CFD simulations were presented of flammability factor for hydrogen and methane jets. Turbulence intermittency was modelled using the correlation of Kent & Bilger (1976) and a two-part PDF was used, based on a delta function and a Gaussian distribution, weighted by intermittency. The model performance was compared to measurements of the PDF of mixture fraction and ignition probability. For the former quantity, predictions were in fair agreement with the measurements, and for the ignition probability, on the axis of the jets the model performed well. However, at radial positions far downstream from the jet source, the performance deteriorated, although the correct qualitative behaviour was still captured. Schefer *et al*. (2010) stated that they planned to extend their work to consider releases of hydrogen affected by walls, wind and the ground, with the

objective of helping determine safety distances for codes and standards regulations for flammable gases.

5.3 PRACTICABLE CFD MODEL

The model developed by Alvani & Fairweather (2008) is highly complex, particularly the Reynolds stress model variant, and it would be extremely difficult and costly to implement it fully in a commercial CFD code. However, it is possible to derive a simpler version which shares many of its features. In developing this simpler model careful consideration needs to be given to the practicality of its implementation in commercial CFD software. The key requirements are the introduction of additional transport equations for new variables such as turbulent intermittency, and the modification of existing transport equations. In this section these issues were examined in the context of the ANSYS CFX software[5], which is one of the CFD packages used at the Health and Safety Laboratory and in widespread use in industry.

The specific needs are as follows:

a.) **Mean and Variance of Mixture Fraction**: Additional transport equations for the mean and variance of mixture fraction need to be introduced. Although ANSYS CFX already has these transport equations coded in the software, they are only available when combustion is being modelled. For consistency with existing work on CFD modelling of flammability factor, transport equations for mixture fraction, rather than fuel mass fraction, are preferred.

b.) **Intermittency**: An additional transport equation for turbulent intermittency needs to be introduced.

c.) **Turbulence Model Constants**: Constants in the k-ε turbulence model need to be modified to match those used by Alvani & Fairweather (2008).

d.) **Turbulent viscosity**: An additional intermittency-related term needs to be added to the expression for the turbulent viscosity.

e.) **Turbulence dissipation rate**: An additional source term related to turbulent intermittency needs to be introduced into the in the dissipation rate equation.

f.) **PDF**: The computed mean and variance of mixture fraction, and the intermittency, need to be post-processed in order to determine the shape of the PDF, and then the PDF needs to be integrated between the upper and lower flammability limits to determine the flammability factor.

Discussions with ANSYS have established that in principle the requirements of a.) to e.) can be met by CFX. The determination of the PDFs for requirement f.) is not trivial. However, it is essentially a post-processing task, since the PDF is only used to determine the flammability factor and it has no effect on the modelled flow field. It may therefore be easiest to export the computed mean and variance of mixture fraction, and the intermittency data from the CFD model and import this into software such as MatLab or Octave in order to perform the necessary operations.

Given that these steps can be achieved in practice, a summary of the mathematical formulae for the proposed model are provided below. Since the transport equations for mean mixture

[5] http://www.ansys.com, *accessed July 2010.*

fraction and its variance are the same as that already coded into CFX, these are not described. The background to this model is described in Appendix C.

5.3.1 Intermittency

There are two approaches that can be used to determine the turbulence intermittency in the CFD model. The first is to adopt the simple empirical correlation of Kent & Bilger (1976) that was described in Section 4. This model is based on a comparison of measured intermittency for jets in still and co-flowing air, and a heated plane wake, against a parameter comprising mixture fraction mean and its variance.

The alternative and more general-purpose approach is to solve a transport equation for turbulence intermittency, which is given below in Cartesian tensor notation. The variables in this equation take on their standard meaning, i.e. U_j is the component of mean velocity in the j-direction, see for example Alvani (2004) or Versteeg & Malalasekera (2007) for a full nomenclature. The Reynolds stresses which appear in the C_{I1} term are closed by the usual eddy viscosity-based Boussinesq approximation.

$$U_j \frac{\partial I}{\partial x_j} = \frac{\partial}{\partial x_j}\left[(1-I)\frac{\nu_t}{\sigma_y}\frac{\partial I}{\partial x_j}\right] \underbrace{- C_{I1} I}(1-I)\frac{\overline{u_i u_j}}{k}\frac{\partial U_i}{\partial x_j} + C_{I2}\frac{k^2}{\varepsilon}\frac{\partial I}{\partial x_j}\frac{\partial I}{\partial x_j} - C_{I3} I(1-I)\frac{\varepsilon}{k}\Gamma \qquad (5.1)$$

In Alvani (2004) and Alvani & Fairweather (2008), the underbraced term in the above expression is incorrectly written as "$+C_{I1}I$". The final term, Γ, is given below in the form used by Cho & Chung (1992) and is the same as that used by Alvani & Fairweather (2008), although Alvani (2004) used a slightly modified version that is valid for compressible flow.

$$\Gamma = \frac{k^{5/2}}{\varepsilon^2}\frac{U_i}{(U_k U_k)^{1/2}}\frac{\partial U_i}{\partial x_j}\frac{\partial I}{\partial x_j} \qquad (5.2)$$

5.3.2 Turbulent Viscosity

The turbulence viscosity is modified as follows:

$$\nu_t = C_\mu\left[1 + C_{\mu I}\frac{k^3}{\varepsilon^2} I^{-3}(1-I)\frac{\partial I}{\partial x_k}\frac{\partial I}{\partial x_k}\right]\frac{k^2}{\varepsilon} \qquad (5.3)$$

5.3.3 Turbulence Dissipation Rate

The k and ε transport equations are unchanged from their standard form (Jones & Launder, 1972), with the sole exception of an additional positive source term in the ε-equation:

$$\frac{\varepsilon^2}{k} C_{\varepsilon 4} \Gamma \qquad (5.4)$$

This additional term is written incorrectly in Alvani & Fairweather (2008) and also in parts of Alvani's thesis (2004).

5.3.4 Model Constants

The new constants related to intermittency in the above equations are given by Cho & Chung (1992):

$$C_{I1} = 1.6 \quad C_{I2} = 0.15 \quad C_{I3} = 0.16 \quad C_{\mu I} = 0.10 \quad C_{\varepsilon 4} = 0.10 \qquad (5.5)$$

Alvani (2004) used the same set of constants, although Alvani & Fairweather (2008) used slightly modified values to optimise predictions, with C_{I1} = 1.85 and C_{I2} = 0.20.

Alvani & Fairweather (2008) also used a non-standard value for the $C_{\varepsilon 1}$ constant in the dissipation rate equation: a value of 1.48 rather than the standard value of 1.44. This was found to give a best fit to a range of round turbulent jet data. In effect, it was a simple correction to resolve the round/plane jet anomaly[6] (Pope, 1978). In order to compare to the previous work of Alvani & Fairweather (2008), $C_{\varepsilon 1}$ should be given the value of 1.48.

5.3.5 Probability Density Function

There are two PDFs that could be used to determine the flammability factor. The simpler is the two-part PDF of Janicka & Peters (1982) comprising a delta function to model the intermittency spike and a beta function to model the fully turbulent part of the flow, weighted by intermittency:

$$P(\tilde{f}) = (1-I)\delta(\tilde{f}) + IP_\beta(\tilde{f}) \qquad (5.6)$$

The initial steps in the numerical integration of the beta function are outlined by Versteeg & Malalasekera (2007). Schefer & Dibble (2001) also showed how to convert between the fuel mole fraction and the mixture fraction.

The more advanced PDF, which Alvani & Fairweather (2008) found to give the best performance across a range of jets and wake data, is given by:

$$P(\tilde{f}) = (1-I)\delta(\tilde{f}) + I\left[\underbrace{sP_s(\tilde{f})}_{} + (1-s)P_\beta(\tilde{f})\right] \qquad (5.7)$$

This was developed originally by Effelsberg & Peters (1983) for describing the behaviour of conserved scalars in turbulent shear flows – thus having a wider applicability than just jets. The δ and P_β functions account for the outer region and fully turbulent inner regions,

[6] *The standard set of model constants accurately captures spreading rates for a plane jet, but not a round jet.*

respectively. The underbraced term which accounts for the transition between these two regions, called the 'viscous superlayer', is modelled as follows:

$$P_s(\tilde{f}) = \frac{1-k}{(\tilde{f})^k} L(\tilde{f}) \qquad (5.8)$$

$$L(\tilde{f}) = \int_{\tilde{f}}^{1} (\tilde{f}_t)^{k-1} P_\beta(\tilde{f}_t) d\tilde{f}_t \qquad (5.9)$$

According to Effelsberg & Peters (1983), $\tilde{f}_t$ is "*a random variable whose statistics are equal to that of the fully turbulent part of the flow*" and "*instantaneously* $\tilde{f}_t$ *is the value at the boundary*" (between the fully turbulent part and the superlayer). Values for the variables *s* and *k* are calculated through an involved iterative procedure, but Effelsberg & Peters (1983) also provided some simple expressions for these quantities, based upon correlations developed for the heated plane wake behind a circular cylinder studied by LaRue & Libby (1974):

$$s = (1-I^2)^{0.25} \qquad (5.10)$$

$$k = 1-I^2 \qquad (5.11)$$

Alvani & Fairweather (2008) found that in the case of turbulent jets these simple expressions for *s* and *k* gave better performance than the involved iterative procedure, and consequently they adopted these simple forms. However, Effelsberg & Peters (1983) commented that "*These approximations can by no means be expected to be universal, but they do display a general tendency*", so there is some uncertainty as to their wider applicability.

5.3.6 Buoyancy Effects

The treatment of buoyancy in the turbulent transport equations was examined by Alvani (2004). For the variable density natural gas jet of Birch *et al*. (1978), Alvani found that incorporation of buoyancy effects made practically no difference to the predictions of mean and variance of mixture fraction. Whilst this observation is valid in the momentum-dominated region of the buoyant jet, it should not be assumed that this would hold for all flows of interest. Therefore, the effects of buoyancy should be included in the turbulent transport equations. This is an option which is already commonly available within commercial CFD software, such as ANSYS CFX.

5.3.7 Numerical Considerations

Although it is not possible to provide firm guidelines on mesh resolution in CFD simulations of flammability factor, it seems likely that a relatively fine mesh will be needed to resolve the spatial gradients of flow variables, particularly for the source terms in the intermittency transport equation.

It is not clear whether an implementation of sub-models for flammability factor may lead to numerical instabilities, but this is a possibility. The mixture fraction and intermittency should be bounded between zero and unity. If such bounds can be explicitly included in the model, this may aid numerical stability.

5.4 CODE VERIFICATION AND VALIDATION

5.4.1 Mean and Variance of Mixture Fraction

The first step in the implementation of the flammability factor model in commercial CFD software should be the testing of transport equations for the mean and variance of mixture fraction. If these equations are not already coded in the CFD software, they should be relatively straightforward to code, with turbulent scalar fluxes being modelled using an eddy viscosity-based gradient diffusion approximation. The performance of the model should then be tested against measurements of the mean and variance of mixture fraction for jets. For this purpose, comparisons can be made to the predictions shown in Chapter 4 of Alvani (2004) and the experimental datasets for natural gas jets of Birch *et al*. (1978) and the propane jet of Schefer & Dibble (2001). It is recommended to use the flow profiles of Alvani (2004) as appropriate inlet boundary conditions when simulating the Birch *et al*. (1978) experiments. Whilst Smith *et al*. (1986) presented data for mean mixture fraction measured on the axis of jets of natural gas, propane and simulated town gas, these data contribute little extra to that of Birch *et al*. (1978) and Schefer & Dibble (2001), apart from measurements at greater axial distances.

5.4.2 Probability Density Function

The second step in the implementation of the flammability factor model should be the integration of an appropriate PDF over the upper and lower flammability limits of a release. Initially, the two-part PDF of Janicka & Peters (1982) could be used, in conjunction with the turbulent intermittency correlation of Kent & Bilger (1976). For these sub-models, predictions for the PDF of mixture fraction on the axis of jets should be in good agreement with measurements. Appropriate datasets for model validation would again be those of Birch *et al*. (1978) and Schefer & Dibble (2001), which include measured PDFs on the axis of jets as well as at certain radial locations.

In addition to comparisons with measurements, it would be useful to also compare predictions at this stage to some of the earlier work of Alvani & Fairweather (2002), where they tested the performance of this two-part PDF with the correlation of Kent & Bilger (1976). Predictions of the flammability factor could also be compared to measured ignition probability for the data of Birch *et al*. (1979, 1981) and Smith *et al.* (1986). On the axis of the jets the predictions should be in good agreement with measurements and broadly in-line with those presented by Alvani (2004).

5.4.3 Intermittency

The next step should be the implementation of an intermittency transport equation within the framework of a k-ε model, Equations (5.1) to (5.5). Predictions of turbulent intermittency should be compared against measurements obtained in the propane jets by Schefer & Dibble (2001). The model could also be validated against the intermittency measurements for an air jet by Wygnanski & Fiedler (1967). The latter study has the advantage that detailed measurements of the flow field were also produced. For both of these jets, predictions should also be compared against those obtained by Alvani (2004).

5.4.4 Model Refinement

If resources permit, the final step in the implementation of the flammability factor model should be the three-part composite PDF, Equation (5.7). At this stage the performance of the model should be re-compared to the measurements of Birch *et al*. (1978) and Schefer & Dibble (2001) for the PDF of mixture fraction, as well as to ignition probabilities measured by Birch *et al*. (1979, 1981) and Smith *et al.* (1986). The model performance should now be very similar to that demonstrated by Alvani & Fairweather (2008).

Consideration should also be given to validation against other data on turbulent jets, such as that of Papadopoulos & Pitts (1998) for methane and propane, and that of Dowling & Dimotakis (1990), who investigated constant density releases comprising a jet of ethylene into nitrogen, and a jet of propylene into argon.

5.4.5 Crosswind Effects

In addition to the above validation against data on free turbulent jets, it is strongly recommended that predictions be compared to some of the more complex scenarios of practical interest. This could include jets in a crosswind, for which Birch *et al.* (1989) presented measurements of mean concentration on the symmetry plane, as well as on radial planes at four downstream locations. Other scenarios of interest could include impingement on surfaces, for which suitable data may exist in the literature. A short literature review should quickly establish the availability of further relevant data for model validation, although this is unlikely to extend to detailed PDFs or measurements of ignition probability.

5.4.6 Resource Implications

The effort required to implement and validate models for the prediction of flammability factor in commercial CFD software should not be under-estimated. For a full implementation of the above models this is likely to be of the order of a few months of effort, rather than a few weeks. However, if resources are very constrained then worthwhile benefits could still be realised using the simpler two-part PDF coupled with the intermittency correlation of Kent & Bilger (1976), as demonstrated by Schefer *et al*. (2010). Implementation and validation of this model would probably take about one month of effort if validation was restricted to data on jets.

5.5 APPLICATIONS

The issues which have been considered in the development and validation of CFD models for the prediction of ignition probability have largely been within the context of free turbulent flammable jets. This is unsurprising, as this class of flows has been investigated in great detail and so it provides a firm foundation for making modelling recommendations. However, the potential applications of CFD models are far wider-ranging than such simple flows – which in any case can conveniently be modelled using the empirical model described in Section 4.

The potential applications of a CFD model for the prediction of ignition probability could include:

- **Incident Investigations**: For incidents involving fires or explosions, the model could be used to help determine likely sources of ignition or to indicate the probability of

ignition of flammable releases which fortuitously did not ignite. The model is suitable for a wide range of flammable gases: natural gas, propane, ethylene, hydrogen, or mixtures of gases including inert gases such as carbon dioxide or nitrogen. The only data required in order to model a different substance is the static flammability limits, which are readily available or can be determined for mixtures, see for example Drysdale (1999) or Kondo *et al*. (2006).

- **Prediction of hazard range**: One of the key findings of the research on ignition probabilities is that gas clouds can be ignited in regions of the flow where the mean concentration is well below the LFL. Provision of the hazard range based on ignition probability may provide a firmer basis for decisions on hazard range than those based on criteria such as the common "50% of the LFL". Using the flammability factor model, the hazard range could be determined for flammable releases in complex industrial plant (both on- and off-shore), releases impinging on or affected by solid surfaces, releases affected by crosswinds or buoyancy, or any combination of these complexities.

- **Toxic Load**: It is possible to extend the flammability factor concept to analyse the toxic load a person may receive from atmospheric exposure to fluctuating concentrations of a toxic gas, aerosol or dust. In particular, the model would be useful for those chemicals for which the Specified Level of Toxicity (SLOT) and Significant Likelihood of Death (SLOD) are highly sensitive to the concentration of the toxic substance[7]. For instance, the toxic load for CO_2 is proportional to its concentration to the power eight ($TL \propto \tilde{c}^8$). In atmospheric releases involving CO_2, it is therefore important to account not only for the mean gas concentration but also the fluctuations about the mean, which could rapidly cause toxic loads to reach SLOT or even SLOD levels. The methods described in this report could readily be applied to study the toxic loads, since it involves essentially the same principles of determining the proportion of time a gas concentration remains at a given level.

[7] http://www.hse.gov.uk/hid/haztox.htm, *accessed July 2010.*

6 CONCLUSIONS

Explosion measurements have been presented for premixed CO_2 and propane or methane mixtures in two different scale tests: a 20 litre sphere and a 1.04 m diameter pipe. The explosion overpressures were found to decrease monotonically as the CO_2 concentration was increased in both sets of tests. For the 20 litre sphere, concentrations greater than 15% vol/vol in the CO_2-methane-air mixture were needed in order to suppress the explosion completely. The results were broadly in agreement with previous results published in the literature. In the larger-scale pipe tests, no ignition of the gas mixture was found to occur for a CO_2 concentration of 12% vol/vol. The fact that this concentration was lower than the value achieved in the 20 litre sphere tests was attributed to incomplete mixing of the gases in the larger scale tests.

A brief introduction was provided to various analytical techniques that can be used to assess the flammability of non-premixed gas flows. A simple empirically-based model was then presented for the flammability factor in free, unobstructed, gas jets. This was validated against the previously published works of Birch *et al*. (1981) and Smith *et al*. (1986), and used to predict the ignition probability in free-jets of methane and CO_2, for which new experimental data was also presented.

The results showed that the ignitable region in a jet of methane containing 20% CO_2 in the feed gas was smaller than that in the equivalent pure methane release, as expected. The model and the experiments demonstrated that it is possible to ignite gas jets at points in the flow where the mean concentration was either below the LFL or above the UFL. This has implications for safety cases involving MAH events associated with new plants or de-commissioning of existing hydrocarbon containing process plant.

The agreement between the flammability factor predicted by the empirical model and the measured ignition probability was reasonably good in the near-field of the jet but was found to deteriorate further downstream. The model predictions were significantly higher here than those measured, with the measured ignition probabilities remaining below 60% even where it was predicted for gas concentrations to be within the flammable range for the vast majority of the time. The difference between modelled and measured behaviour was attributed to the effect of the wind in the experiments, which were conducted in a walled courtyard that was open to the atmosphere. The results provide an important lesson and demonstrate that care should be exercised in applying free-jet flammability factor models to assess hazards in realistic environments, where the effects of even moderate winds may be significant.

Bulk ignition experiments were also conducted, in which jets of methane mixed with varying quantities of CO_2 were released in air and ignited using a propane blow torch. Three different release velocities were examined and the resulting ignition behaviour was classified according to a set of five criteria. The results showed that in some situations where a stable flame could not be sustained, the fuel present in the CO_2-methane jet still promoted combustion. If, in a MAH event, a partially inerted mixture was released onto a continuous ignition source, such as an on-going hydrocarbon fire, these results show that it could potentially add to the severity of the fire.

A final section of this study examined the feasibility of using CFD to extend predictions of the flammability factor beyond simple jet flows. Previous work in this field was examined in detail, and a simplified methodology was proposed which retains many of the benefits of more sophisticated approaches. To implement and test such models would be by no means trivial, but it would enable predictions of ignition probability to be obtained in flows that are of practical importance in risk assessment and incident investigation.

Models for the flammability of hydrocarbon and CO_2 gas clouds can easily be extended to consider other gas mixtures. Applications include discharges from storage tanks with nitrogen-inerting systems, and hydrogen and inert gas mixtures used in pre-combustion CO_2-capture power stations. The same fundamental principles of the flammability factor can also be used to analyse the toxic load a person may receive from atmospheric exposure to fluctuating concentrations of a toxic gas, aerosol or dust.

7 REFERENCES

ALVANI, R. F. (2004) *Mathematical modelling of the ignition characteristics of flammable jets*. PhD Thesis, University of Leeds.

ALVANI, R. F. & FAIRWEATHER, M. (2002) Ignition characteristics of turbulent jet flows. *Trans IChemE,* 80, p917-923.

ALVANI, R. F. & FAIRWEATHER, M. (2008) Prediction of the ignition characteristics of flammable jets using intermittency-based turbulence models and a prescribed pdf approach. *Computers and Chemical Engineering,* 32, p371-381.

ASTM (2005) Standard practices for determining limits of flammability of chemicals at elevated temperature and pressure. ASTM E918 - 83(2005), ASTM International, West Conshohocken, Pennsylvania, USA.

ASTM (2009) Standard test method for concentration limits of flammability of chemicals (vapors and gases). ASTM E681 - 09, ASTM International, West Conshohocken, Pennsylvania, USA.

BECKER, H. A., HOTTEL, H. C. & WILLIAMS, G. C. (1967) The nozzle-field concentration field of the round turbulent, free jet. *J. Fluid Mech.,* 30, p285-303.

BEYLER, C. L. (2002) Flammability limits of premixed and diffusion flames. In DINENNO, P. J., DRYSDALE, D., BEYLER, C. L., WALTON, W. D., CUSTER, R. L. P., HALL, J. R. & WATTS, J. W. (Eds.) *SFPE Handbook of Fire Protection Engineering*, Society of Fire Protection Engineers, Bethesda, Maryland.

BILGER, R. W. (1980) Turbulent flows with non-premixed reactants. In LIBBY, P. A. & WILLIAMS, F. A. (Eds.) *Turbulent Reacting Flows*, Springer-Verlag.

BIRCH, A. D., BROWN, D. R., COOK, D. K. & HARGRAVE, G. K. (1988) Flame stability in under-expanded natural gas jets. *Combust. Sci. and Tech.,* 58, p267-280.

BIRCH, A. D., BROWN, D. R. & DODSON, M. G. (1981) Ignition probabilities in turbulent mixing flows. *18th Symposium (International) on Combustion*, p1775-1780.

BIRCH, A. D., BROWN, D. R., DODSON, M. G. & THOMAS, J. R. (1978) The turbulent concentration field of a methane jet. *J. Fluid Mech.,* 88, p431-449.

BIRCH, A. D., BROWN, D. R., DODSON, M. G. & THOMAS, J. R. (1979) Studies of flammability in turbulent flows using laser Raman spectroscopy. *17th Symposium (International) on Combustion*, The Combustion Institute, p301-314.

BIRCH, A. D., BROWN, D. R., FAIRWEATHER, M. & HARGRAVE, G. K. (1989) An experimental study of a turbulent natural gas jet in a cross-flow. *Combust. Sci. and Tech.,* 66, p217-232.

BSI (2004) Determination of explosion limits of gases and vapours. BS EN 1839:2003, The British Standards Institution, London, UK.

CANT, S. R. & MASTORAKOS, E. (2008) *An introduction to turbulent reacting flows*. Imperial College Press.

CHATWIN, P. C. & SULLIVAN, P. J. (1990) A simple and unifying physical interpretation of scalar fluctuation measurements from many turbulent shear flows. *J. Fluid Mech.*, 212, p533-556.

CHATWIN, P. C. & SULLIVAN, P. J. (1993) The structure and magnitude of concentration fluctuations. *Boundary-Layer Meteorology*, 62, p269-280.

CHEN, C. J. & RODI, W. (1980) *Vertical turbulent buoyant jets: a review of experimental data*. Pergamon Press.

CHEN, J. Y. (1987) Second-order conditional modelling of turbulent non-premixed flames with a composite PDF. *Combust. Flame*, 69, p1-36.

CHO, J. & CHUNG, M. K. (1992) A k-ε-γ equation turbulence model. *J. Fluid Mech.*, 237, p301-322.

COWARD, H. F. & JONES, G. W. (1952) Limits of flammability of gases and vapors. Bulletin 503, Bureau of Mines, U.S. Government Printing Office.

DE SMEDT, G., DE CORTE, F., NOTELÉ, R. & BERGHMANS, J. (1999) Comparison of two standard test methods for determining explosion limits of gases at atmospheric conditions. *J. Hazardous Mater.*, A70, p105-113.

DOPAZO, C. (1977) On conditional averages for intermittent turbulent flows. *J. Fluid Mech.*, 81, p433-438.

DOWLING, D. R. & DIMOTAKIS, P. E. (1990) Similarity of the concentration field of gas-phase turbulent jets. *J. Fluid Mech.*, 218, p109-141.

DRYSDALE, D. (1999) *An Introduction to Fire Dynamics*. John Wiley & Sons.

EFFELSBERG, E. & PETERS, N. (1983) A composite model for the conserved scalar PDF. *Combust. Flame*, 50, p351-360.

FAIRWEATHER, M., JONES, W. P., LEDIN, H. S. & LINDSTEDT, R. P. (1992) Predictions of soot formation in turbulent non-premixed propane flames. *24th Symposium (International) on Combustion*, The Combustion Institute, p1067-1074.

GANT, S. E. (2009) Quality and reliability issues with large-eddy simulation. Health and Safety Laboratory Report MSU/2008/10.

ISHIZUKA, S. & TSUJI, H. (1981) An experimental study of effect of inert gases on extinction of laminar diffusion flames. *18th Symposium (International) on Combustion*, The Combustion Institute, p695-703.

ISO (2010) Gases and gas mixtures - determination of fire potential and oxidising ability for the selection of cylinder valve outlets. ISO 10156:2010, International Organization for Standardization (ISO), Geneva, Switzerland.

JANICKA, J. & PETERS, N. (1982) Prediction of turbulent jet diffusion flame lift-off using a PDF transport equation. *Proceedings of the Combustion Institute*, 19, p367-374.

JONES, W. P. (1994) Turbulence modelling and numerical solution methods for variable density and combusting flows. In LIBBY, P. A. & WILLIAMS, F. A. (Eds.) *Turbulent Reactive Flows*, Academic Press.

JONES, W. P. & LAUNDER, B. E. (1972) The prediction of laminarization with a two-equation model of turbulence. *Int. J. Heat Mass Transfer*, 15, p301-314.

JONES, W. P. & MUSONGE, P. (1988) Closure of the Reynolds stress and scalar flux equations. *Phys. Fluids*, 31, p3589-3604.

KENT, J. H. & BILGER, R. W. (1976) The prediction of turbulent diffusion flame fields and nitric oxide formation. *16th Symposium (International) on Combustion*, The Combustion Institute, p1643-1656.

KONDO, S., TAKIZAWA, K., TAKAHASHI, A. & TOKUHASHI, K. (2006) Extended Le Chatelier's formula for carbon dioxide dilution effect on flammability limits. *J. Hazardous Mater.*, A138, p1-8.

LARUE, J. C. & LIBBY, P. A. (1974) Temperature fluctuations in the plane turbulent wake. *Phys. Fluids*, 17, p1956-1967.

LAUNDER, B. E. & SANDHAM, N. D. (2002) *Closure strategies for turbulent and transitional flows*. Cambridge University Press.

LIBBY, P. A. (1975) On the prediction of intermittent turbulent flows. *J. Fluid Mech.*, 68, p273-295.

MOLE, N. (2006) The α-β model for concentration moments in turbulent flows. *Environmetrics*, 6, p559-569.

MOLNARNE, M., MIZSEY, P. & SCHRÖDER, V. (2005) Flammability of gas mixtures. Part 2: Influence of inert gases. *J. Hazardous Mater.*, A121, p45-49.

PAPADOPOULOS, G. & PITTS, W. M. (1998) Scaling the near-field centerline mixing behavior of axisymmetric turbulent jets. *AIAA J.*, 36, p1635-1642.

POPE, S. B. (1978) An explanation of the turbulent round-jet/plane-jet anomaly. *AIAA Journal*, 16, p279-281.

RANGA DINESH, K. K. J., SAVILL, A. M., JENKINS, K. W. & KIRKPATRICK, M. P. (2010) LES of intermittency in a turbulent round jet with different inlet conditions. *Computers & Fluids*, 39, p1685-1695.

SAIMA, A. & HIGAKI, M. (1988) Turbulent diffusion of fuel gas jet without flames. *Experimental Heat Transfer, Fluid Mechanics and Thermodynamics*.

SAVILL, A. M. (2002a) By-pass transition using conventional closures. In LAUNDER, B. E. & SANDHAM, N. D. (Eds.) *Closure strategies for turbulent and transitional flows*, Cambridge University Press.

SAVILL, A. M. (2002b) New strategies in modelling by-pass transition. In LAUNDER, B. E. & SANDHAM, N. D. (Eds.) *Closure strategies for turbulent and transitional flows*, Cambridge University Press.

SCHEFER, R. W. & DIBBLE, R. W. (2001) Mixture fraction field in a turbulent nonreacting propane jet. *AIAA J.*, 39, p64-72.

SCHEFER, R. W., EVANS, G. H., ZHANG, J., RUGGLES, A. J. & GREIF, R. (2010) Ignitability limits for combustion of unintended hydrogen releases: experimental and theoretical results. *Int. J. Hydrogen Energy*, Accepted for publication.

SHAUGHNESSY, E. J. & MORTON, J. B. (1977) Laser light-scattering measurements of particle concentration in a turbulent jet. *J. Fluid Mech.,* 80, p129-148.

SMITH, M. T. E., BIRCH, A. D., BROWN, D. R. & FAIRWEATHER, M. (1986) Studies of ignition and flame propagation in turbulent jets of natural gas, propane and a gas with a high hydrogen content. *21st Symposium (International) on Combustion*, The Combustion Institute, p1403-1408.

THYER, A. M., KAY, J. & GANT, S. E. (2009) Investigations into the flammability of propane/carbon dioxide, hydrogen/carbon dioxide and hydrogen/nitrogen mixtures. *Proc. IChemE Hazards XXI Symposium & Workshop,* Manchester, UK.

TRIANTAFYLLIDIS, A., MASTORAKOS, E. & EGGELS, R. L. G. M. (2009) Large eddy simulation of forced ignition of a non-premixed bluff-body methane flame with conditional moment closure. *Combust. Flame,* 156, p2328-2345.

VERSTEEG, H. K. & MALALASEKERA, W. (2007) *An introduction to computational fluid dynamics: the finite volume method*. Pearson Education Ltd.

WYGNANSKI, I. & FIEDLER, H. (1967) Some measurements in the self-preserving jet. *J. Fluid Mech.,* 38, p577-612.

ZABETAKIS, M. G. (1965) Flammability characteristics of combustible gases and vapors. Bulletin 627, Bureau of Mines, U.S. Government Printing Office.

8 APPENDIX A: EXPERIMENTAL DATA

8.1 20 LITRE EXPLOSION SPHERE

Table 4 Explosion tests results for mixtures of methane, CO_2 and air in the 20 litre sphere.

Test Number	*CH_4 (%$^v/_v$)*	*CO_2 (%$^v/_v$)*	*CH_4 (%$^v/_v$)*	*CO_2 (%$^v/_v$)*	*Air (%$^v/_v$)*	*P_{max} (barg)*	*dP/dt (bar s^{-1})*
	—Feed Concentrations—		*————Final Concentrations———*				
1	100	0	10	0	90	7.403	382.9
2	50	50	10	10	80	5.795	74.2
3	40	60	10	15	75	2.724	3.3
5	37	63	10	17	73	0	0
4	33	67	10	20	70	0	0

Table 5 Explosion tests results for mixtures of propane, CO_2 and air in the 20 litre sphere.

Test Number	*C_3H_8 (%$^v/_v$)*	*CO_2 (%$^v/_v$)*	*C_3H_8 (%$^v/_v$)*	*CO_2 (%$^v/_v$)*	*Air (%$^v/_v$)*	*P_{max} (barg)*	*dP/dt (bar s^{-1})*
	—Feed Concentrations—		*————Final Concentrations———*				
1	100	0	5	0	95	7.672	360.7
3	33	67	5	10	85	4.931	23.7
4	25	75	5	15	80	0.627	2.4
5	22	78	5	17.5	77.5	0.303	1.1
2	20	80	5	20	75	0	0

8.2 1.04 M DIAMETER PIPE

Table 6 Explosion tests results for mixtures of methane, CO_2 and air in the 1.04 m diameter pipe.

Test Number	*CH_4 (%$^v/_v$)*	*CO_2 (%$^v/_v$)*	*CH_4 (%$^v/_v$)*	*CO_2 (%$^v/_v$)*	*Air (%$^v/_v$)*	*P_{max} (barg)*
	—Feed Concentrations—		*————Final Concentrations———*			
1	100	0	9.3	0	90.7	0.724
3	71.8	28.2	9.4	3.7	86.9	0.360
4	60.0	40.0	10.5	7.0	82.5	0.211
2	40.6	59.4	8.2	12.0	79.8	0.000

8.3 JET CONCENTRATION ANALYSIS

8.3.1 Axial measurements for pure methane jet

Distance from Release point (cm)	*CH_4 (% vol/vol)*
5	59.9
10	34.4
20	18.2
25	13.8
30	8.6
40	6.7
50	5.4
70	3.2
90	1.6

8.3.2 Axial measurements for 80% methane, 20% CO_2 jet

Distance from release point (cm)	*CH_4 (% vol/vol)*	*CO_2 (% vol/vol)*	*Combined (% vol/vol)*
5	46.0	14.2	60.2
10	26.9	8.6	35.6
20	13.4	3.7	17.2
25	10.5	2.7	13.2
30	7.1	1.7	8.8
40	5.5	1.3	6.8
50	3.5	0.9	4.4
70	2.9	0.8	3.7
90	2.3	0.7	3.0

8.3.3 Measurements at radial offset of 4cm for pure methane jet

Distance from release point (cm)	*CH_4 (% vol/vol)*
30	6.1
40	6.5
70	3.3

8.3.4 Measurements at radial offset of 4cm Offset for 80% methane, 20% CO_2 jet

Distance from release point (cm)	*CH_4 (% vol/vol)*	*CO_2 (% vol/vol)*	*Combined (% vol/vol)*
30	3.8	0.9	4.8
40	4.9	1.2	6.1
70	2.6	0.7	3.3

8.4 JET IGNITION ANALYSIS

8.4.1 Axial measurements for pure methane jet

Distance from release point (cm)	*Attempts*	*Ignitions*	*Probability*
20	463	60	0.13
25	271	77	0.28
30	188	108	0.57
40	189	107	0.57
50	324	107	0.33
70	200	0	0.00

8.4.2 Axial measurements for 80% methane, 20% CO_2 jet

Distance from release point (cm)	*Attempts*	*Ignitions*	*Probability*
20	339	108	0.32
25	190	108	0.57
30	185	108	0.58
40	233	107	0.46
50	166	2	0.01
70	200	0	0.00

8.4.3 Measurements at radial offset of 4cm for pure methane jet

Distance from release point (cm)	*Attempts*	*Ignitions*	*Probability*
30	326	105	0.32
40	277	105	0.38

8.4.4 Measurements at radial offset of 4cm Offset for 80% methane, 20% CO_2 jet

Distance from release point (cm)	*Attempts*	*Ignitions*	*Probability*
30	364	69	0.19
40	359	70	0.19

8.5 IGNITION RESPONSE

Figure 43 compares the pure methane flame produced at the three different exit velocities of 17.1 m/s, 29.5 m/s and 53.1 m/s. Using image analysis, the flame stand off height was determined to be 0.8 cm at the lowest velocity, 4.1 cm at the intermediate velocity and 8.3 cm at the highest velocity. This demonstrated the competition between the advancing gas velocity and the flame front speed in determining the stability of the flame.

Figure 44 shows an example of a Class 3 ignition for a gas mixture containing 16.7% vol/vol CO_2 with a release velocity of 53.1m/s. In the initial frames it can be seen that the gas burnt in the presence of the pilot flame, however once this was removed the flame front was blown downstream and extinguished.

Figures 45, 46 and 47 show images from the flame stability tests for exit velocities of 17.7 m/s, 29.5 m/s and 53.1 m/s respectively. For each exit velocity the first three images show flames that had either Class 5 or 4 stability, i.e. it was not necessary to use a pilot light to maintain the flame. In each series of photographs it is seen that the flame front stand off distance increased with an increase in the CO_2 concentration, demonstrating that the flame front velocity deceased as the concentration of CO_2 increased. Beyond the threshold CO_2 concentration of 33.3% vol/vol, 20% vol/vol and 11.1% vol/vol, for exit velocities of 17.7 m/s, 29.5 m/s and 53.1 m/s, respectively, it was not possible to maintain a stable flame.

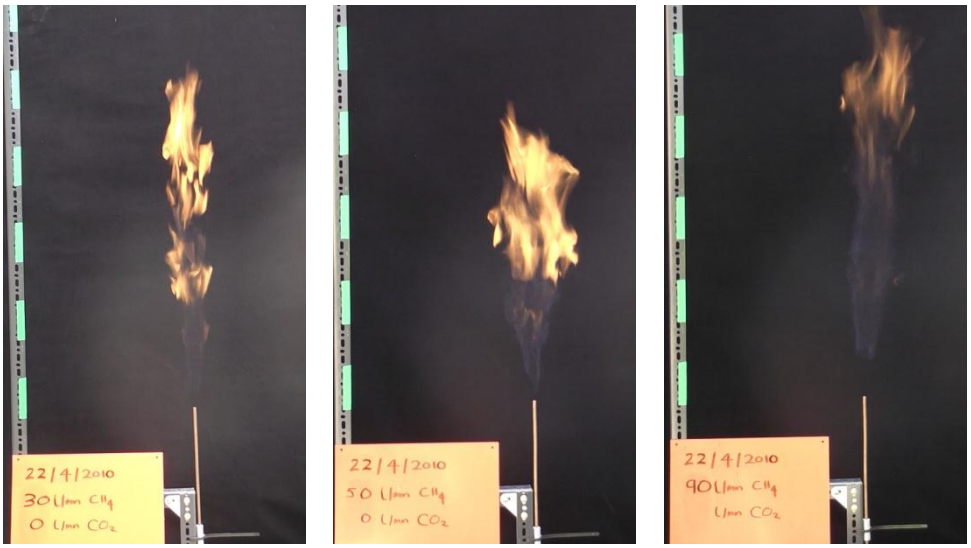

(a) 17.1 m/s **(b) 29.5 m/s** **(c) 53.1 m/s**

Figure 43 Comparison of the pure methane flames at different exit velocities

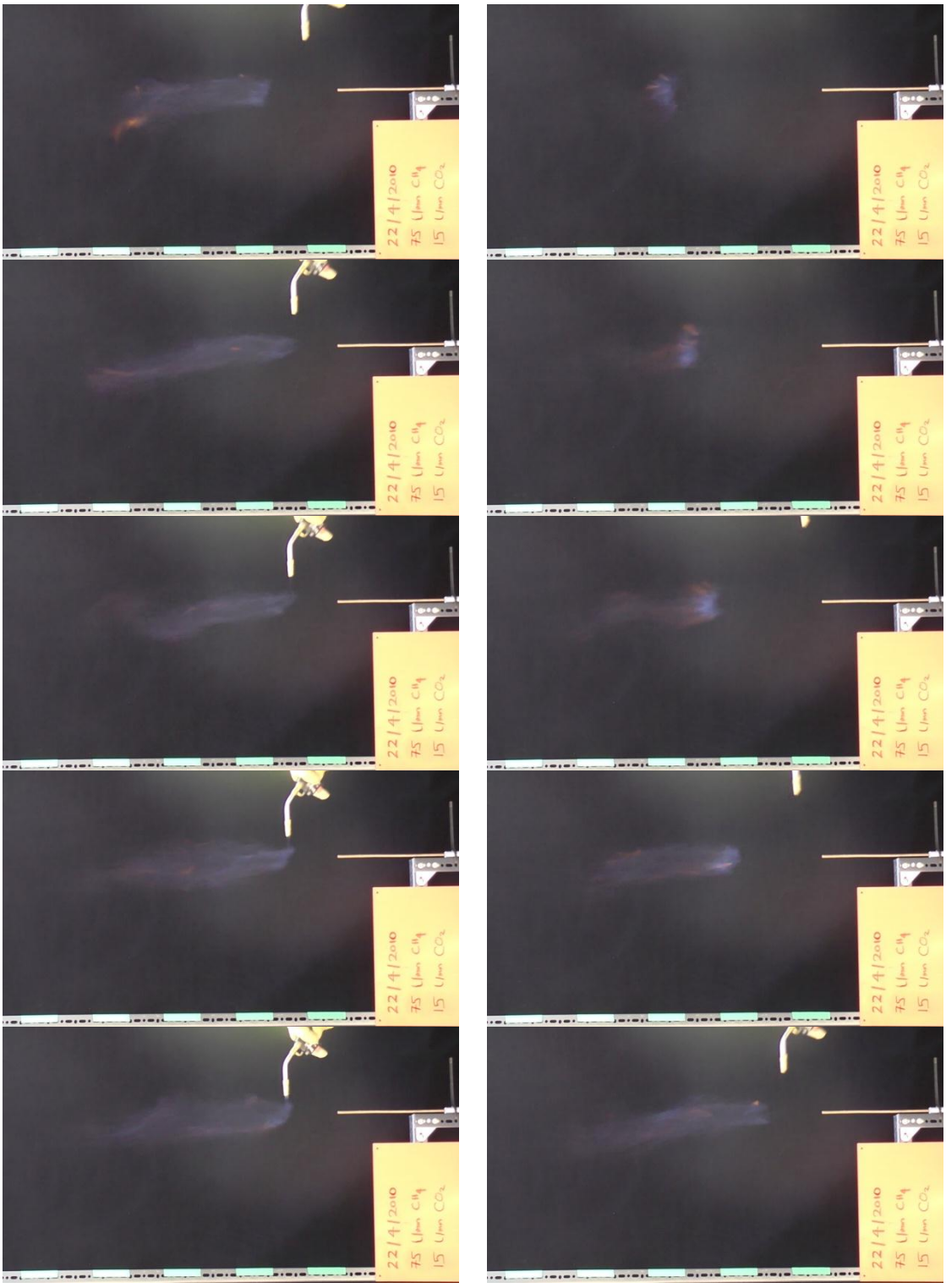

Figure 44 Class 3 ignition response with a gas mixture containing 16.7% CO_2. The release velocity was 53.1 m/s and the image time step was 1/25 s.

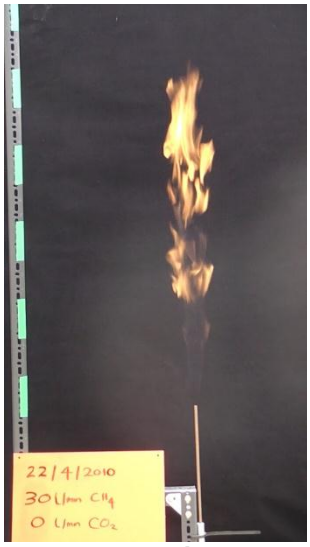

0% CO_2: Class 5

16.7% CO_2: Class 5

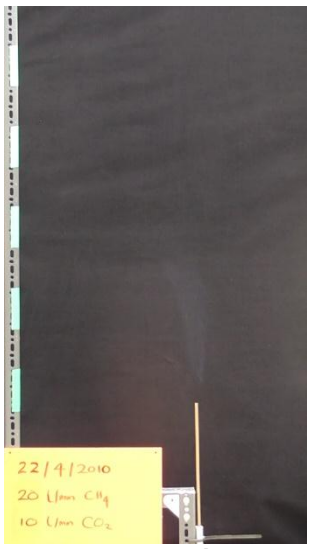

33.3% CO_2: Class 4

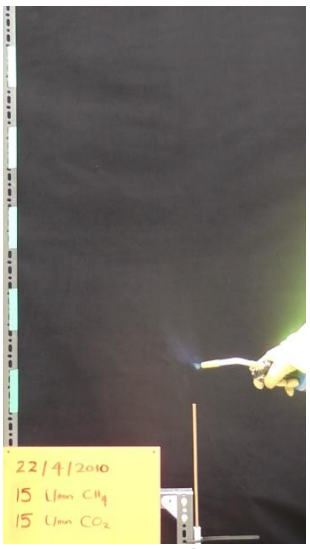

50% CO_2: Class 2

Figure 45 Ignition class tests for an exit velocity of 17.7 m/s and CO_2 concentrations from 0% to 60% vol/vol.

0% CO_2: Class 5

10% CO_2: Class 5

20% CO_2: Class 4

30% CO_2: Class 3

40% CO_2: Class 2

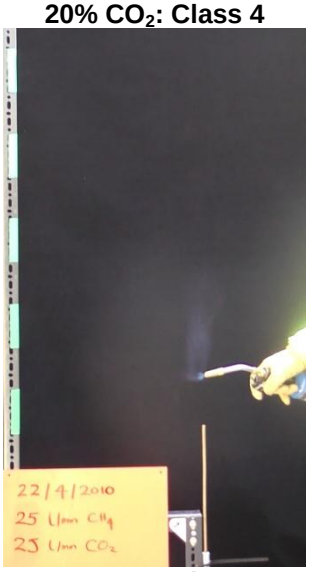

50% CO_2: Class 2

60% CO_2: Class 1

Figure 46 Ignition class tests for an exit velocity of 29.5 m/s and CO_2 concentrations from 0% to 60% vol/vol.

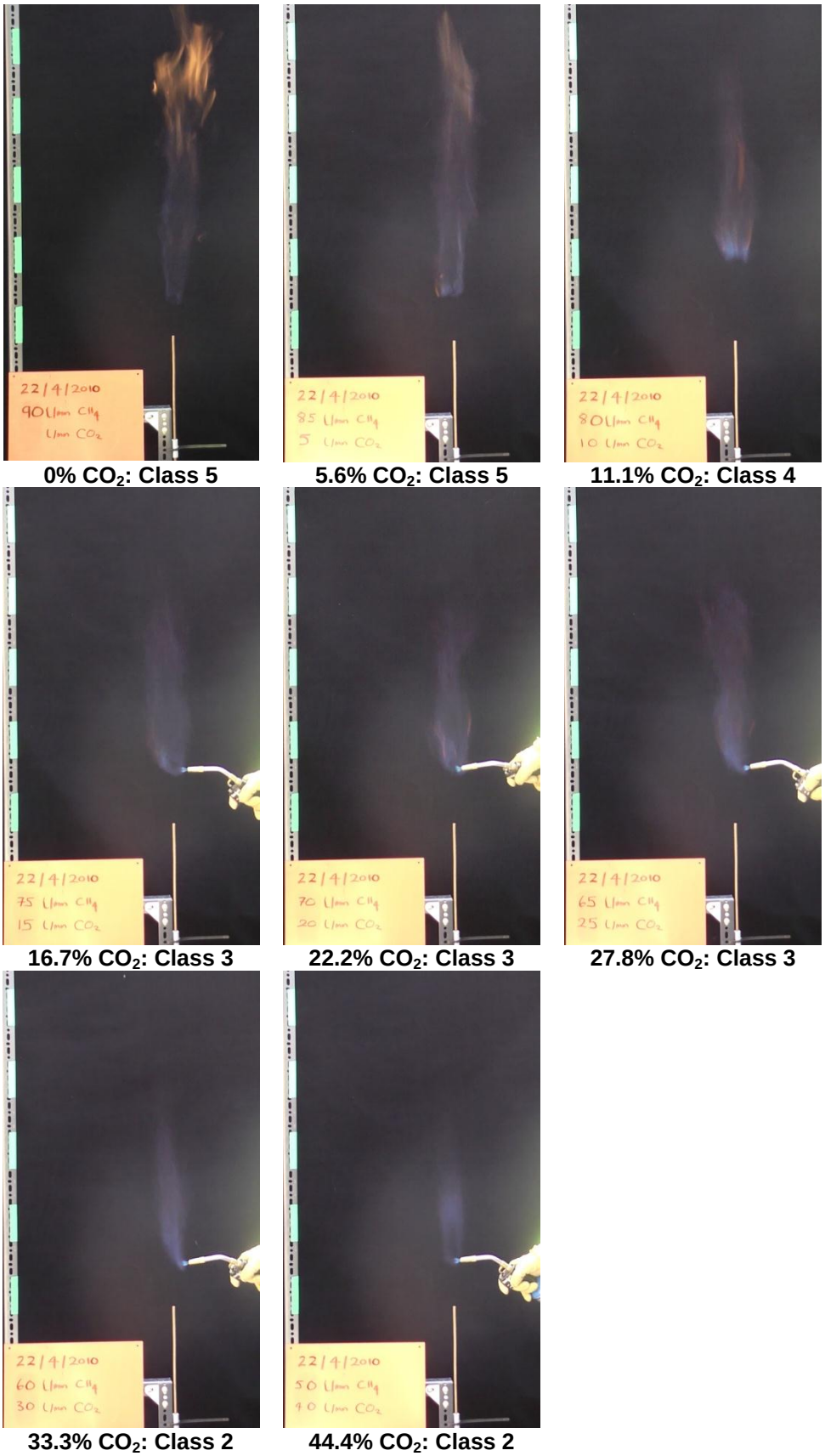

Figure 47 Ignition class tests for an exit velocity of 53.1 m/s and CO_2 concentrations from 0% to 44.4% vol/vol.

9 APPENDIX B: EMPIRICAL FLAMMABILITY FACTOR MODEL

9.1 SIMPLE MODEL FOR JET AXIS

The simple model for the flammability factor, described below, provides practically identical predictions to that of the free-jet model presented in Section 4. It is also slightly easier to implement and so can be readily coded into Microsoft Excel. However, it is only valid along the jet centreline, whereas the model presented in Section 4 can be used to calculate the flammability factor at radial positions away from the jet axis.

The principal simplifications of the model are that it does not require the turbulence intermittency to be calculated, the mathematical formula for the RMS concentration profile is considerably simpler and a pure Gaussian profile is adopted for the concentration PDF instead of a two-part PDF. Although the tails of the Gaussian PDF may in theory provide unphysical values (i.e. concentrations volume fractions below zero and above one), along the centreline where the jet is flammable the effect of this is small.

9.1.1 Mean Concentration

The mean velocity and concentration profiles along the centreline are identical to those presented in Section 4, Equations (4.1) to (4.5), with the same choice of model constants.

9.1.2 RMS Concentration

In the self-similar region of the jet, the centreline RMS values of the velocity and concentration (u' and c') both tend to constant fractions of the local mean velocity and concentration. To determine the RMS concentration, rather than use the α-β model of Chatwin & Sullivan (1990), it can therefore be determined from the mean concentration as follows:

$$\left(\frac{c'}{C}\right)_{cl} = b \qquad (9.1)$$

where b is a constant. From their review of previous experiments, Chen & Rodi (1980) found that the ratio $(c'/C)_{cl}$ takes a value of between 0.21 and 0.24 in round jets with density ratios close to unity. Following the work of Smith *et al*. (1986), in the present simple model the value of b is taken as 0.22. The sensitivity of the flammability factor to variations in b between values of 0.2 and 0.3 are shown in Figure 48.

9.1.3 Probability Density Function

Along the centreline of a free-jet, the concentration PDF is approximated as a Gaussian distribution:

$$P(\tilde{c}) = \frac{1}{\sqrt{2\pi\overline{c^2}}} \exp\left[-\frac{(\tilde{c}-C)^2}{2\overline{c^2}}\right] \qquad (9.2)$$

To determine the flammability factor, this PDF is integrated between the upper and lower flammability limits (c_U and c_L).

Although the Gaussian distribution cannot be integrated analytically, most mathematical modelling packages such as MatLab and Excel have subroutines to efficiently calculate error functions (*ERF*) which can be used for this purpose. The error function is defined as follows:

$$ERF(x) = \frac{2}{\sqrt{\pi}} \int_0^x \exp\left(-y^2\right) dy \qquad (9.3)$$

and the flammability factor is then determined as follows:

$$F = \frac{1}{2}\left[ERF\left(\frac{c_U - C}{\sqrt{2\overline{c^2}}} \right) - ERF\left(\frac{c_L - C}{\sqrt{2\overline{c^2}}} \right) \right] \qquad (9.4)$$

This can be implemented in MatLab using, for example, the following commands:

```
etaU(i) = (ufl/100.0 - c0(i)) / (max(cRMS0(i) , tiny) * sqrt(2.0));
etaL(i) = (lfl/100.0 - c0(i)) / (max(cRMS0(i) , tiny) * sqrt(2.0));
ff0(i)=0.5 * (erf( etaU(i) ) - erf( etaL(i) ) );
```

where `ufl` and `lfl` are the upper and lower flammability limits (in percent by volume), `c0` and `cRMS0` are mean and RMS concentrations and `ff0` is the resulting flammability factor. The parameter `tiny` is a very small number that is introduced to ensure the calculation remains bounded when the RMS concentration falls to zero. In the present work it was set to a value of 10^{-8} and tests were conducted to ensure that it had no effect on the results.

In Microsoft Excel, the equivalent formulae are implemented as follows:

```
etaU(i) = (ufl/100.0 - c0(i)) / (max(cRMS0(i) , tiny) * sqrt(2.0));
etaL(i) = (lfl/100.0 - c0(i)) / (max(cRMS0(i) , tiny) * sqrt(2.0));
ff0(i)=0.5 * ( SIGN(etaU(i)) * ERF( ABS(etaU(i)) ) -
                                SIGN(etaL(i)) * ERF( ABS(etaL(i)) ) );
```

9.1.4 Results

Predictions of the flammability factor using the simple model described above are compared in Figure 48 to those obtained using the more complex model described in Section 4. The results shown are for the natural gas jet experiments studied by Smith *et al*. (1986), which involved an exit velocity of 50 m/s, orifice diameter of 6.35 mm and Reynolds number of 21,750. Figure 48 shows that the simple model with a coefficient of b = 0.20 provides practically identical results to those obtained with the more complex flammability factor model presented in Section 4. Results with a coefficient of b = 0.22 are just a few percent different, whilst those obtained with b = 0.30 show a more marked deviation, with a reduction in the peak flammability factor and a wider spread along the axis of the jet. The results obtained by Smith *et al*. (1986), using their own flammability factor model were presented earlier in Figure 23.

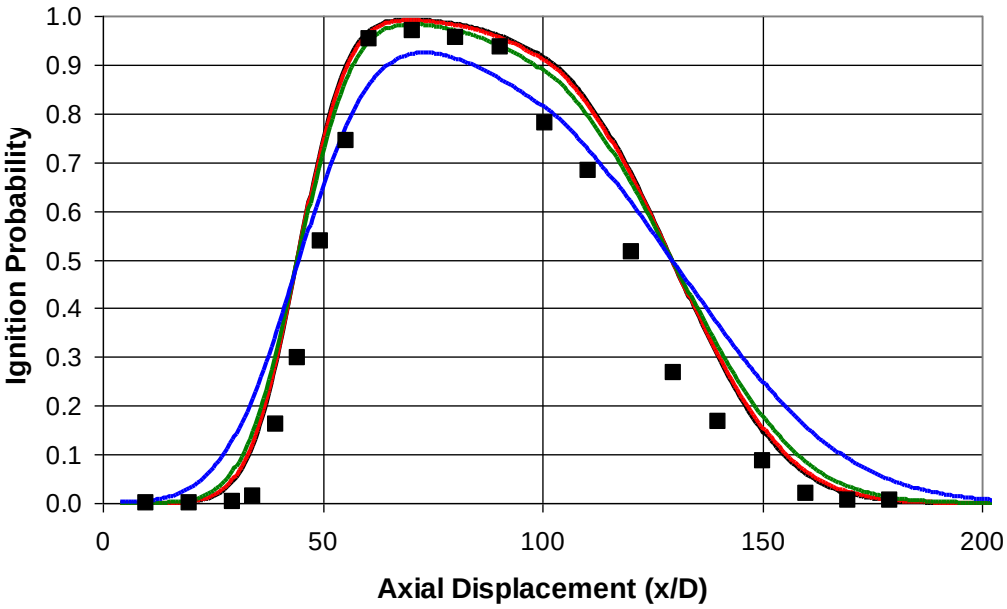

Figure 48 Flammability factor predicted by the standard model (**–**), and the simple model using constants: – b = 0.20; – b = 0.22; – b = 0.30; compared to the ignition probability (■) measured in the natural gas jet experiments of Smith *et al*. (1986).

9.2 FREE-JET MODEL IMPLEMENTATION AND SENSITIVITY

9.2.1 Implementation Issues

To implement the free-jet flammability factor model described in Section 4, a number of numerical clips and limiters were used to ensure that the model provided bounded results and did not produce numerical errors. These are described below.

Maximum Mean Concentration and Velocity

Close to the pipe orifice, in the potential core of the jet, the mean concentration on the jet centreline is equal to that in the pipe (i.e. a volume fraction of gas of unity) and the mean velocity is equal to the velocity at the orifice (which is assumed here to have a top-hat velocity profile). In implementing the free-jet model, on the centreline of the jet the maximum value of the mean concentration was therefore limited to a volume fraction of 1.0 and the mean velocity was limited to the jet exit velocity. The empirical profiles, given by Equations (4.2) and (4.3), are such that the mean concentration and velocity can otherwise exceed the values at the orifice, which is clearly unphysical.

Intermittency

The turbulent intermittency is bounded between values of zero and one. It is not physically possible to have negative intermittency or values greater than one. The Kent & Bilger (1976) intermittency model, which is written mathematically:

$$I = \frac{K+1}{\left[\left(\frac{\overline{c^2}}{C^2}\right)+1\right]} \tag{9.5}$$

was therefore implemented as follows:

$$I = \min\left\{\frac{(K+1)C^2}{\max\left[\left(\overline{c^2}+C^2\right), tiny\right]}, 1\right\} \tag{9.6}$$

The 'max' clip in the denominator of this expression is used to ensure that the model remains bounded at the fringes of the jet, where the mean and RMS concentrations fall to zero. The parameter *tiny* was a very small number that in the present work was set to a value of 10^{-8}. Tests were conducted to ensure that changing its magnitude had no effect on the results.

Conditional Mean Concentration and Variance

To avoid divide-by-zero problems when the intermittency was zero (i.e. outside the jet), expressions for the conditional mean concentration and variance were derived from Equations (4.7, 4.8 and 4.9) as follows:

$$C_c = C_{cl} S \tag{9.7}$$

$$\overline{c_c^2} = C_{cl}^2\left[\beta(\alpha - T)S - S^2 - ST\right] \tag{9.8}$$

where parameters *S* and *T* are given by:

$$S = \max\left[\frac{\alpha\beta + (1-\beta)T}{(K+1)}, T\right] \tag{9.9}$$

$$T = \exp\left[-K_C\left(\frac{r}{x'}\right)^2\right] \tag{9.10}$$

At large radii, outside the jet, where *T* tends to zero, the conditional mean concentration and variance tend to the following values:

$$C_c\big|_{r\to\infty} = C_{cl}\frac{\alpha\beta}{(K+1)} \tag{9.11}$$

$$\overline{c_c^2}\Big|_{r\to\infty} = C_{cl}^2 K\left[\frac{\alpha\beta}{(K+1)}\right]^2 \tag{9.12}$$

9.2.2 Model Sensitivity

Decay Rate of Centreline Mean Concentration and Velocity

In the intermediate region of the free-jet, at a dimensionless axial distance, *x**, between 0.5 and 5.0, the mean centreline velocity and concentration are given by:

$$U_{cl} = a_U U_0 Fr^{-1/10} \left(\frac{\rho_0}{\rho_a} \right)^{9/20} \left(\frac{x'}{D} \right)^{-4/5} \qquad (9.13)$$

$$C_{cl} = a_C C_0 Fr^{1/8} \left(\frac{\rho_0}{\rho_a} \right)^{-7/16} \left(\frac{x'}{D} \right)^{-5/4} \qquad (9.14)$$

Values of 7.1 and 4.2 are taken for the constants a_U and a_C, respectively. These differ slightly from the values given by Chen & Rodi (1980) and Smith *et al*. (1986) who used, respectively, a_U = 7.26 and a_C = 0.44, and a_C = 4.4. The values have been chosen in the present study to produce smooth transitions in velocity and concentration between the momentum-dominated and intermediate regions, whereas the values given by used by Chen & Rodi (1980) and Smith *et al*. (1986) produce steps in the profiles, as shown by Figures 49 to 51. The choice of constant a_C = 0.44 by Chen & Rodi (1980) appears to be a typographical error which was corrected by Smith *et al*. (1986) to a_C = 4.4.

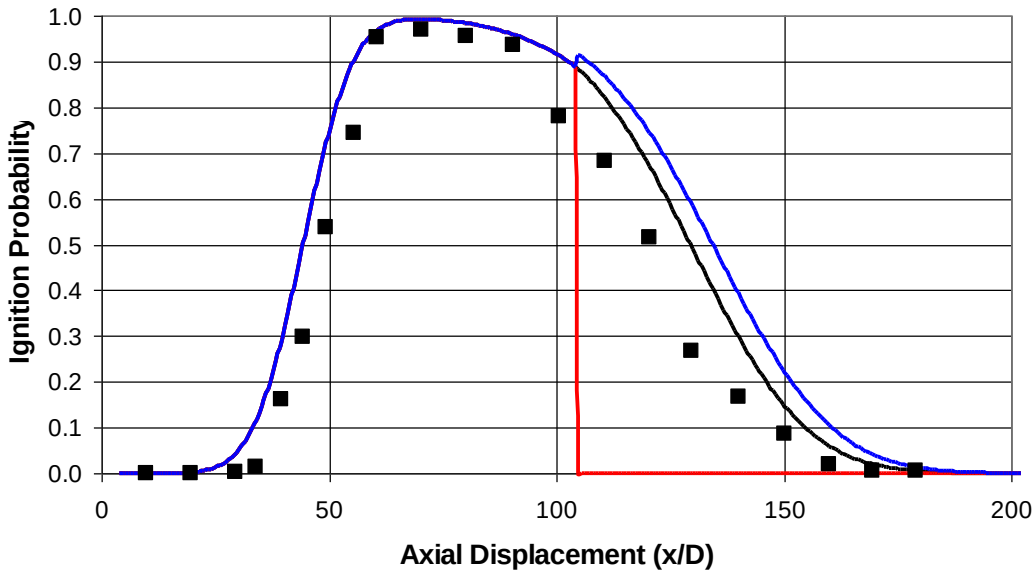

Figure 49 Predicted flammability factor on the centreline of a natural gas jet with orifice diameter 6.35mm and release velocity 50 m/s using the emprical mean concentration profile of Chen & Rodi (1980) with their value of constant a_c of 0.44 (**–**), the Smith *et al*. (1986) value of a_C = 4.4 (**–**) and the present model constant of a_C = 4.2 (**–**). Symbols show measured ignition probabilities of Smith *et al*. (1986).

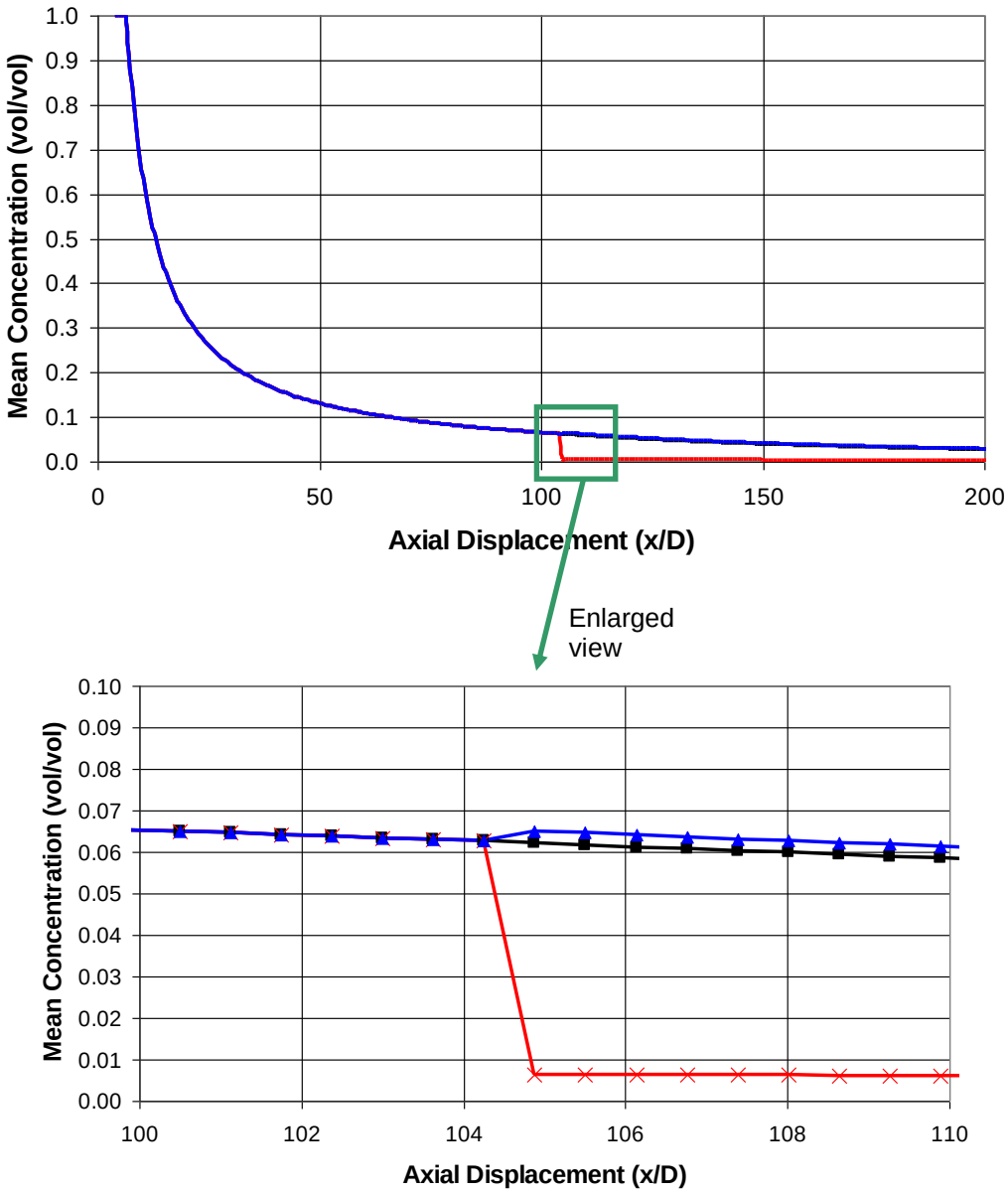

Figure 50 Mean concentration on the centreline of a natural gas jet with orifice diameter 6.35mm and release velocity 50 m/s using the emprical mean concentration profile of Chen & Rodi (1980) with their value of constant a_C of 0.44 (**–**), the Smith *et al*. (1986) value of a_C = 4.4 (**–**) and the present model constant of a_C = 4.2 (**–**).

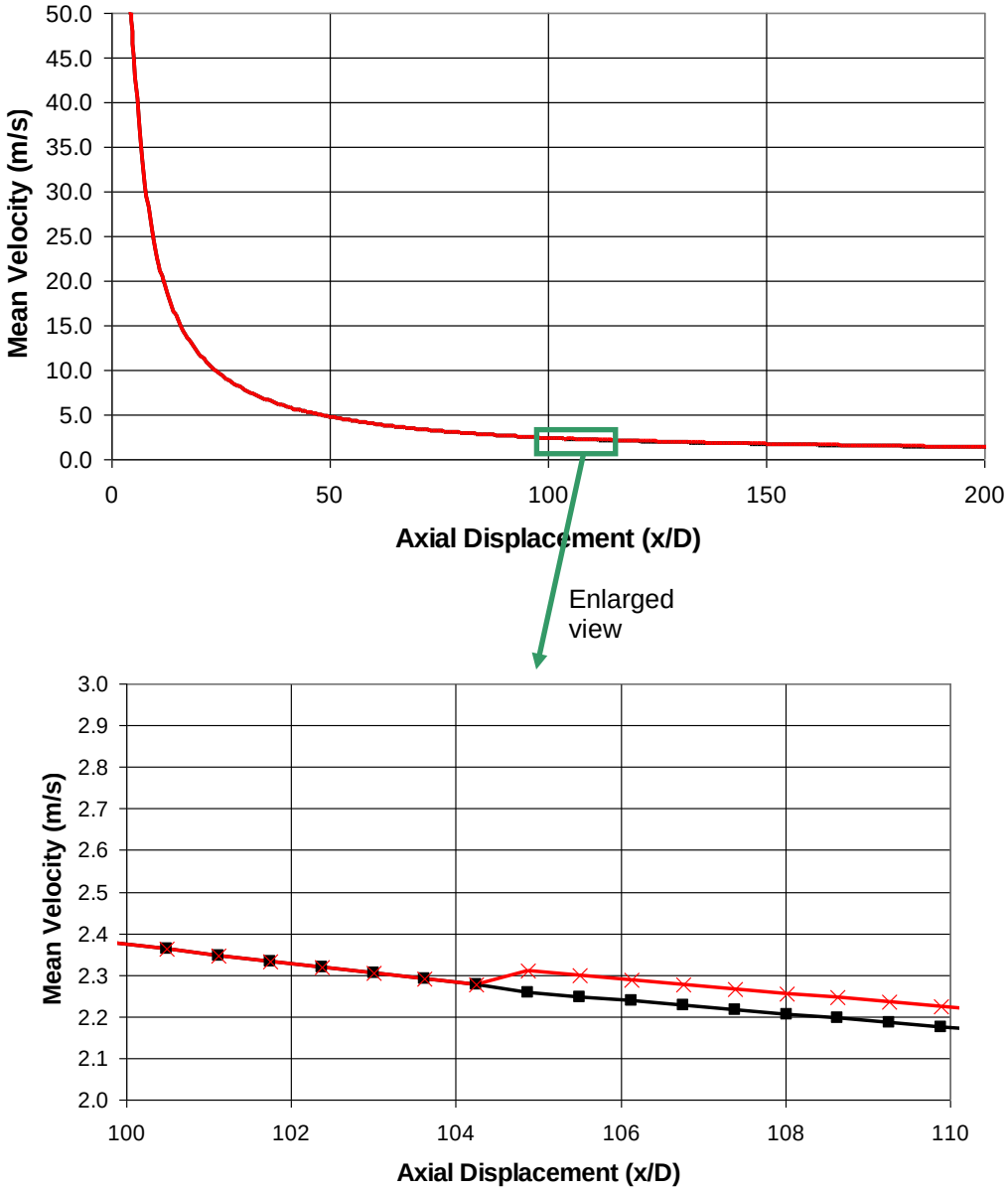

Figure 51 Mean centreline velocity for a natural gas jet with orifice diameter 6.35mm and release velocity 50 m/s using the emprical correlation of Chen & Rodi (1980) with their constant of a_U = 7.26 (**–**), and the present model constant of a_U = 7.1 (**–**).

Spreading Rate of Radial Mean Concentration

In the radial direction, the mean concentration profile is approximated in the flammability factor model using a Gaussian distribution:

$$\frac{C}{C_{cl}} = \exp\left[- K_C \left(\frac{r}{x'} \right)^2 \right] \qquad (9.15)$$

In the present work, the model constant K_C is taken to be 73.6, based on value obtained by Birch *et al*. (1978). The effect of changing K_C to the value of 57 recommended by Chen & Rodi (1980) is shown in Figure 52. The flammability factor predictions agree best with the measured ignition probability of Birch *et al*. (1981), using K_C = 73.6.

The choice of the K_C affects the radius at which the mean concentration falls to half of the centreline value, a measure which is often examined in model validation studies. The concentration half-width can be related to the constants K_C as follows:

$$r_{0.5C} = \sqrt{\ln 2 / K_C} \qquad (9.16)$$

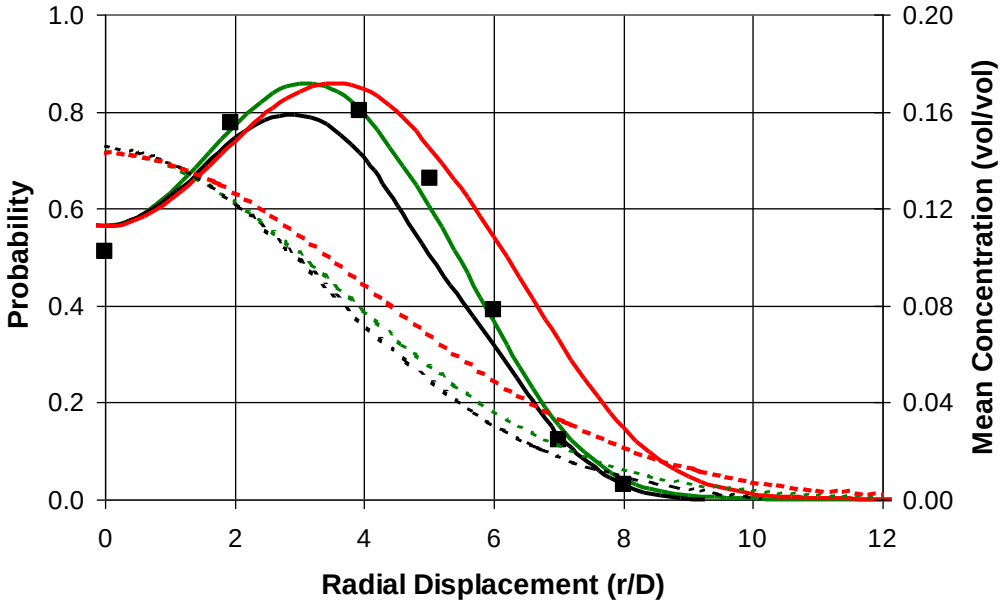

Figure 52 Comparison of flammability factor predictions (solid lines) and mean concentrations (dashed lines) to ignition probability measurements (symbols) for the natural gas jets studied by Birch *et al*. (1981). The black lines are the previous predictions of Birch *et al*. (1981), and the coloured lines are the present model predictions with exit velocities of 25.7 m/s and model constant K_c equal to: – 57 (from Chen & Rodi, 1980); – 73.6 (from Birch *et al*., 1978).

Radial Profiles of RMS Concentration

In the flammability factor model, the RMS concentration in the radial direction is determined from the α-β model of Chatwin & Sullivan (1990), with α and β constants assigned values of 1.27 and 0.14, respectively, based on Chatwin & Sullivan's (1990) analysis of the methane jet data experiments of Birch *et al*. (1978). The effect of small variations in the values of these constants on the resulting flammability factor contours is shown in Figure 53. In addition to the standard model constants, results are shown using α = 1.31 and β = 0.16, and α = 1.24 and β = 0.12. The former values are suggested by Chatwin & Sullivan (1990) as best matching the experiments of Becker *et al*. (1967), and the latter as best matching the experiments of Shaughnessy & Morton (1977). The difference in the predicted flammability factor is relatively modest and, overall, best agreement is obtained using the coefficients derived for methane jet data experiments of Birch *et al*. (1978) (i.e. α = 1.27 and β = 0.14).

Although radial profiles of the RMS concentration were presented in the review of experimental data by Chen & Rodi (1980), no empirical curve-fit to the data was provided and the measurements extended to only limited radial distances. Their data was therefore not used in the present work.

Further applications of the α-β model to predict concentration fluctuations in environmental flows are discussed by Chatwin & Sullivan (1993) and Mole (2006).

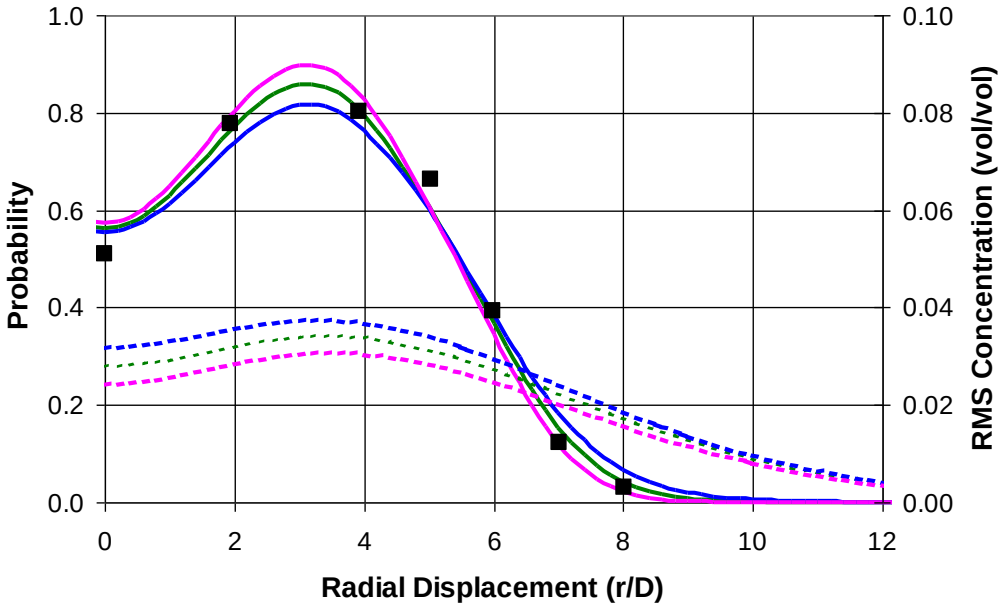

Figure 53 Comparison of flammability factor predictions (solid lines) and RMS concentrations (dashed lines) to ignition probability measurements (symbols) for the natural gas jets studied by Birch *et al*. (1981). All of the results are based on an exit velocity of 25.7 m/s with constants: – α = 1.31 and β = 0.16, – α = 1.27 and β = 0.14 , – α = 1.24 and β = 0.12.

Intermittency

The turbulent intermittency, I, is calculated in the present work using the Equation (9.5), with the model constant K set to 0.25, as recommended by Kent & Bilger (1976). The effect of changing the value of K to 0.3, as used by Alvani & Fairweather (2002), is shown in Figure 54. The difference in the predicted flammability factor using K = 0.25 or K = 0.30 is practically negligible.

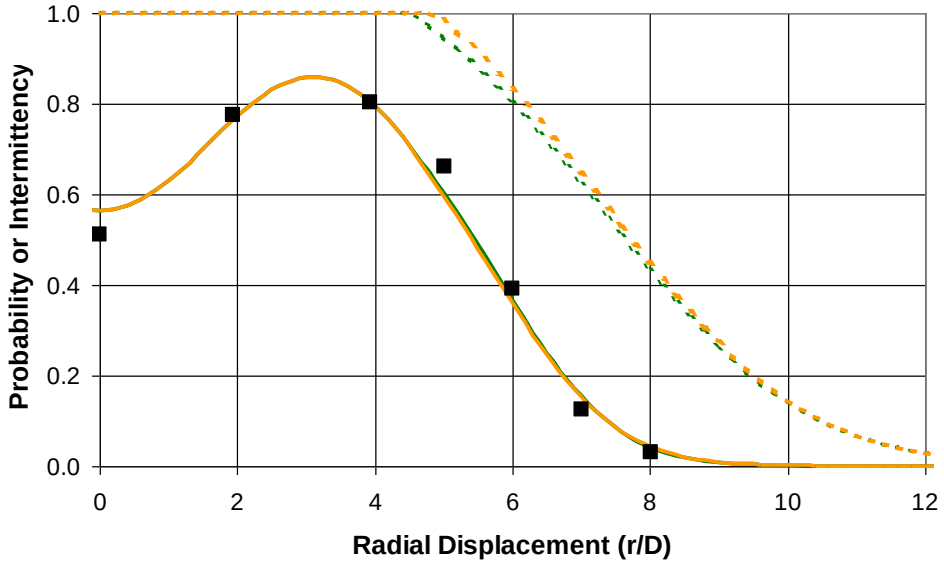

Figure 54 Comparison of flammability factor predictions (solid lines) and turbulent intermittency (dashed lines) to ignition probability measurements (symbols) for the natural gas jets studied by Birch *et al*. (1981). All of the results are based on an exit velocity of 25.7 m/s with constants: – K = 0.25, – K = 0.30.

9.3 FURTHER EXAMINATION OF THE TRUNCATED GAUSSIAN PDF

The flammability factor model presented in the present report determines the likelihood of ignition by integrating the concentration PDF between the upper and lower flammability limits. A two-part PDF is used, comprising the sum of a delta function and a truncated Gaussian. The delta function component has no influence on the computed flammability factor, since it is only finite when the concentration approaches zero (i.e. well below the lower flammability limit). The flammability factor is therefore determined solely by the truncated Gaussian component of the PDF, the shape of which is specified by the conditional mean concentration, C_c, and the variance, $\overline{c_c^2}$ (Equation 4.10).

The shape of the truncated Gaussian is shown in Figure 55 for four different mean concentrations of C_c = 0.05, 0.1, 0.2 and 0.3, with the variance held constant at $\overline{c_c^2} = 0.01$. Negative gas concentrations are unphysical and therefore any concentrations below zero are truncated. As the mean concentration is reduced from 0.3 to 0.05, a greater proportion of the Gaussian therefore becomes truncated. Since the integral of the probability across all concentrations must be unity, the peak of the probability also increases as C_c is reduced, to maintain the same area beneath the curve.

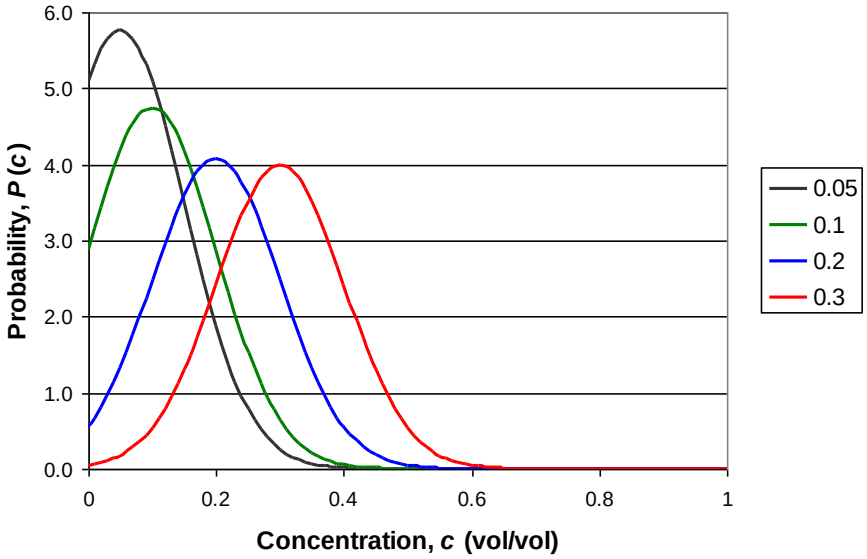

Figure 55 Truncated Gaussian PDFs with C_c = 0.05, 0.1, 0.2 and 0.3 and $\overline{c_c^2} = 0.01$.

One of the features of the truncated Gaussian distribution is that the mean used to specify the shape of the Gaussian distribution, C_c, can be different from the mean of the resulting truncated PDF, μ. This behaviour is illustrated in Figure 56, which shows the value of C_c and μ for two cases. For the case shown in black, the shape of the Gaussian is specified with C_c = 0.05 whilst the mean of the truncated Gaussian, μ, is approximately 0.1. In physical terms, this means that there is an equal likelihood of the concentration being either greater than or less than the mean value of 0.1.

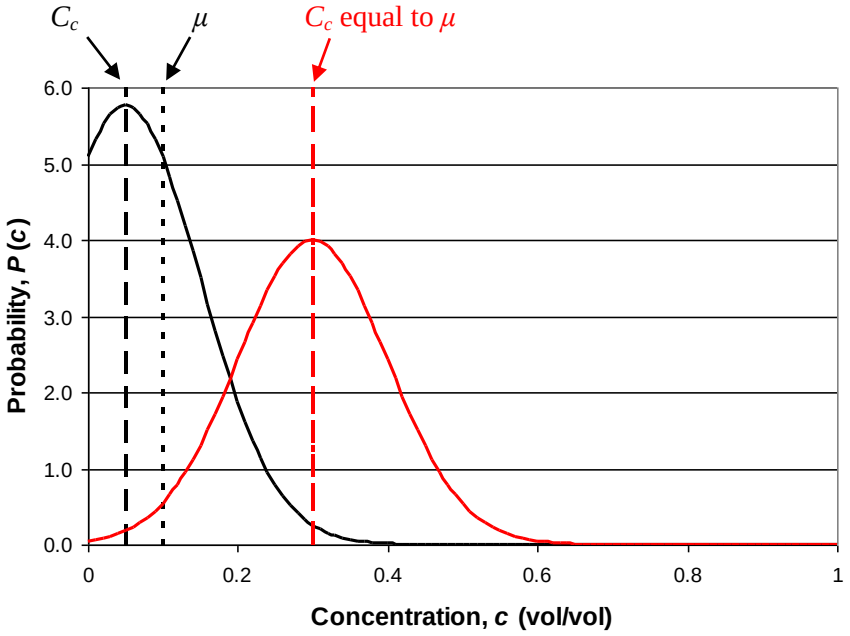

Figure 56 Truncated Gaussian PDFs with C_c = 0.05 and 0.3 and $\overline{c_c^2} = 0.01$.

This difference between C_c and μ is only significant when a large proportion of the Gaussian is truncated. This is illustrated by the red curve in Figure 56, which shows that for C_c = 0.3 (where the Gaussian is hardly truncated at all) the values of C_c and μ are identical.

The mean value of the truncated Gaussian distribution, μ, is calculated from the mean and variance, C_c and $\overline{c_c^2}$, as follows:

$$\mu = C_c + \frac{\phi\left(\frac{a-C_c}{\sqrt{\overline{c_c^2}}}\right) - \phi\left(\frac{b-C_c}{\sqrt{\overline{c_c^2}}}\right)}{\Phi\left(\frac{b-C_c}{\sqrt{\overline{c_c^2}}}\right) - \Phi\left(\frac{a-C_c}{\sqrt{\overline{c_c^2}}}\right)} \sqrt{\overline{c_c^2}} \qquad (9.17)$$

where constants a and b are the upper and lower limits of integration. In the present work, the PDF has physical bounds in terms of volume fractions of zero and unity, hence a = 0 and b = 1. The functions $\phi(x)$ and $\Phi(x)$ represent the Gaussian PDF and Cumulative Density Function (CDF) respectively:

$$\phi(x) = \frac{1}{\sqrt{2\pi}} \exp\left(-\frac{x^2}{2}\right) \qquad (9.18)$$

$$\Phi(x) = \frac{1}{\sqrt{2\pi}} \int_{-\infty}^{x} \exp\left(-\frac{t^2}{2}\right) dt = \frac{1}{2}\left[1 + erf\left(\frac{x}{\sqrt{2}}\right)\right] \qquad (9.19)$$

Truncation of the Gaussian PDF also changes its variance, which is calculated as follows:

$$s^2 = \overline{c_s^2}\left\{1 + \frac{\frac{a-C_c}{\sqrt{\overline{c_c^2}}}\phi\left(\frac{a-C_c}{\sqrt{\overline{c_c^2}}}\right) - \frac{b-C_c}{\sqrt{\overline{c_c^2}}}\phi\left(\frac{b-C_c}{\sqrt{\overline{c_c^2}}}\right)}{\Phi\left(\frac{b-C_c}{\sqrt{\overline{c_c^2}}}\right) - \Phi\left(\frac{a-C_c}{\sqrt{\overline{c_c^2}}}\right)} - \left[\frac{\phi\left(\frac{a-C_c}{\sqrt{\overline{c_c^2}}}\right) - \phi\left(\frac{b-C_c}{\sqrt{\overline{c_c^2}}}\right)}{\Phi\left(\frac{b-C_c}{\sqrt{\overline{c_c^2}}}\right) - \Phi\left(\frac{a-C_c}{\sqrt{\overline{c_c^2}}}\right)}\right]^2\right\} \qquad (9.20)$$

The empirical profiles developed by Birch *et al*. (1978, 1981) were based on the measured conditional mean concentration, μ, and variance, s^2, not on the parameters which determine the mean and variance of the (un-truncated) Gaussian PDF, C_c and $\overline{c_c^2}$. Up to this point, however, it has been assumed by the flammability factor model that $\mu = C_c$ and $s^2 = \overline{c_c^2}$. Figure 56 illustrates that under certain conditions this assumption is incorrect.

To assess the magnitude of this discrepancy, the model has been changed to use empirical profiles (Equations 4.11 and 4.12) based on the values of μ and s^2, not, as was assumed, the values of C_c and $\overline{c_c^2}$. The shape of the truncated Gaussian PDF has also been specified to achieve a given μ and s^2. This is not trivial, since it requires values of C_c and $\overline{c_c^2}$ to be determined from specified values of μ and s^2. An analytical solution is not possible, and therefore an iterative numerical method has been used, which adjusts the width of the PDF and the location of its peak and until a good fit is obtained with the input values of μ and s^2. The particular method used, based on Maximum Likelihood Estimation (MLE), is well established in the statistical sciences although it may be unfamiliar to many scientists and engineers. A short description of it is therefore provided below.

The method starts from the expression for the likelihood, l, which is the product of n multiple samples of the truncated Gaussian PDF :

$$l = f(\tilde{c}_1) f(\tilde{c}_2) \ldots f(\tilde{c}_n) \qquad (9.21)$$

where

$$f(\tilde{c}_i) = \frac{1}{\Phi\left(\frac{b-C_c}{\sqrt{\overline{c_c^2}}}\right) - \Phi\left(\frac{a-C_c}{\sqrt{\overline{c_c^2}}}\right)} \frac{1}{\sqrt{2\pi\overline{c_c^2}}} \exp\left[-\frac{(\tilde{c}_i - C_c)^2}{2\overline{c_c^2}}\right] \qquad (9.22)$$

Values of C_c and $\overline{c_c^2}$ that need to be selected in order to best match the desired values of μ and s^2 are found when the value of the likelihood, l, is largest. Rather than simply find the maximum of l, the method finds the maximum of the logarithm of l. This simplifies the derivation and avoids numerical round-off errors associated with taking the product of small values. Since when l is maximum, $\ln(l)$ is also maximum, this has no effect on the results of the method. Equations (9.21) and (9.22) are then written:

$$\ln(l) = \underbrace{-n \ln\left[\Phi\left(\frac{b-C_c}{\sqrt{\overline{c_c^2}}}\right) - \Phi\left(\frac{a-C_c}{\sqrt{\overline{c_c^2}}}\right)\right]}_{A1} \underbrace{- n\ln\left(\sqrt{2\pi}\right)}_{A2} \underbrace{- n\ln\left(\sqrt{\overline{c_c^2}}\right)}_{A3} \underbrace{- \sum_{i=1}^{n}\left[\frac{(\tilde{c}_i - C_c)^2}{2\overline{c_c^2}}\right]}_{A4} \qquad (9.23)$$

The second term, $A2$, can be ignored in the subsequent analysis since it has only an additive effect. Equation (9.23) is then divided through by the number of samples, n, (a constant) and the third term on the right-hand-side, $A3$, is expanded as follows:

$$\frac{1}{n}\sum_{i=1}^{n}\left[\frac{(\tilde{c}_i - C_c)^2}{2\overline{c_c^2}}\right] = \frac{1}{2\overline{c_c^2}} \frac{1}{n}\sum_{i=1}^{n}\left(\tilde{c}_i^{\,2} - 2\tilde{c}_i C_c + C_c^2\right) \qquad (9.24)$$

$$= \frac{1}{2\overline{c_c^2}}\left[\frac{1}{n}\sum_{i=1}^{n}\left(\tilde{c}_i^{\,2}\right) - 2C_c \frac{1}{n}\sum_{i=1}^{n}\left(\tilde{c}_i\right) + C_c^2\right]$$

Since the mean of the truncated Gaussian distribution, μ, is by definition:

$$\mu = \frac{1}{n}\sum_{i=1}^{n}\tilde{c}_i \qquad (9.25)$$

and the variance, s^2, is:

$$s^2 = \frac{1}{n}\sum_{i=1}^{n}(\tilde{c}_i - \mu)^2 = \frac{1}{n}\sum_{i=1}^{n}\left(\tilde{c}_i^{\,2}\right) - \mu^2 \qquad (9.26)$$

Equation (9.23) simplifies to:

$$\frac{\ln(l)}{n} = -\ln\left[\Phi\left(\frac{b-C_c}{\sqrt{\overline{c_c^2}}}\right) - \Phi\left(\frac{a-C_c}{\sqrt{\overline{c_c^2}}}\right)\right] - n\ln\left(\sqrt{\overline{c_c^2}}\right) - \frac{1}{2\overline{c_c^2}}\left(s^2 + \mu^2 - 2C_c\mu + C_c{}^2\right) \quad (9.27)$$

It is then necessary to find the optimum values of C_c and $\overline{c_c^2}$ for which the maximum value of $\ln(l)/n$ is obtained, based on given values of the mean and variance of concentration (μ and s^2). Different techniques exist in order to determine the maxima of a function with two variables. In the present work, the `fminsearch` function in MatLab has been used. Since this determines the minima of a function, the negative of Equation (9.27) has been used.

To check that the above derivation and numerical coding of the model were correct, a verification test was performed which involved the following steps:

1. The shape of the truncated PDF was set using specified values of C_c and $\overline{c_c^2}$
2. The mean and variance of the truncated PDF concentration (μ and s^2) was calculated from Equations (9.17) and (9.20).
3. The calculated values of μ and s^2 from Step 2 were used to determine values of C_c and $\overline{c_c^2}$, using the MLE method based on `fminsearch` (Equation 9.27).

The results of these tests are not shown here, but they demonstrated that the values of C_c and $\overline{c_c^2}$ input in Step 1 were equal to the values output in Step 3, confirming that the model derivation and its implementation were correct.

Results from using the flammability factor model with mean and variance of concentration of μ and s^2, instead of C_c and $\overline{c_c^2}$, are presented in Figures 57 to 60 for the natural gas jet experiments of Smith *et al*. (1986). The results using the new approach are practically identical to those obtained assuming $\mu = C_c$ and $s^2 = \overline{c_c^2}$. Along the centreline of the jet, there are no perceptible differences in the predicted flammability factor. Towards the jet periphery, Figure 58 shows that there are some very small differences in the flammability factor predictions (less than 1% difference), which result from the differences between μ and C_c, and between s^2 and $\overline{c_c^2}$, shown in Figure 59. The resulting truncated Gaussian PDF is shown Figure 60 at a position in the jet where differences between the two approaches are most significant. Even here, the difference between μ and C_c is relatively small (around 0.1 % vol/vol).

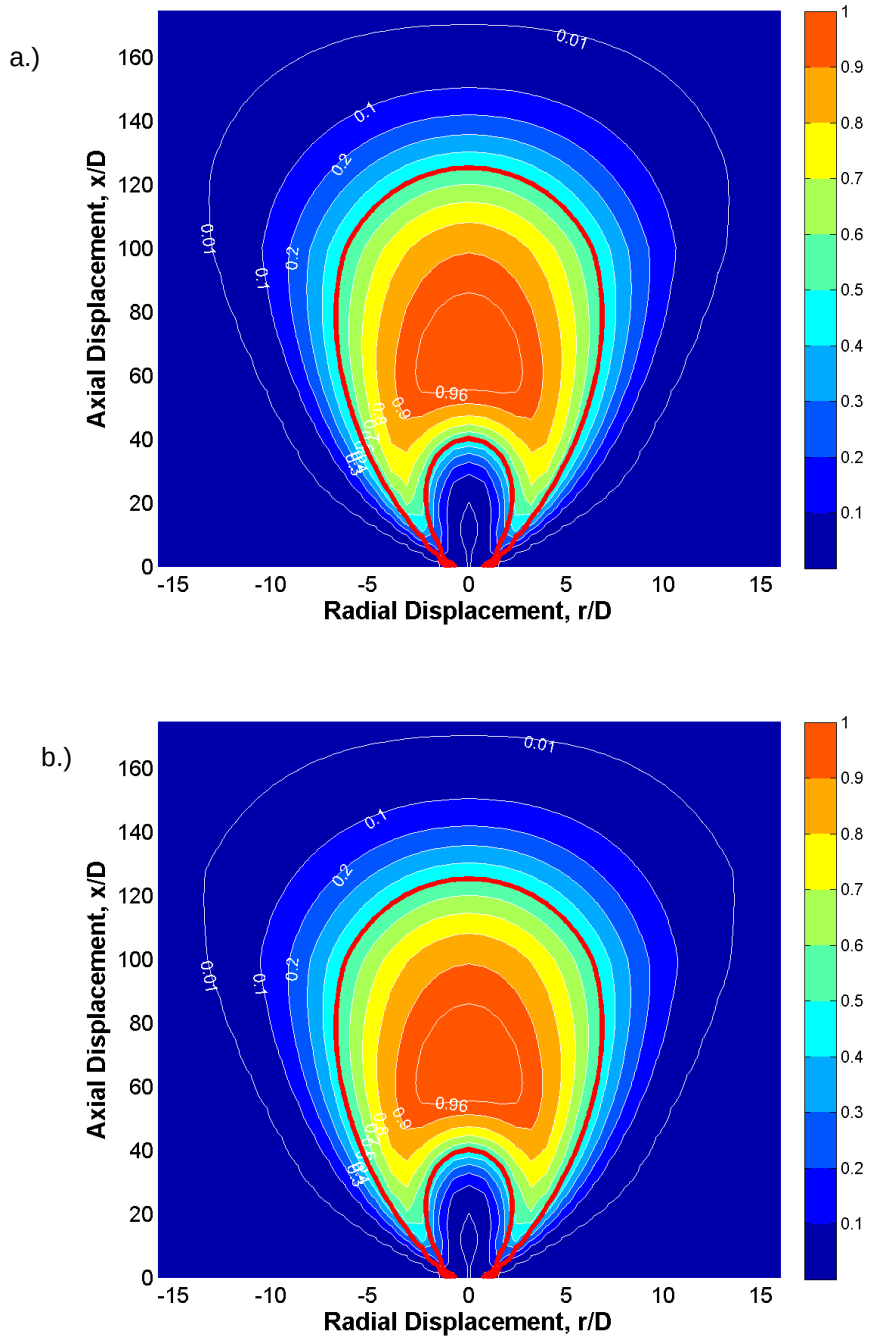

Figure 57 Predicted flammability factor for the natural gas jet studied by Smith *et al*. (1986) using a.) C_c and $\overline{c_c^2}$; b.) μ and s^2;. Red lines indicate the position of the LFL and UFL, based on the predicted mean gas concentration

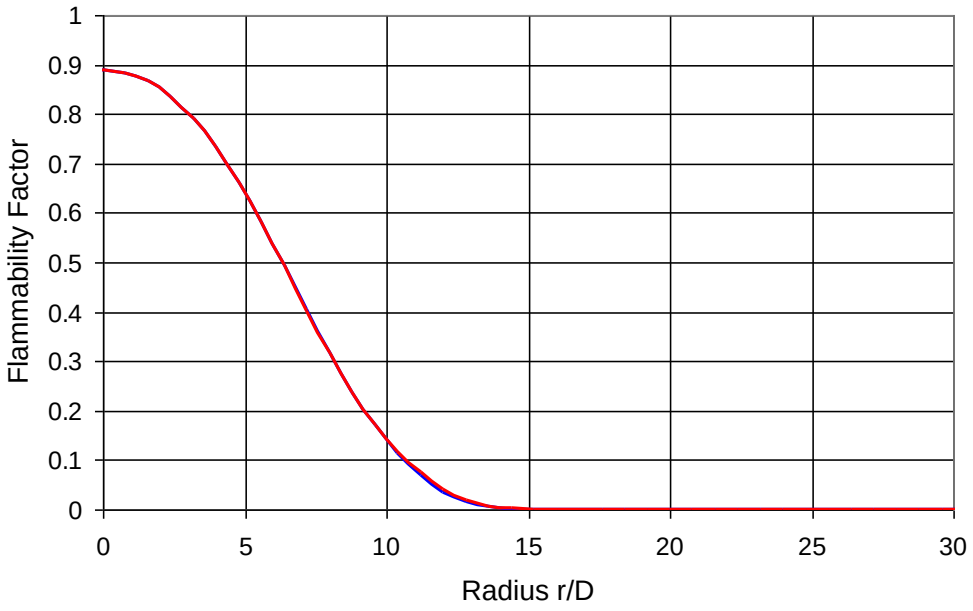

Figure 58 Radial profile of the predicted flammability factor at an axial position 100 diameters from the jet source using: — C_c and $\overline{c_c^2}$; — μ and s^2.

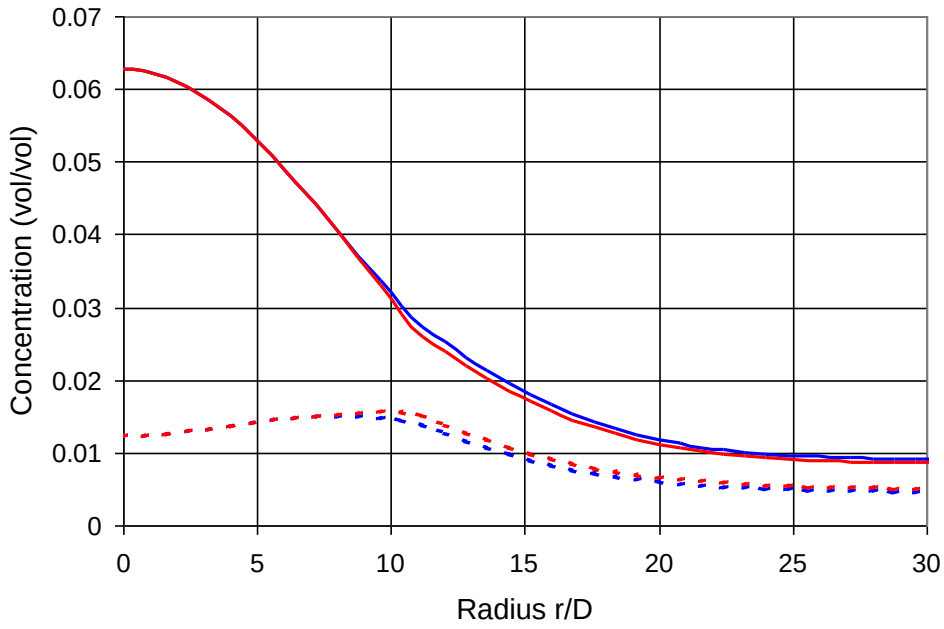

Figure 59 Radial profiles of the predicted conditional mean concentration (solid lines) and RMS concentration (broken lines) at an axial position 100 diameters from the jet source using : — C_c and $\overline{c_c^2}$; — μ and s^2.

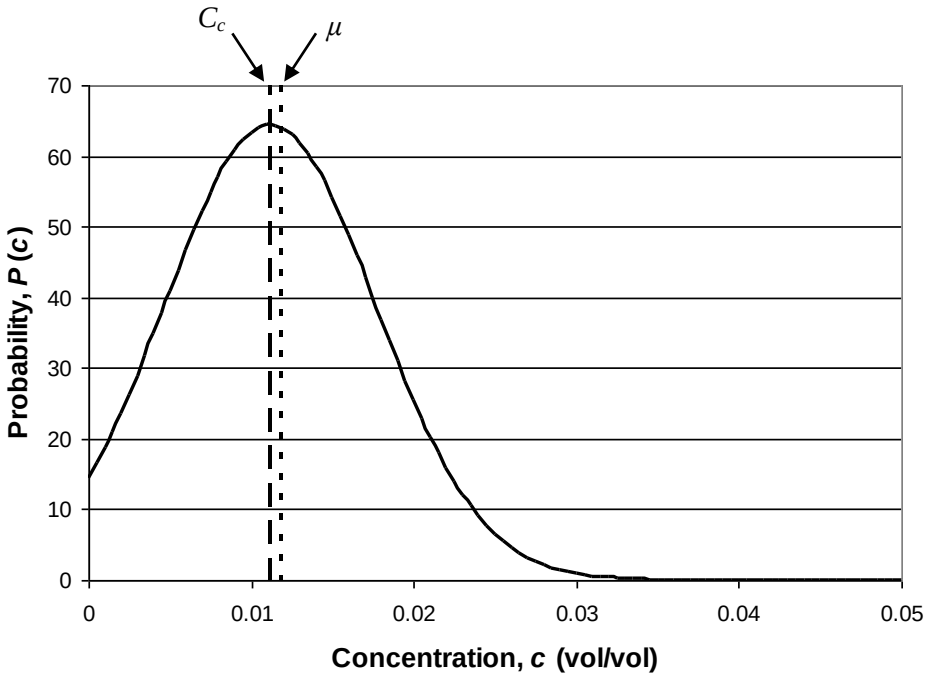

Figure 60 Concentration PDF at an axial position of 100 diameters and radial position of 20 diameters.

The results from these tests show that for the free-jet flammability factor model it is reasonable to assume that $\mu = C_c$ and $s^2 = \overline{c_c^2}$. This assumption is valid where mean concentrations are relatively high, since the Gaussian PDF is not truncated. Where mean concentrations are lower (around a few percent by volume or less) the concentration variance is also low and therefore only a relatively small fraction of the PDF is truncated. Differences between μ and C_c, and between s^2 and $\overline{c_c^2}$, therefore remain small. Assuming $\mu = C_c$ and $s^2 = \overline{c_c^2}$ has the advantage of simplifying considerably the implementation of the model.

10 APPENDIX C – ANALYSIS OF CFD MODELS

In Section 5, a flammability factor model was proposed that should be practicable to implement in commercial CFD codes. The sub-models selected for use in that model were chosen following detailed analysis of the previous work of Alvani and Fairweather (Alvani, 2004, Alvani & Fairweather, 2002, 2008). The following sections provide a description of these previous works and a rationale for the choice of sub-models.

10.1 ALVANI AND FAIRWEATHER MODELS

10.1.1 Mixture Fraction

Alvani and Fairweather formed PDFs for the mixture fraction, *f*, rather than PDFs of the concentration in terms of the volume fraction, *c*. Before presenting the PDF which Alvani and Fairweather found to give the best overall performance, it is necessary therefore to digress a little to discuss the mixture fraction, which is determined from:

$$f = \frac{Z_i - Z_{i2}}{Z_{i1} - Z_{i2}} \qquad (10.1)$$

where Z_i is the mass fraction for element *i*; for example, the mass fraction of hydrogen originating from a hydrocarbon fuel at any point in the flow. Subscripts 1 and 2 refer to the composition of the two feeds (fuel and air) at their source. The normalisation which is implied by the denominator in the above equation ensures that mixture fraction has a value of unity in a fuel feed and zero in an oxidiser feed.

The mixture fraction at any point in the flow can be understood in physical terms as the mass fraction of material that originated from the fuel stream (Bilger, 1980, Cant & Mastorakos, 2008). As this is identical to the fuel mass fraction (prior to combustion only), the question then arises as to why Alvani and Fairweather did not simply use PDFs for fuel mass fraction, rather than the mixture fraction. There are several reasons, but probably the main one is that many of the CFD sub-models needed to compute turbulent mixing for the purposes of ignition probability can conveniently be drawn from the field of non-premixed combustion – in which the use of mixture fraction as a flow variable is very widespread, as it offers several benefits:

- Mixture fraction is a conserved scalar, i.e. it is neither created nor destroyed, merely being convected and diffused by mixing within the flow domain (even during combustion), whereas the mass fraction of fuel is not conserved during combustion and so needs an additional 'sink' term in its transport equation to be modelled.

- Mixture fraction allows for the possibility that the fuel and/or oxidiser feeds can be in several separate streams, such that there could be more than one source of fuel feed (for example, two or more separate leak sources of the same fuel in a hazard scenario).

- If the molecular diffusivities of the elements are the same, or can be assumed to be negligible in comparison to turbulent mixing, then the mixture fraction is independent of the element used for its definition. A single transport equation for the mixture fraction then defines the mixing of all chemical species.

The transport equations for the mean and variance of the mixture fraction, denoted F and $\overline{f^2}$ respectively, were given by Alvani (2004) and are also described in most textbooks on combustion (Bilger, 1980, Cant & Mastorakos, 2008).

10.1.2 Turbulence Model

Alvani and Fairweather investigated the performance of two turbulence models: a standard k-ε model (Jones & Launder, 1972) and the Reynolds stress transport model (*RS*) of Jones & Musonge (1988). The k-ε model is the most commonly-used turbulence model in engineering applications of CFD, whilst the model of Jones & Musonge (1988) is a variant of a wider class of Reynolds stress transport models. Details of the Reynolds stress model are given by Alvani (2004) and Alvani & Fairweather (2008), but as the relevant expressions are very lengthy they are not repeated here. When the turbulence transport equations are coupled with intermittency transport equations, they are referred to as the k-ε-I and *RS*-*I* models.

The key role played by these turbulence models, in the context of simulations of flammability factor, is to provide closure for turbulent scalar flux terms which must be modelled in the transport equations for mean and variance of the mixture fraction. These terms consist of correlations between fluctuations in mixture fraction and velocity. In the case of the k-ε model they are simply closed using a gradient-diffusion expression, in which ν_t is the turbulent kinematic viscosity and σ_t is a turbulent Prandtl number:

$$\overline{uf} = \frac{\nu_t}{\sigma_t}\frac{\partial F}{\partial x_i} \qquad (10.2)$$

In the case of the Reynolds stress model, the turbulent scalar fluxes are found by solving their transport equations. These transport equations are rather complex; details are given by Fairweather *et al*. (1992) and Alvani (2004).

Overall, Alvani and Fairweather demonstrated that the Reynolds stress turbulence model provided better predictions than the simpler k-ε–I model. However, this comes at the cost of greatly increased modelling complexity. Alvani & Fairweather (2008) note that: "*Predictions of the k-ε-I model are in general inferior to those of the latter approach (RS-I), although still sufficiently accurate for most design purposes*". Figures 41 and 42 show that either model offers predictions of flammability factor that compare well with measured ignition probability. Similarly, for the propane jet measurements of Schefer & Dibble (2001), Figure 61 shows that good predictions can be obtained using either a k-ε-I or *RS*-*I* turbulence model. Simulations obtained using either a k-ε or *RS* turbulence model in which intermittency, I, is not modelled, are much less satisfactory for this case.

10.1.3 PDF

A number of different types and combinations of prescribed generic PDF were examined by Alvani and Fairweather (Alvani, 2004, Alvani & Fairweather, 2002, 2008). Their examination was conducted in a rigorous fashion by comparing model predictions for specific PDFs against measured PDFs for natural gas jets from Birch *et al*. (1978) and propane jets from Schefer & Dibble (2001), as well as PDF data for the plane wake behind a heated circular cylinder (LaRue & Libby, 1974). The best performance across a range of jets and wake data was obtained using the following form:

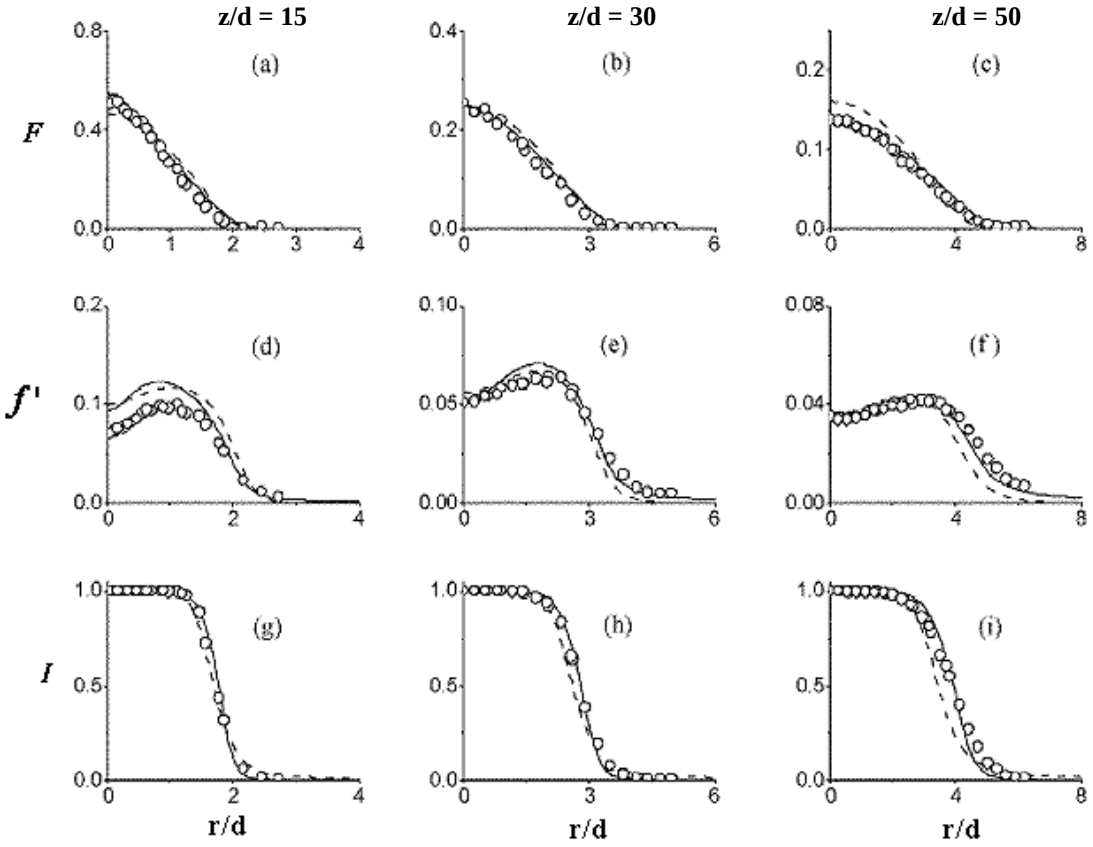

Figure 61 Radial profiles of mean mixture fraction, *F*, RMS mixture fraction *f'* and turbulence intermittency, *I*, in the jet of Schefer & Dibble (2001). Solid line: *RS-I* turbulence model; dashed-line: *k-ε-I* turbulence model; symbols: measurements. Reproduced with the permission of Prof. Fairweather, University of Leeds.

$$P(\tilde{f}) = (1-I)\delta(\tilde{f}) + I\left[sP_s(\tilde{f}) + (1-s)P_\beta(\tilde{f})\right] \qquad (10.3)$$

This is a three-part PDF, initially developed by Effelsberg & Peters (1983) for describing the behaviour of conserved scalars in turbulent shear flows – thus having a wider applicability than just jets. Effelsberg & Peters (1983) identified the three regions to be the fully turbulent part, the outer flow in which large eddies engulf ambient fluid into the turbulent region, and a transition layer between these two regions, called the 'viscous superlayer'. A description of the models used in these three regions was provided earlier in Section 5.3.

10.1.4 Intermittency

In order to integrate the PDF and determine the flammability factor, it is necessary to calculate the turbulence intermittency, *I*. Alvani and Fairweather computed this variable by solving a transport equation for turbulence intermittency, using a slightly modified version of a *k-ε-I* turbulence model developed by Cho & Chung (1992). This model was based on the earlier theoretical work of Dopazo (1977) who took as the starting point for the derivation of the

intermittency transport equation the instantaneous mass conservation equation which was subsequently "*conditioned ... by an intermittency indicator function*". Dopazo's transport equation for turbulence intermittency was, in turn, based on the pioneering theoretical work of Libby (1975), who was the first to postulate and derive a transport equation for an intermittency function. Dopazo (1977) provided an intermittency transport equation which involved physically meaningful but unknown flow variables. Cho & Chung (1992) subsequently modelled the un-closed terms in this equation and coupled it to a k-ε turbulence model. The modelled transport equation for the turbulence intermittency was given earlier in Section 5.3, see Equations (5.1) to (5.5).

Details of the intermittency model used by Alvani and Fairweather in conjunction with a Reynolds stress transport turbulence model (RS-*I* model), were given by Alvani (2004) and Alvani & Fairweather (2008). The transport equation for turbulence intermittency was little different from that used for the k-ε-I model, except that the diffusion term was replaced by a generalised gradient diffusion expression. An additional term related to intermittency also appeared in each of the Reynolds stress transport equations and the Γ-term in the ε-equation took on a different form.

Cho & Chung (1992) tested their intermittency model against measurements for a plane jet and round jet (using Pope's (1978) correction for the round/plane jet anomaly), plane wake and plane mixing layer. In every case there was found a significant improvement in the computed results over those obtained from k-ε or Reynolds stress turbulence models without intermittency effects. Cho & Chung's (1992) k-ε-I model also gave good agreement with measurements of intermittency in the far-field plane wake. The results for Cho and Chung's model, compared to the measured intermittency in the propane jet of Schefer & Dibble (2001) are given in Figure 61, and it can be seen to be in close agreement with measurements.

10.1.5 Model Implementation

Finally, it should be noted that the computations carried out by Alvani and Fairweather were made using a 2-D parabolic CFD code, rather than the 3-D elliptic codes used in commercial CFD software. In parabolic codes the solution is stepped downstream so that only the current and subsequent row of radially-arranged mesh cells needs to be stored. This is for reasons of efficiency, as jets can essentially be treated as being parabolic in behaviour. Since a parabolic code was used, Alvani and Fairweather were able to use a very fine computational mesh in the radial direction. However, we understand from communications with Professor Fairweather that such fine meshes are not necessary in practice.

10.2 ANALYSIS OF ALTERNATIVE MODELLING APPROACHES

10.2.1 PDF

Alvani and Fairweather (Alvani, 2004, Alvani & Fairweather, 2002, 2008) found that the three-part composite PDF, given by Equation (10.3), produced the best overall agreement with data on jets and, in particular, with the plane wake data of LaRue & Libby (1974). Unfortunately, however, this PDF is complex, especially that part relating to the superlayer. Moreover, the correct implementation of $\widetilde{f}_t$ in the superlayer part of the PDF, Equation (5.9), is also unclear. Neither Effelsberg & Peters (1983) nor Alvani (2004) provided details of how this PDF is best implemented in a CFD code. There is also the question of the validity in other flows of the expressions for variables s and k in the model equations (see Section 5.3.5). Chen (1987)

applied the same three-part composite PDF to simulate non-premixed flames, but used a different expression for variable *s* to that of Effelsberg & Peters (1983).

Alvani (2004) also evaluated the performance of two simpler PDFs: a beta PDF, P_β, and a two-part PDF developed by Janicka & Peters (1982) comprising a delta function plus a beta function, weighted by intermittency:

$$P(\tilde{f}) = (1-I)\delta(\tilde{f}) + IP_\beta(\tilde{f}) \qquad (10.4)$$

The delta function was used to model the intermittency spike whilst the beta function accounted for the fully turbulent part of the flow.

The evaluation of all three different PDFs by Alvani (2004) was undertaken using experimental measurements (where available) as input parameters to the PDF to minimise errors due to other aspects of the modelling. Both of the simpler PDFs were found to perform poorly for the plane wake of LaRue & Libby (1974) and the beta PDF also performed poorly when compared to the jet data at locations not on the jet axis (Figures 62 and 63).

Curiously, results for the three-part composite PDF in which variables *s* and *k* were calculated using the full iterative procedure mentioned in Section 5.3 were significantly worse than when these variables are evaluated using the simple prescriptions of Equations (5.10) and (5.11).

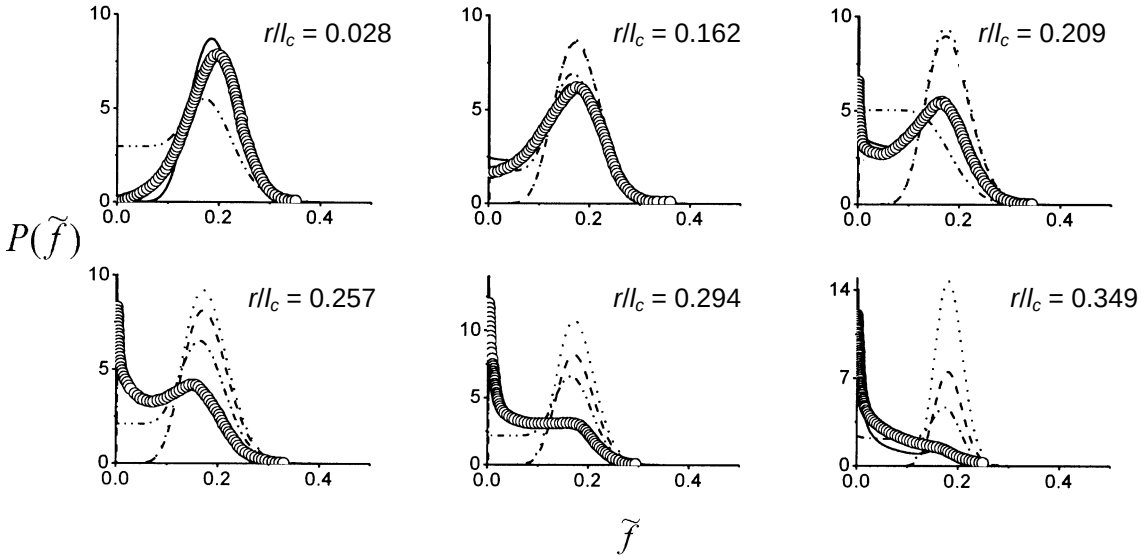

Figure 62 PDFs of mixture fraction for the plane wake behind a heated cylinder of length l_c, at different radial positions. Symbols: measurements of LaRue & Libby (1974); solid line: three-part PDF with constants *s* and *k* calculated from Equations (5.10) and (5.11); dash-dot-dot line: three-part PDF with constants *s* and *k* calculated by full iteration; dashed line: two-part PDF; dotted line: beta PDF. Reproduced with the permission of Prof. Fairweather, University of Leeds.

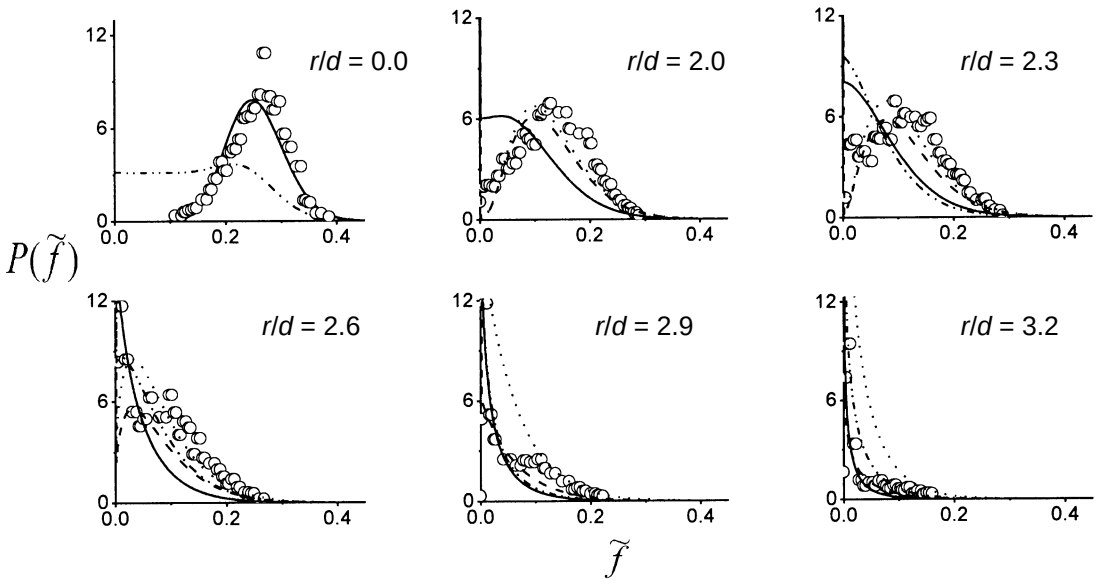

Figure 63 PDFs of mixture fraction for a propane jet at different radial positions using experimental mreasurements for the mean and variance of mixture fraction, and the intermittency, in the calculated PDF. Symbols: measurements of Schefer & Dibble (2001); solid line: three-part PDF with constants *s* and *k* calculated from Equations (5.10) and (5.11); dash-dot-dot line: three-part PDF with constants *s* and *k* calculated by full iteration; dashed line: two-part PDF; dotted line: beta PDF. Reproduced with the permission of Prof. Fairweather, University of Leeds.

Figure 63 suggests that for free jets there is little advantage in using the three-part PDF instead of the two-part PDF. Neither the two-part nor three-part PDFs capture the bi-modal behaviour of the PDF at certain radial locations, such as the r/d = 2.3, 2.6 and 2.9 positions in Figure 63. Much the same conclusion can be drawn from similar results presented by Alvani (2004) for the natural gas jet studied by Birch *et al*. (1978). The validity of these PDFs for other turbulent shear flows of interest, such as impinging flows, is unclear.

There appears to be some latitude for error in the shape of the PDF when computing the flammability factor. Since the flammability factor is calculated by integrating over the PDF, a small difference between the calculated and 'correct' shape of PDF may not lead to a significant difference in the computed flammability factor. This is illustrated by Figure 64, which shows measured and computed PDF of mixture fraction for the natural gas jet of Birch *et al*. (1978). Although neither turbulence model gives very close agreement with the measured PDFs, when these PDFs are integrated to give flammability factor the comparison was quite acceptable, as shown in Table 7.

Taking all of the above factors into consideration, it is recommended that to calculate the flammability factor using commercial CFD software, initially it is sufficient use two-part PDF of Janicka & Peters (1982), and only later consider implementing the three-part composite PDF of Effelsberg & Peters (1983), if resources permit.

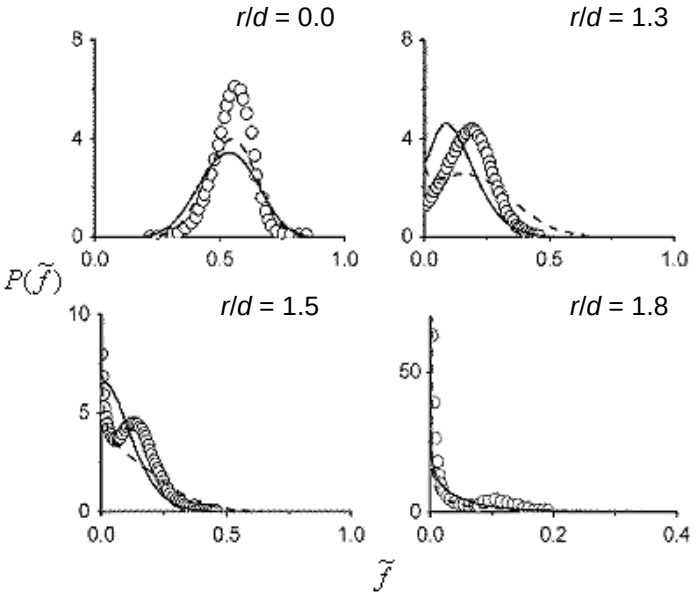

Figure 64 PDFs of mixture fraction for a natural gas jet four radial positions, at an axial distance of *x*/*d* = 10. Symbols: measurements of Birch *et al*. (1978); solid line: *RS-I* turbulence model, dashed-line: *k-ε-I* turbulence model. Reproduced with the permission of Prof. Fairweather, University of Leeds.

Table 7 Flammability factor calculated from the measured and computed PDFs in the natural gas jet of Birch *et al*. (1978), at the axial location *x*/*d* = 10.

r/d	*Measured*	*k-ε-I*	*RS-I*
0.0	0.00	0.00	0.00
1.3	0.31[8]	0.40	0.28
1.5	0.40	0.43	0.37
1.8	0.28	0.27	0.29

10.2.2 Intermittency

The turbulent intermittency model of Cho & Chung (1992) results in improved performance over turbulence models which omit intermittency effects in a variety of shear flows, including plane and round jets, plane wakes and plane mixing layers. Whether the model performs as well for more complex shear flows, involving phenomena such as flow impingement, is unknown. Nevertheless, it does seem to offer the prospect of a valid means of computing a local value of turbulence intermittency, and this variable is needed if predictions of flammability factor are to be made using an intermittency-based PDF.

[8] *The value given by Birch et al. (1979, 1981) is given as 0.21, but this is incorrect (Alvani, 2004).*

In the empirical model described in Section 4.2, turbulent intermittency is provided by an alternative means, i.e. from Kent & Bilger's (1976) empirical correlation:

$$I = \frac{K+1}{\left[\left(\frac{\overline{f^2}}{F^2}\right)+1\right]} \qquad (10.5)$$

where K is a constant whose value varies between 0 and 0.44. Kent & Bilger (1976) obtained the best fit to data for jets in still or co-flowing air, and a heated plane wake, with $K = 0.25$.

Alvani (2004) referred to a number of other empirical correlations for turbulent intermittency. A different value of 0.3 was used for the constant K in Equation (10.5) by Alvani and Fairweather (Alvani, 2004, Alvani & Fairweather, 2008), as apparently recommended by Janicka & Peters (1982). The validity of this expression was also checked by Alvani (2004) against the propane jet experiments of Schefer & Dibble (2001). The intermittency was found to correlate well to the parameter for mixture fraction mean and variance, as shown in Figure 65.

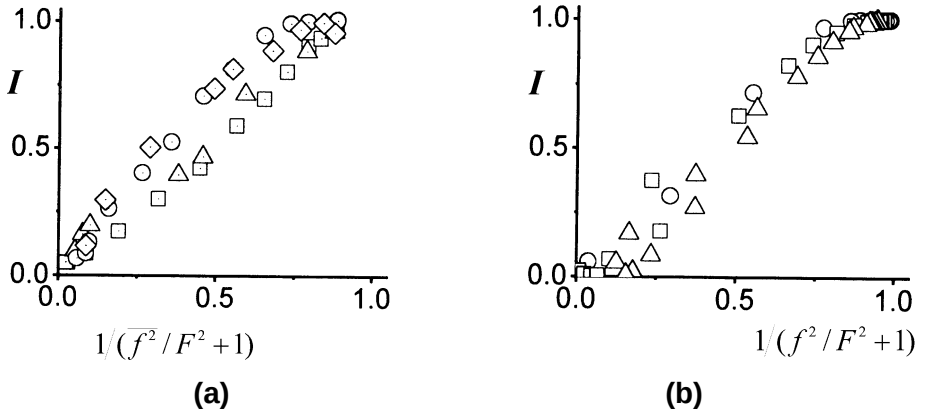

Figure 65 Correlation between intermittency and mixture fraction fluctuation intensity. a) ○: air jet, □ and △: heated jet in a co-flow, ◇: heated plane wake; b) Propane jet of Schefer & Dibble (2001) with ○: x/d = 5, □: x/d = 30, △: x/d = 50. Reproduced with the permission of Prof. Fairweather, University of Leeds.

Alvani (2004) also performed CFD simulations with the intermittency determined from Kent & Bilger's (1976) correlation, rather than from the solution of the intermittency transport equation. Results were presented for the PDF of mixture fraction for the gas jets of Birch *et al*. (1978) and Smith *et al.* (1986). The computed PDF were found to be closer to the measured PDF when a transport equation for turbulent intermittency was solved, rather than when Kent and Bilger's (1976) correlation was used. However, when these PDFs were integrated to determine the flammability factor, the two methods gave fairly similar results, as shown by Table 8. On the axis of jets, the mixture fraction PDF, and thus the flammability factor, are in close agreement with data, irrespective of whether Kent and Bilger's (1976) correlation is used to obtain the intermittency or a transport equation is solved.

Table 8 Flammability factor calculated from the measured and computed PDFs in the natural gas jet of Birch *et al*. (1978), at the axial location *x*/*d* = 10. Values are shown for turbulence models in which intermittency is calculated using Kent and Bilger's (1976) correlation (*k-ε, RS*), or with the intermittency determined from solution of its transport equation (*k-ε-I, RS-I*).

r/d	*Measured*	*k-ε*	*RS*	*k-ε-I*	*RS-I*
0.0	0.00	0.00	0.00	0.00	0.00
1.3	0.31	0.19	0.32	0.40	0.28
1.5	0.40	0.35	0.35	0.43	0.37
1.8	0.28	0.31	0.14	0.27	0.29

For simple turbulent shear flows, such as jets or wakes, there would appear to be only a modest overall advantage gained from solving a transport equation for turbulent intermittency, over that offered by use of Kent & Bilger's (1976) correlation. The situation for more complex flows, such as impinging jets, or for jets in cross-winds, is unclear. However, the philosophy which underlies the solution of turbulent transport equations, such as that for turbulent kinetic energy and its dissipation rate in the *k-ε* turbulence model, is to compute local turbulence properties rather than to rely on empirical correlations. Such correlations do exist for turbulent shear flows and are used in simplistic turbulence model approaches based on the concept of a 'mixing length'. The reason why they are not used for more complex flows is that they have limited validity, being restricted to the particular flows in which they are calibrated. A similar concern could apply to the use of Kent and Bilger's (1976) correlation if applied to complex flows, especially when these are likely to be the class of flows for which the use of CFD would be required.

Set against this concern is the effort needed to code a transport equation for turbulent intermittency. As outlined in Section 5.3, this is significant, and could be error-prone.

On balance, it is recommended that if a CFD model is to be used for calculating the flammability factor, that the intermittency should be obtained by solving its transport equation. It is noteworthy that Schefer *et al*. (2010) used Kent and Bilger's (1976) correlation in their initial CFD simulations of hydrogen jets, but stated that: "*Reduced empiricism in the predicted flammability factor can be achieved by replacing the intermittency correlation with a transport equation…*".

Although Alvani and Fairweather (Alvani, 2004, Alvani & Fairweather, 2008) used a slightly modified set of values for intermittency constants than those of Cho & Chung (1992) (see Section 5.3), these would appear to be optimised for jets. For validity across a wider range of flows, the values of constants as defined by Cho & Chung (1992) are to be preferred.

10.2.3 Turbulence model

Alvani and Fairweather (Alvani, 2004, Alvani & Fairweather, 2002, 2008) found that the best overall predictions of the mixture fraction PDF and the flammability factor were obtained using a Reynolds stress transport model with the turbulent scalar fluxes modelled from their own separate transport equations. However, the turbulence model was very complex with some very

specific features. It was based on the model of Jones & Musonge (1988) but with a revised set of constants from Jones (1994). The turbulent scalar fluxes were modelled following the approach of Fairweather *et al*. (1992). The effect of intermittency on the turbulence was incorporated by the addition of source terms in both the Reynolds stress and dissipation rate equations, following the approach of Savill (2002a, 2002b). The Intermittency transport equation followed the same basis as that of Cho & Chung (1992), but with a diffusion term modified to reflect turbulence anisotropy. The constants applied by Alvani and Fairweather in this intermittency transport equation were partly drawn from Cho & Chung (1992) and partly from Savill (2002a, 2002b). Finally, in the dissipation rate equation, the value of the $C_{\varepsilon 2}$ constant was reduced to 1.8, to improve the spreading rate predictions for a round turbulent jet flame, following the approach of Fairweather *et al*. (1992). It is only when all of the above adjustments were applied that the full performance of the Reynolds stress model was realised.

Although commercial CFD software usually incorporates one or more Reynolds stress transport turbulence models, the form of the model as used by Alvani and Fairweather (Alvani, 2004, Alvani & Fairweather, 2002, 2008) was very specific indeed. It would require a great deal of effort to replicate this exact form of Reynolds stress model in commercial CFD software. Often, such software does not include transport equations for the turbulent scalar fluxes, which are instead modelled using Equation (10.2). Coding these transport equations would add to the difficulties.

Importantly, Alvani & Fairweather (2008) concluded that the *k-ε-I* turbulence model gave results of sufficient accuracy for design purposes, even though it did not perform as well as the Reynolds stress model. Therefore, it is recommended that the *k-ε-I* turbulence model be used for predictions of flammability factor, rather than the Reynolds stress approach.

Nevertheless, it should be borne in mind that simple two-equation turbulence models do have their limitations. It is possible to overcome some of these limitations without having recourse to a full Reynolds stress transport model, by using more advanced forms of two-equation model (Launder & Sandham, 2002), but this may require further coding effort.

A brief mention was made in Section 3 of the possibility of using advanced turbulence modelling techniques, based on Large-Eddy Simulation (LES), to capture the detailed time-varying structure of turbulent shear flows. In such approaches the PDF of mixture fraction is calculated as an outcome of the simulations, rather than being prescribed. Ranga Dinesh *et al*. (2010) demonstrated the viability of LES for computing turbulence intermittency and the PDF of mixture fraction in a co-axial jet. However, the resource implications are daunting. Some 2.4 million mesh cells were required to resolve the spatial structure of the jet, together with many thousands of time-steps to generate appropriate flow statistics. Unfortunately, Ranga Dinesh *et al*. (2010) also did not include any comparisons with measurements.

Triantafyllidis *et al*. (2009) also presented LES results, in this case applied to the computation of ignition of a non-premixed flame stabilised by a bluff-body burner. Up to 4.9 million mesh cells were required, although a far coarser mesh was used for calculating the mixture fraction field using Conditional Moment Closure techniques. Triantafyllidis *et al*. (2009) compared contours of computed flammability factor and measured values, and found good agreement between the two in terms of both the shape of the profiles and the quantitative accuracy.

Clearly, LES offers the long-term prospect of being able to compute the flammability factor directly. However, the resource implications are presently a major limitation on the practicality of applying such approaches to the analysis and modelling of industrial hazards, and are likely to remain so for some years to come.